7/21

COO-2208-9

HUMAN THORACIC ANATOMY RELEVANT TO IMPLANTABLE ARTIFICIAL HEARTS

Technical Report

G.B. Jacobs, R.J. Kiraly and Y. Nosé

Department of Artificial Organs
The Cleveland Clinic Foundation
Cleveland, Ohio 44106

October 1976

Prepared For
THE U.S. ENERGY RESEARCH AND DEVELOPMENT ADMINISTRATION
UNDER CONTRACT NO. E(11-1)-2208

DISCLAIMER

NOTICE

FOREWORD

This report is the culmination of a study initiated in 1972 under ERDA (then AEC), Contract E(11-1)-2208. The study described in this report, as well as other specific studies under this same contract and separately reported, were conducted in the Department of Artificial Organs, Division of Research, Cleveland Clinic Foundation. Dr. Y. Nosé, Department Head, was Principal Investigator and R.J. Kiraly was Co-investigator. Mr. G. B. Jacobs was Project Leader and the major contributor to the study.

The authors acknowledge the substantial contribution of a number of individuals who provided effort to obtain and analyze the data: Drs. O. Sudilovsky, N. Taslitz and R. Seale provided the cadaver data. Drs. K. Hayashi and T. Meaney provided radiographs of living humans. Dr. T. Agishi extracted and digitized the radiographic data. Data compilation and analysis was performed by R. Ecker, R. Louie, R. Kobetic, B. Kluger and H. Sullivan.

TABLE OF CONTENTS

ABSTRACT

The objective of study is to define the human thorax in a quantitative statistical manner such that the information will be useful to the designers of cardiac prostheses, both total replacement and assist devices. This report pertains specifically to anatomical parameters relevant to the total cardiac prosthesis. This information will also be clinically useful in that the proposed recipient of a cardiac prosthesis can by simple radiography be assured of an adequate fit with the prosthesis prior to the implantation.

Methods have been developed for generating an integrated, statistical model of the anatomical structures within the human thorax relevant to artificial heart implantation. These methods involve definition of anatomy in four areas: chest wall, pericardium, vascular connection locations, and great vessels.

A model for the prediction of thorax features from radiograms is finalized. The models have been combined with radiograms to arrive at a size distribution representing the adult male and female populations.

Results are presented in three scale views of the human thorax showing the main features relevant to cardiac prosthesis implantation. Data is available for size distribution as a function of the population having specific sizes. Data was obtained from a number of sources and represents both normal and diseased patients. The ERDA total artificial heart was shown to successfully fit the fifty percentile adult male human.

1.0 INTRODUCTION AND MOTIVATION

Research and development efforts on cardiac prostheses have been underway by a large number of investigators for almost two decades. Even with a fairly well standardized experimental animal, the calf, present day devices have experienced failures due to mismatches in the geometry, kinking at the vascular connections, and pumps that are oversized for the animal's anatomy (1). In hindsight, it is obvious that progress could have been much greater had a comprehensive, quantitative study of the calf anatomy been done at the start. As a result of the prostheses development programs without the benefit of this data, current devices are being implanted in larger and larger animals in order to obtain a reasonable fit (2, 3). Clearly, many of these cannot be fitted into even the largest of human patients. We cannot lose sight of the fact that the goal is to have devices for use in humans and that the calf serves only as a test bed for the human-fitting device. With the approach of the first clinical applications of total replacement and assist devices, it is necessary to lay the groundwork so that dangerous anatomical mismatches be avoided in humans.

Figure 1 shows a mockup of the ERDA thermal converter and blood pump. This report concerns only the available thorax space for the pump.

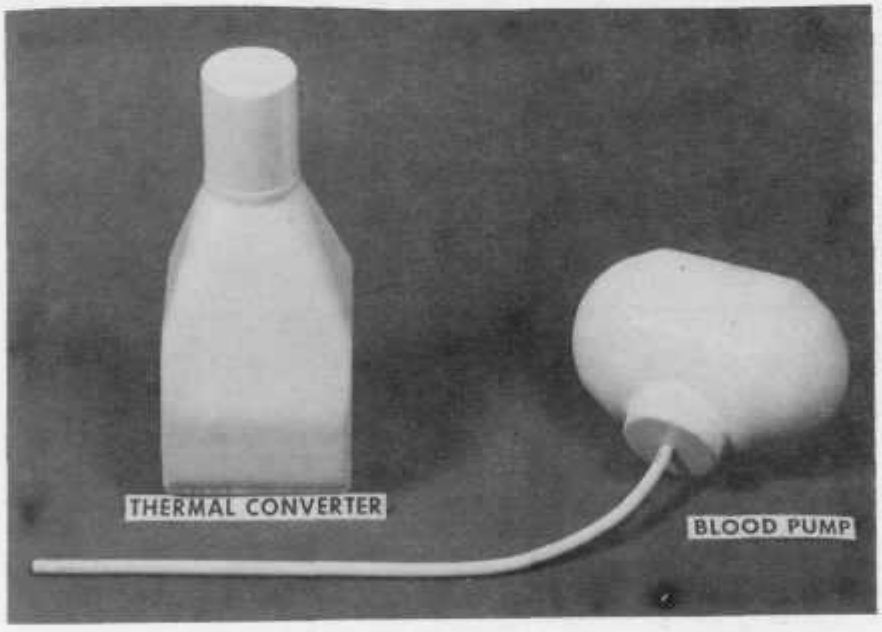

Figure 1

The problem can be broken down into two main areas according to the mode of geometrical mismatch between the mechanical heart and the recipient. After excising the natural heart, the surgeon is presented with four vascular connection points with varying distances and orientations (direction of a vector parallel to blood flow in the vessel) between them. The first category (mode 1) of failure can occur if either the distances between the connection points of the artificial heart are incorrect, or if the orientation of a

connection point on the prosthesis does not match the orientation of the corresponding blood vessel. This results in stretching (and possible tearing) or kinking at the anastomosis points, ending in either a fatal experiment or sharply curtailed blood flow.

A second mode of failure can occur even if perfect joints are made; this happens when the heart, hanging from its four bonds, encounters either relatively hard structures (chest wall, aorta) or soft structures (vena cava). The first failure mode defines dimensional relationships between connection points on the surface of the blood pump, while the second failure mode dictates constraints on the external boundaries of the device.

In Figure 2 is shown a transverse section of the thorax at the approximate level of the mitral and tricuspid valves. This is also a close estimate to the connection points for the mechanical heart, since it is anticipated that as much natural atrium as possible will be retained in actual implants. Also shown (in hatched region) is the lower edge of the lung hilus area. As can be seen, overly large dimensions for the anterior wall of the cardiac prosthesis will result in a mode 2 failure, in which the heart is forced posteriorly against the two atria, decreasing the effective volume and possible cutting off flow altogether (heavy arrows). In Figure 3 is pictured the same failure in the lateral view. Again, excessive dimensions in the anterior direction will either compress the sensitive hilus region or possibly cause a counterclockwise rotation, pivoting around this same point. Figure 4 indicates a mode 2 failure occurring in the lower region of the chest. Here, an abnormally large heart will be forced backwards (heavy arrow), perhaps compressing fatally the inferior vena cava. Aortic compression while highly unlikely due to its relative rigidity, could occur if blood pump dimensions are excessive.

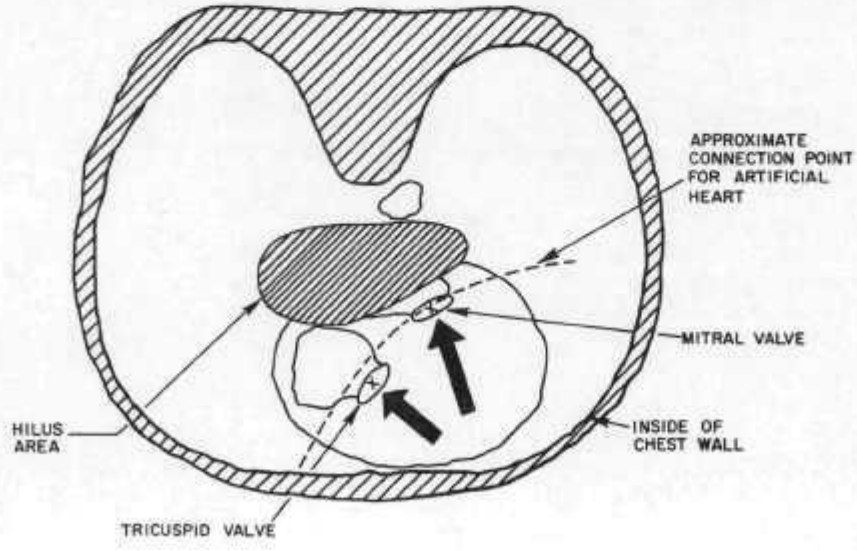

TRANSVERSE SECTION IN UPPER REGION OF PERICARDIUM
(Heavy arrows indicate possible compression)

Figure 2

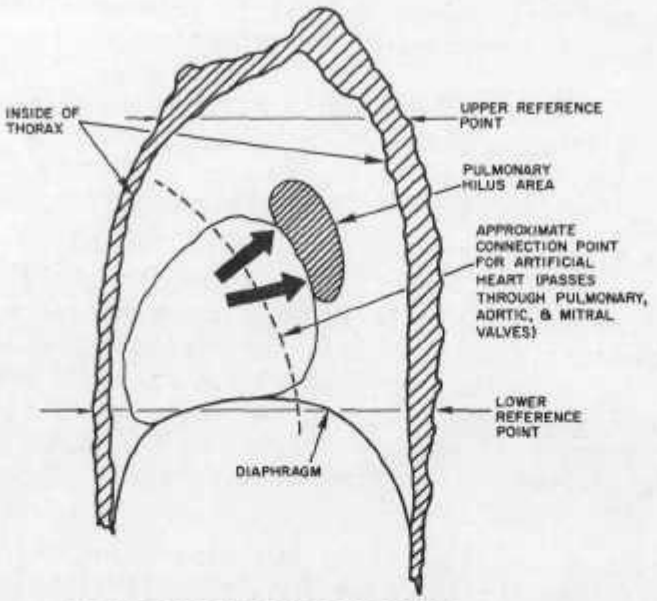

SAGITAL SECTION AT LEFT ROOT OF LUNG
(Heavy arrows indicate possible compression)

Figure 3

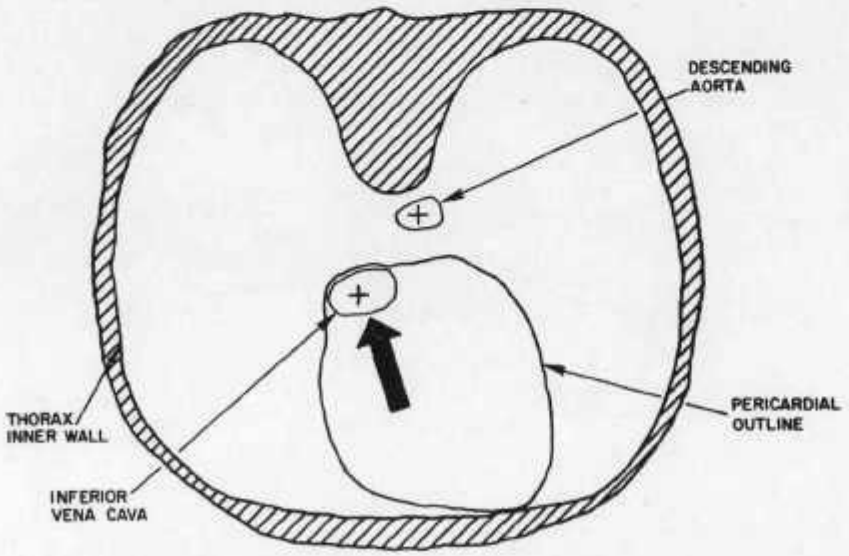

TRANSVERSE SECTION IN LOWER REGION OF HEART
(Heavy arrows indicate possible compression)

Figure 4

To summarize, two failure types must be concentrated on:

A. Kinking or twisting caused by a mismatch at the connection points.

B. Compression of vital soft structures due to abnormally large anterior boundary of the mechanical prosthesis.

Consequently, the region where most of the effort should be directed is enclosed between the dotted lines and the chest wall, as shown in Figures 2 and 3. Structural relationships outside of this area, though not so important, are relevant in that two additional phenomena may occur:

A. Extension of the blood pump's flexible atrium beyond the normal pericardium will result in a decreased atrial compliance (the pliant wall will simply acquire the compliance of surrounding tissue). In such a case, its elasticity will be a function of how far into the lung the atrium extends, and the average lung compliance, which in turn is governed by the lung inflation. Too great a decrease in atrial compliance severely reduces its effectiveness as an accumulator buffering a pulsatile pump.

B. Excessive pressure on the lung by a pump protruding beyond the pericardial limits may cut into the lung's residual volume. In addition, compression of the lung tissue between the thorax wall and the pump may cause necrosis of the lung parenchyma.

2.0 OVERVIEW OF METHOD FOR DEFINING THE HUMAN THORAX

2.1 PREVIOUS WORK

Sources for portions of the necessary data are available in the literature; primarily from the fields of anatomy, radiology, and cardiology. Anatomy texts, especially those with fixed cadaver sections, have proved particularly valuable (4-12). Even if no absolute dimensions are available from these sections, ratio and shape information has been very useful. In the field of radiology, two particular studies have provided valuable raw dimensions on the pericardium for verifying parts of our own data (13-28). These are: first, attempts to estimate total cardiac volume from a limited number of dimensions taken off radiograms, and second, development of methods to correlate certain of these dimensions (cardio-thoracic ratio for example) to specific disease states. However, most of this data represents maximal measurements and contains no shape information. We have therefore used it only as input to our normalizing parameter information. Several recent works of an interdisciplinary nature (29-33) (involving cardiology, radiology, and anatomy) have likewise contributed to substantiating the statistical significance of sections of our data. Other papers, containing subjective information on the spatial arrangement of human heart valves (34-36) have helped in formulating an intravalvular model. Published tomographic data (37), although of limited quantity, has provided a valuable source of measurements for certain aspects of the pericardial and chest wall shape models. A number of general texts (38-40) have helped to identify possible artifacts in our method. Papers relevant to both the mathematics and hardware for defining amorphous, biological shapes have been scarce. Two noteworthy works, however, have general application to the specification of thorax anatomy (41-42).

2.2 CURRENT METHODOLOGY

Because reliable dimensional information is lacking in the literature, some method must be devised for avoiding mode 1 and 2 failures discussed earlier. The approach used must generate not only a set of average dimensions for both the vascular connection points and external boundary of the heart, but tolerances as well, so that the final pump chosen will fit a majority of prospective candidates.

The method finally used was based on the assumption that most organs and structures in the human body have similar configurations, and variations of a particular organ from person to person are due mainly to differences in size. This implies that if these size differences were normalized out of the specific organ under investigation, the organ's "shape," or geometrical

configuration would be the same from person to person. For instance, if various size ellipses displayed symmetrically on the same set of cartesian coordinates (cylindrical coordinates have fewer degrees of freedom) are normalized in both the x and y directions, a single circle with its center at zero and passing through the (1,0) and (0,1) points results. This means that this particular shape, and ellipse in this case, can be characterized by a circle after normalization. Further, the average size of an entire family of ellipses can be expressed by both this circle and the average of the maximum x and maximum y dimensions of the ellipses under investigation.

In Figure 5 is shown the application of this concept to the left posterior boundary (solid line) of a typical transverse section of the human thorax. Maximum x and y values in this quadrant are approximately 8.0 cm and 5.0 cm respectively. The curve, after discretization, consists of a series of points; i.e., (1, .7), (2, 2.4), (3, 3.9), etc. Dividing the coordinates of each of these points by the maximum x and y values respectively (called "normalizing parameters" in this report), results approximately in the middle curve of Figure 5. In the particular case of a thorax section, these "normalizing parameters" were carefully chosen to be observable dimensions in either lateral or P-A radiograms: Specifically, maximum y value in the example appears in lateral view, while greatest x dimension is observed in P-A photo. Note that the maximum x value is the largest dimension in the entire left half of the chest, and may appear in either the posterior or anterior quadrant. For this reason, the end point may not pass through the (1,0) point. This normalized curve, then, represents the "shape" of the left posterior thorax section after size variability has been eliminated.

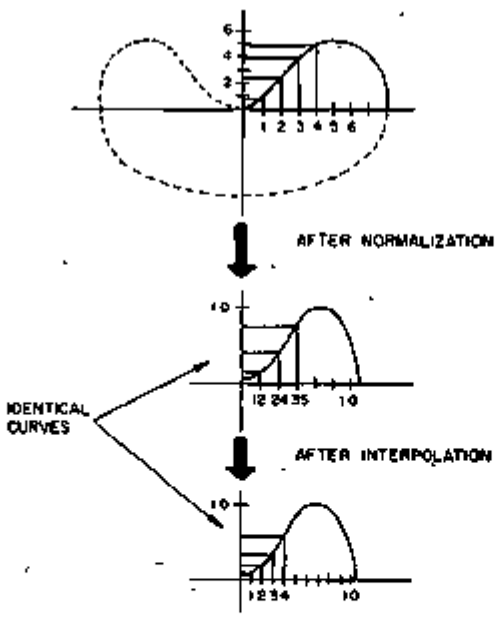

NORMALIZATION AND INTERPOLATION OF RAW DATA

Figure 5

In order to verify this, a statistically significant number of these normalized curves must be averaged together. However, normalization of a second left posterior curve may not result in identical x values, making direct averaging impossible. To avoid this problem, the normalized curve is interpolated to yield a y value for each incremental x value, as shown in the lower curve of Figure 5. A quadratic interpolation scheme that successively straddled each x value in increments of .1, up to 1.0, was found to give excellent results.

The generation of a shape model depends on an accurate interpolation of the normalized data. To check this interpolation method, the following was done. For each integer value of x, there exists the interpolated y value. These were then multiplied by x_{max} and y_{max} and compared with the original curve. This was especially important for shapes similar to the left anterior "type," since there was some discrepancy between these chest wall predictions and the actual outlines (Figures 7-9 in Appendix C). As shown in Figure 6, there is excellent agreement, and the interpolation procedure appears correct.

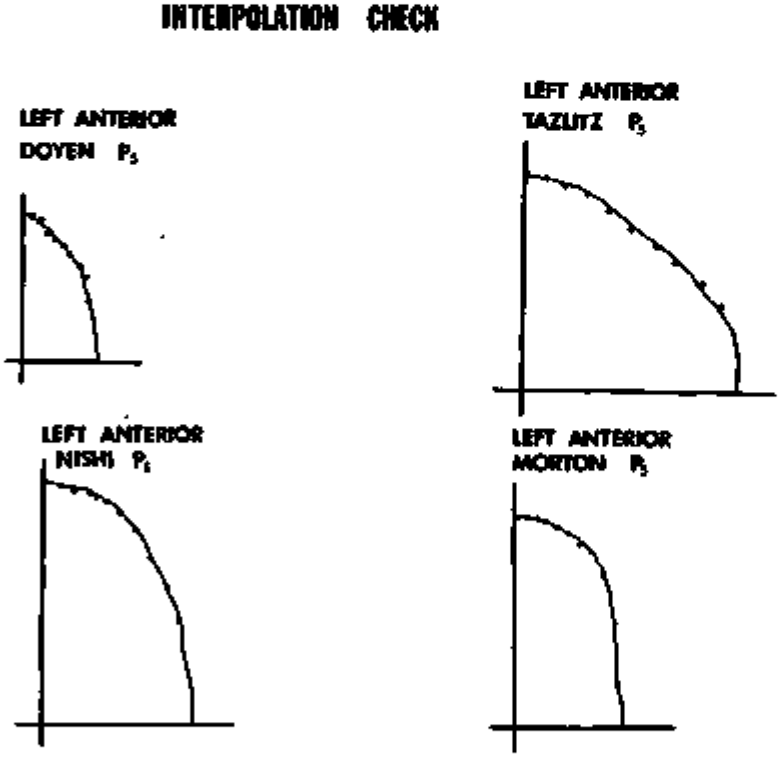

Figure 6

Following interpolation, an average "shape" for any number of samples can be calculated by averaging all y values corresponding to each incremental x value (typical example is Figure 7). If the standard deviation for this curve is sufficiently small, then it can be said to constitute the "shape model" for this particular quadrant of the chest.

Having finalized a configuration for each quadrant, at each level in the chest, the investigator can now measure the "normalizing parameters" from a large number of A-P and lateral radiograms. Using average values of these parameters in conjunction with the shape model allows the reconstruction of the average thorax.

The above is a simple example of a concept that is applied throughout the entire program. A small sample of hard-to-get data is used to determine the form of an organ or structure in terms of normalizing parameters that are easily observed on standard radiograms, a relatively abundant source of data. Final results yield a meaningful average, along with a variability factor (i.e., standard deviation) that can be used for design purposes.

In Figure 8, within the dotted line, appears a general block diagram of the thought processes involved in arriving at a final result. As can be seen, the end product (blood pump shape) is a function of both hard structure (thorax wall) and soft structure (pericardium, great vessels) information. Figure 9 illustrates the application of normalization to acquiring both kinds of information. Average thorax wall definition is generated by combining statistical distributions of "normalizing parameters" (A, B, and C, obtained from A-P and lateral X-ray photographs) with a shape model derived from silastic thorax molds poured in human cadavers. A typical soft structure, the pericardium, is shown to be a function of parameters: level, D, E, F, and G. (Level is the percent vertical distance between an upper and lower reference point located within the thorax (44)). Specifying chest levels in this manner is intended to normalize out variations in chest height encountered from patient to patient. Using certain portions of the ribs to locate high and low reference points follows from the clinical practice of locating heart valves and aspiration points via the rib dependent intercostal spaces (53).

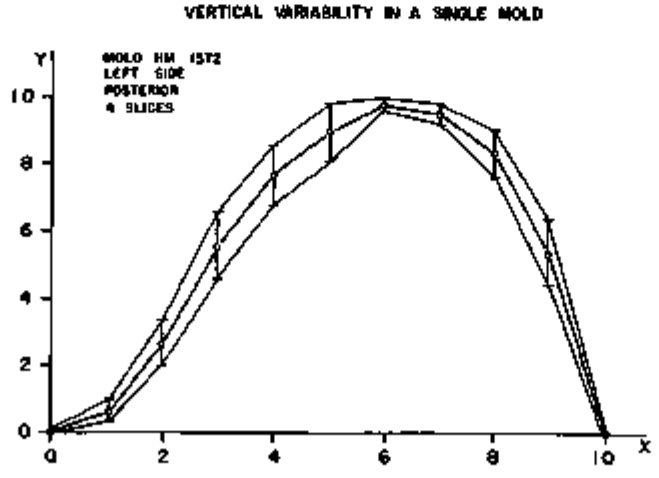

Figure 7

PROGRAM TO DETERMINE SPACE FOR BLOOD PUMP

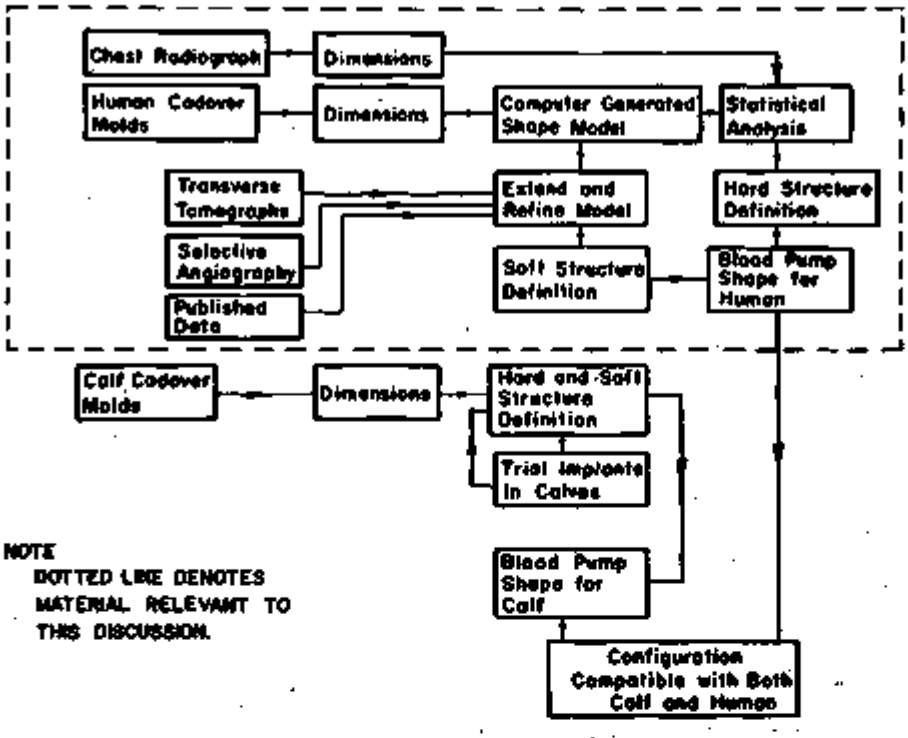

Figure 8

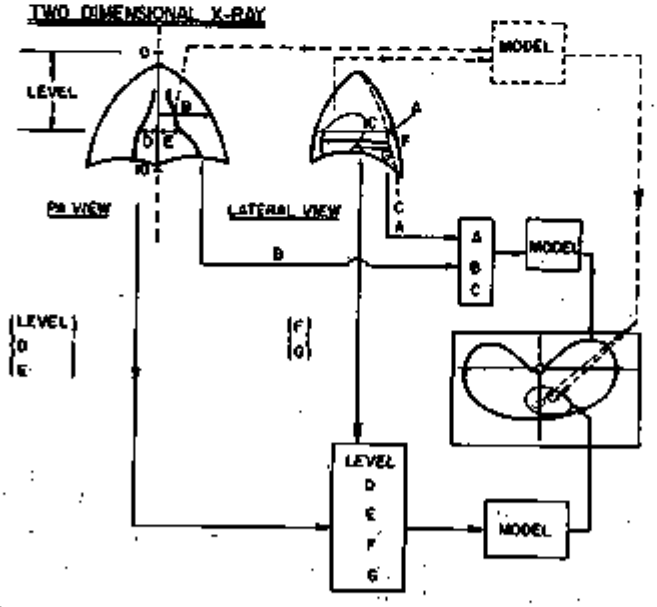

METHOD FOR RELATING TWO DIMENSIONAL MEASUREMENTS TO THREE DIMENSIONAL OBJECTS

Figure 9

The box in the upper right of Figure 9 represents the spatial model for the vascular connection point definition. The question that must be answered is: "What observable points or structures in two-dimensional radiograms should be used as input for a model to predict vascular connections and location of relevant great vessels (both invisible) with respect to the pericardial sac and the chest wall?" Solutions to this problem will be presented in later sections.

A breakdown of the total problem is shown in Figure 10. This includes four basic areas of investigation: chest wall, pericardium, valve and great vessel anatomy. Valves are studied only insofar as they indicate the approximate connection point with the artificial heart. Except for the great vessels, each area is further subdivided into a "shape model" and pertinent normalizing parameters. Dimensions H, I, J, and K are not normalizing parameters in the true sense of the word and will be explained in the detailed section on the valve model.

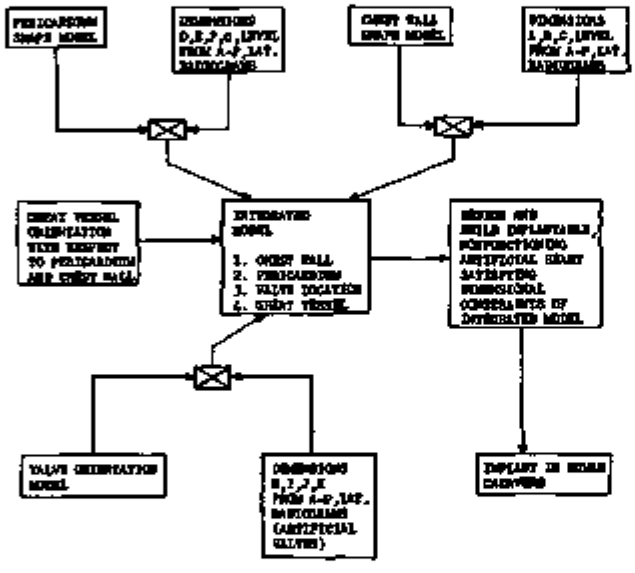

Figure 10

The form of a final integrated model used for design is portrayed in Figure 11. Average values for chest wall, pericardium, valves and great vessels (aorta and vena cava) will be shown with their corresponding tolerances at specified levels in the chest. Vascular connection points in these transverse sections also have vertical tolerances. A complete, reconstructed thorax is generated by stacking each of these sections on top of one another. Distance between sections is simply the average vertical chest length (distance

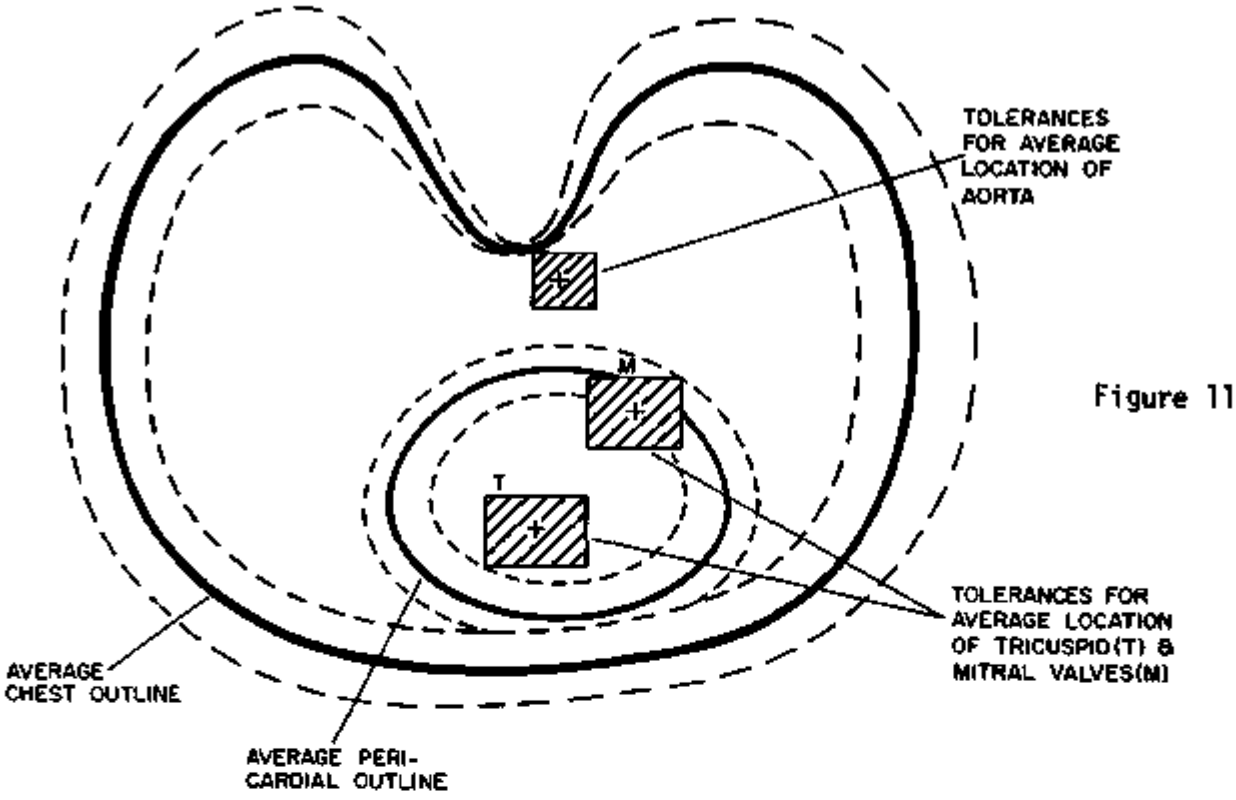

Figure 11

FORM OF FINAL RESULTS AT A PARTICULAR LEVEL IN THE CHEST

between upper and lower reference points) divided by 10. Location of sections with respect to each other is determined by positioning the chest reference point (most anterior portion of vertebra) of each section on the typical curve of a spinal column. This curve is generated from both our own data and published results.

2.3 REFERENCING SYSTEM

Some potential data sources were not usable using our initial referencing system because the ribs were not visible. This reference system, as shown in Figure 12, requires a clear picture of rib location and was chosen to enhance the analysis of radiograms in which vertebrae were not visible. To solve this problem, a correlation was made between the midpoint of each thoracic vertebra and vertical reference level using sources that allowed a good picture of both rib location and vertebra. Seven anatomy texts, seven angiograms, and one cadaver were employed as data banks for deriving a correlation. The accumulated data has been graphed in Figure 13. From this curve, one can estimate accurately vertical reference level if vertebra number is known. This regression line has permitted the inclusion of frozen cadaver data and other sources where rib locations are not available for scrutiny.

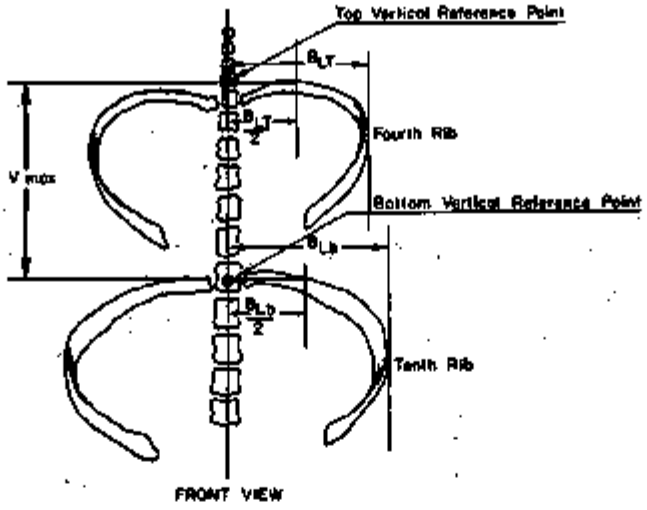

Figure 12

PROCEDURE FOR
LOCATING TOP AND LOWER REFERENCE POINTS

1) Measure B_{LT} and B_{Lb}
2) Upper reference point is intersection of Rib 4 and $B_{LT/2}$
3) Lower reference point is intersection of Rib 10 and $B_{Lb/2}$

VERTICAL REFERENCE LEVEL VS. THORACIC VERTEBRA NUMBER

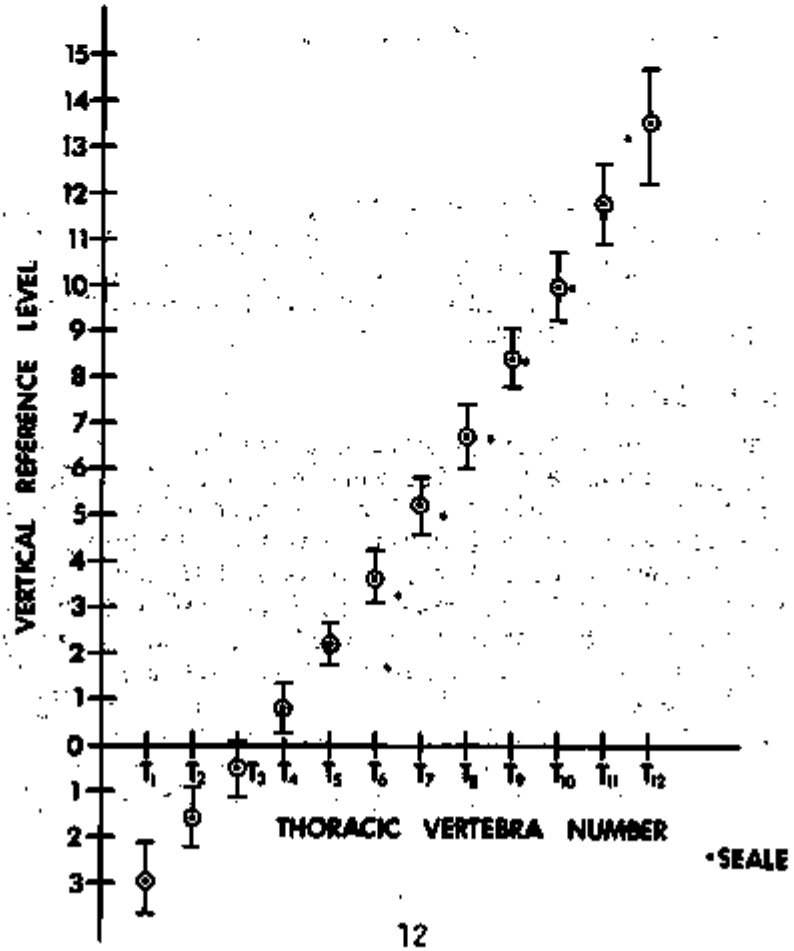

Figure 13

2.4 DATA SOURCES AND VARIABLES

Two broad categories of data had to be gathered; first, shape information and secondly, absolute measurements to determine a statistical distribution for the structure. Typical data sources are shown in Figures 14 to 17. These include molds from cadavers, frozen cross sections of cadavers, published data, and radiograms of living patients. Figure 18 summarizes these sources.

Figures 19 and 20 portray the variables that were recorded and analyzed from this raw data. Because thorax structures are three dimensional, a complete description must necessarily involve dimensions from both the transverse and vertical planes.

These figures will be referred to throughout the report for variable identification.

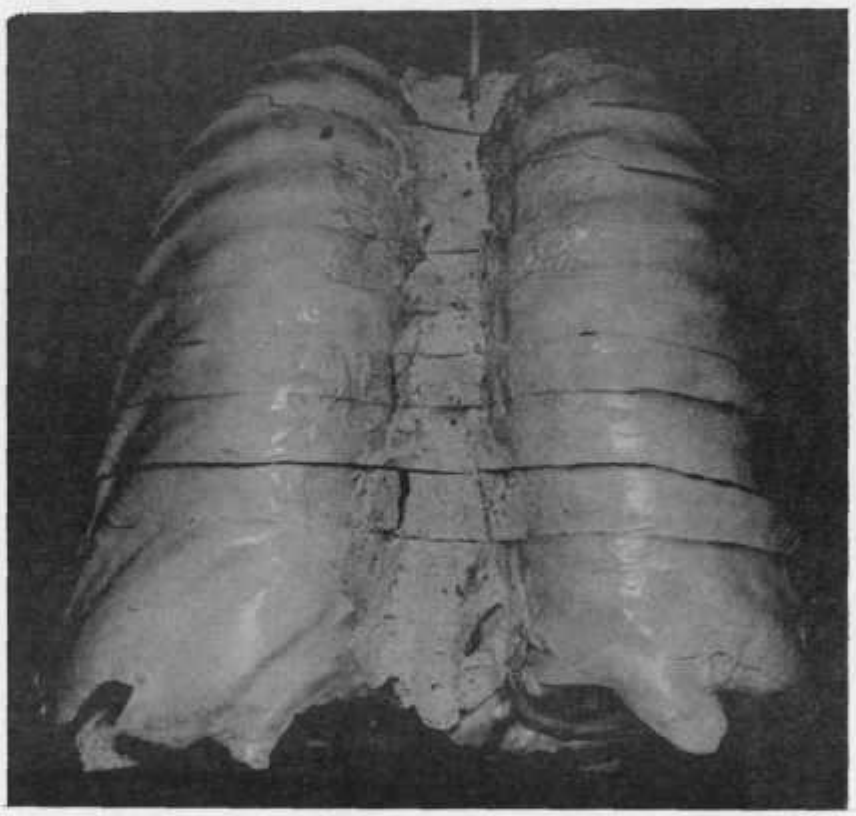

Figure 14: Mold from cadaver thorax.

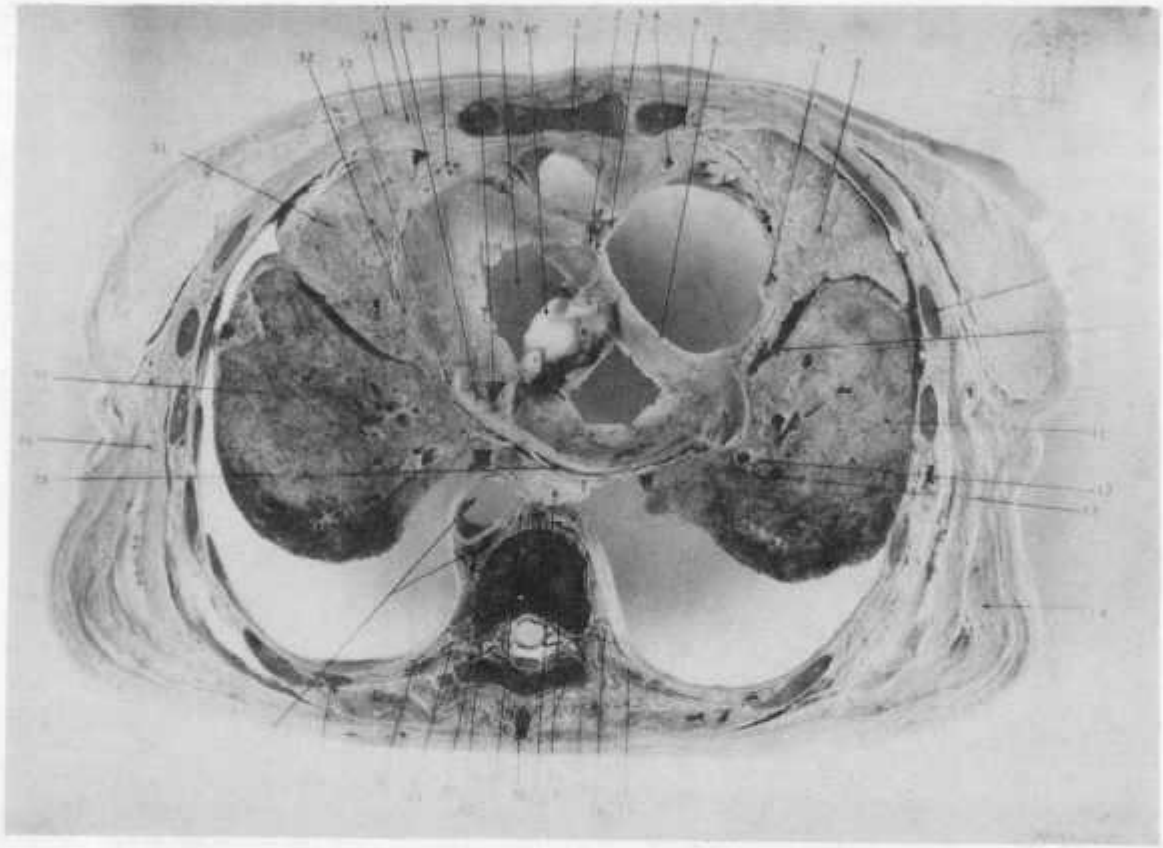

Figure 15

Septum mediastinale
Costa IV
Chordae tendineae
Pulmo [lobus superior]
Ventriculus sinister
Costa V
Atrium sinistrum
Epicardium
Costa VIII
Costa IV
Costa V
Costa VI
Costa VIII

Figure 16
15

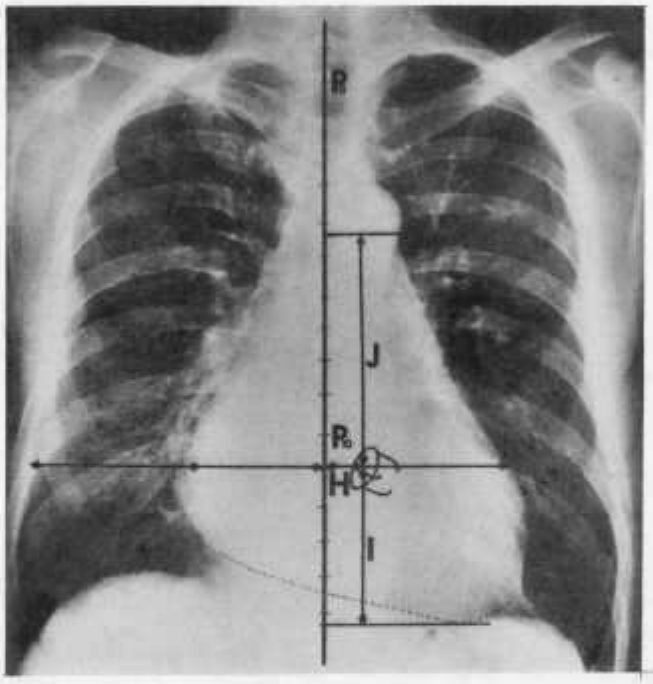

Figure 17

Figure 18

DATA SOURCES FOR RESULTS

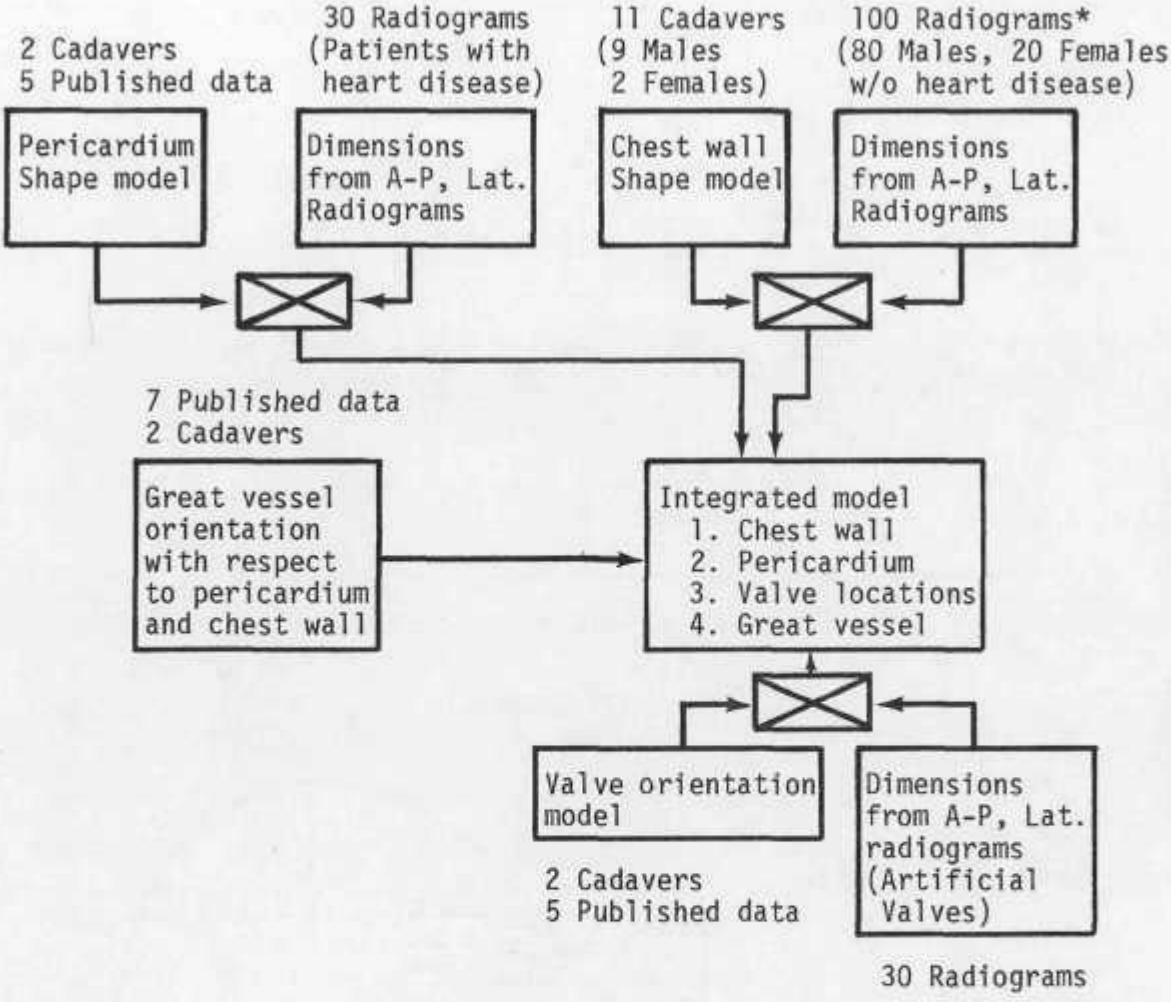

* For some results, 30 radiograms of patients with heart disease were used

VERTICAL REFERENCE

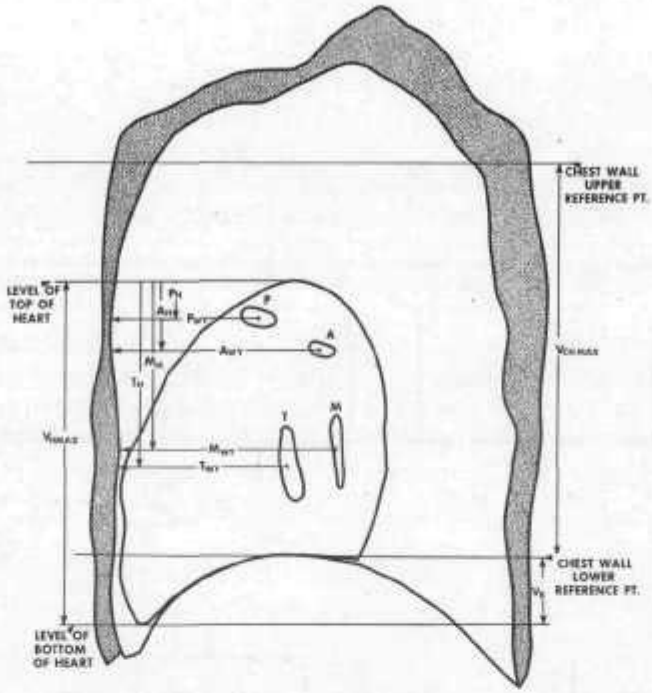

Figure 19

TRANSVERSE REFERENCE

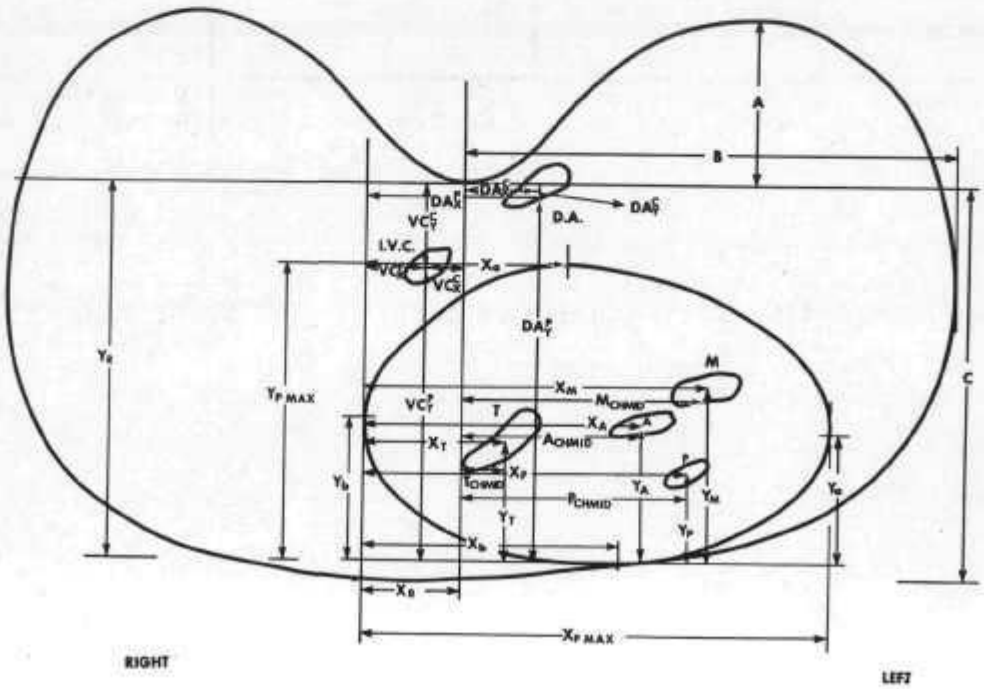

Figure 20

2.5 POSSIBLE ARTIFACTS IN THE METHOD

One of the final goals is the variability of anatomical relation ships within the thorax. There are two sources of this variability: One is the actual, random differences between patients, and the second is error inherent in the method of analyzing the anatomical structures.

Dissimilarities in the thorax region between individuals are significant and qualitatively well documented. Pericardial sac differences alone can be quite remarkable. The sac in an asthenic individual (very low diaphragm) is long and narrow, while that of the sthenic (high diaphragm) is short and broad. Somewhere in between is a so-called "average" individual (13,38). Similarly, there can be great variation in the layout of the great vessels, and an individual can still be considered quite normal (39).

Sources of variability that might be termed artifact, in that they do not reflect purely genetic differences between individuals, may enter the analysis simply because the system under investigation is highly dynamic. This can happen especially in radiological measurements. Cardiac silhouette is known to be highly dependent on respiration phase; hence, standard radiographic procedure dictates that all photos be taken during full inspiration. There may be, however, many different patient views on what constitutes "full inspiration." Cardiac phase has a negligible effect on results for both the cardiac silhouette and valve location (38, 40). However, accidental breathholding by the subject results in the classical valsalva maneuver, resulting in decreased blood inflow to the heart and subsequent marked reductions in cardiac size.

A third source of variability -- disease -- can be considered either an artifact (in dealing with normals), or an important correlation parameter if one is deliberately studying patients with abnormal hearts, prime candidates for an artificial blood pump. The effects of abnormal hemodynamics on pericardial size, valve location and, to some extent, vena cava location, is marked and non-negligible. A detailed discussion of such effects is beyond the present scope of this report, but excellent source materials can be found in references 13, 38, 39 and 52.

In the following sections, the detailed methods used in investigating each of the four main areas outlined in Figure 10 will be discussed. At the same time, the current status of each, and specific methods for detecting errors in the results (if applicable) will be presented.

3.0 DEFINITION OF CHEST WALL AND DIAPHRAGM

The purpose of this section is to define the chest cavity of an adult human. This effort is only the first stage in accomplishing the ultimate goal, that of defining not only the chest cavity, but the relative location of pertinent soft structures within this cavity in the human.

A shape model was made from data taken from transversely sectioned molds of the chest cavity of human cadavers (Figure 21). The normalized shape and curvature of the human chest cavity was determined by analysis of this data on a computer.

The shape model was then combined with the measurements of dimensions on a large number of human plane chest radiographs to determine a distribution of the size of the chest cavity as a function of the percentage of the population having these dimensions.

The ultimately developed technique of the modeling and analysis is also expected to be applicable to clinical cases of artificial heart implantation where standard chest radiographs of the proposed recipient will insure that the prosthesis will fit in the particular patient.

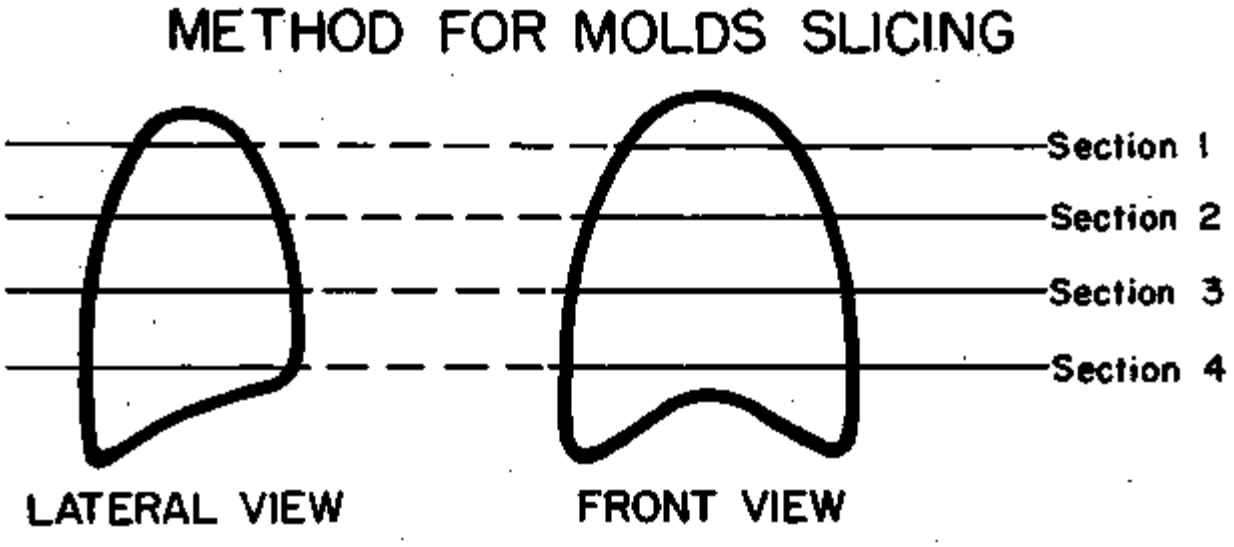

Figure 21

3.1 GENERATION OF SHAPE MODEL

A detailed description of the essential concepts in the model development are included in an earlier report (45). Briefly, shapes generated from molds cast in cadaver thorax cavities were used to determine chest wall curvature after individual size variations had been normalized out of the data (using normalizing parameters A, B, and C, Figure 22). Nine male molds and two female molds have been analyzed and the resulting data used to generate a vertically dependent model. This model consists of a normalized curve for each quadrant (i.e., left anterior, left posterior, etc.) at a known level in the thorax. The vertical level under investigation is specified in terms of the percent vertical distance between two reference points identifiable on the radiograms. Because the individual vertebrae were not distinct in the films, these reference points are specified in terms of rib number and certain X-ray dimensions. They are located roughly at the T4 and T10 regions of the chest (Figure 12, described earlier). A typical normalized curve is shown in Figure 23. This curve represents the model (± 1 standard deviation) for the left anterior portion of a transverse section at approximately the T10 region. Data for this curve is shown at the top of Table 1 under "left anterior." Comparison of Figure 24 with Figure 23 demonstrates graphically the reduction in error when a vertically dependent model is used. Data for the T6 and T4 regions is shown in Tables 2 and 3 respectively. A comparison of the left and right anterior and posterior sections of all model data averaged in the vertical direction is shown in Figures 25 and 26 and clearly demonstrates symmetry of the thoracic wall shape. An example of model use is demonstrated in Appendix A.

To determine a statistical distribution of thorax sizes for the adult population, average values for A, B, and C at each level in the thorax must be determined from a reasonably large sample of X-ray measurements. The procedure used to extract this data from 80 males and 20 females is described next.

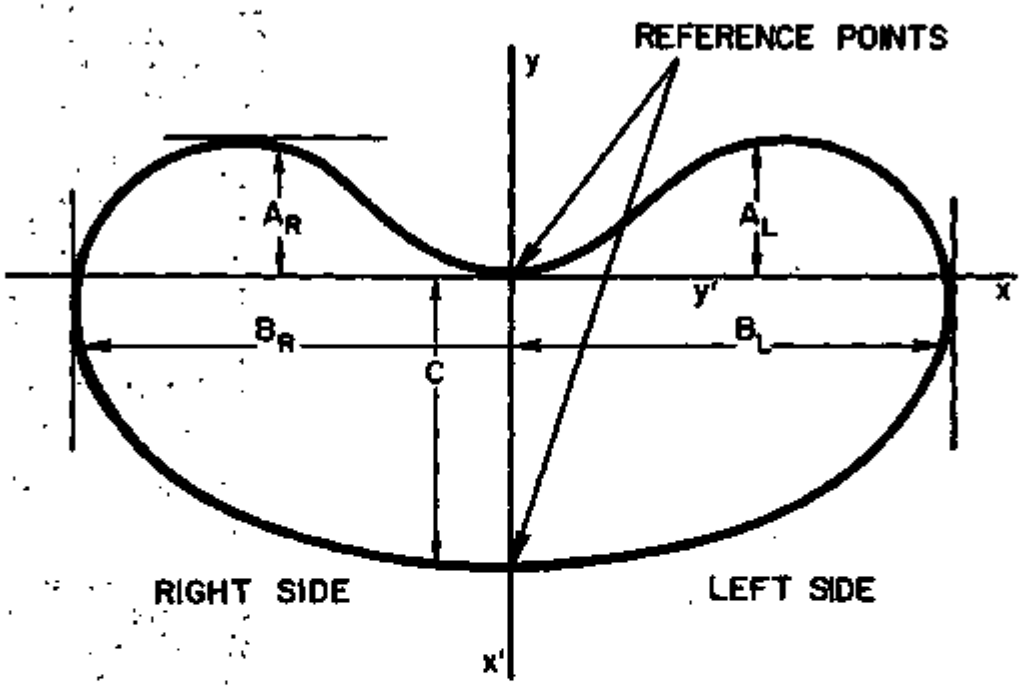

NORMALIZING PARAMETERS FOR A TYPICAL MOLD CROSS SECTION

Figure 22

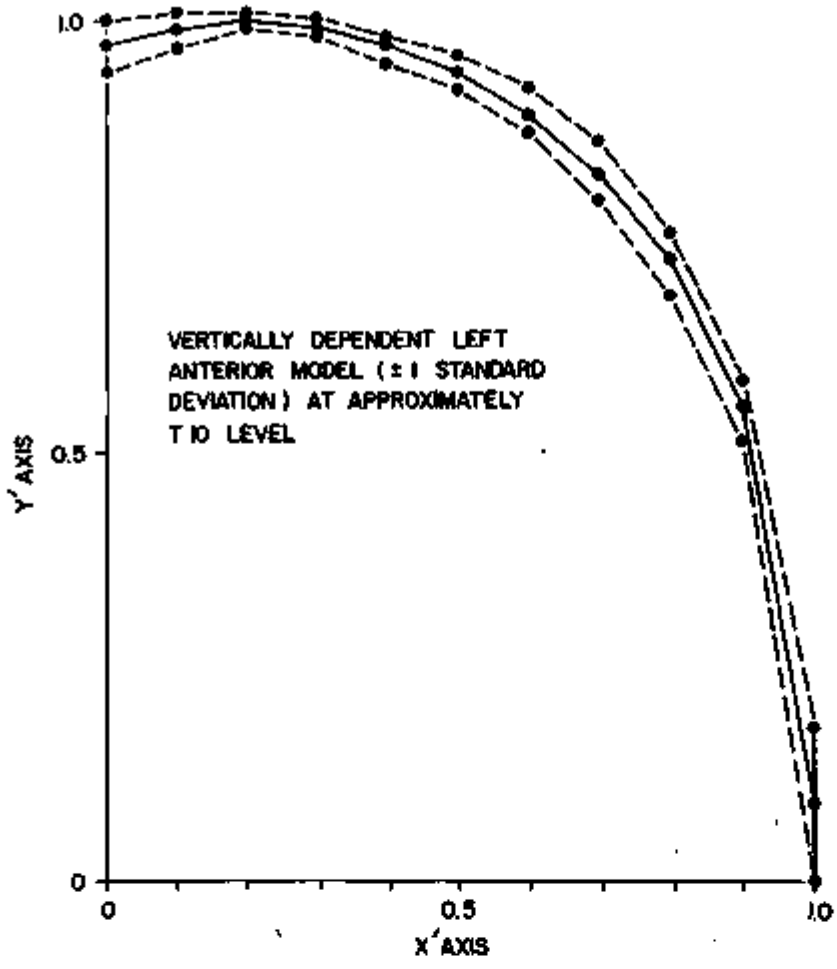

Figure 23

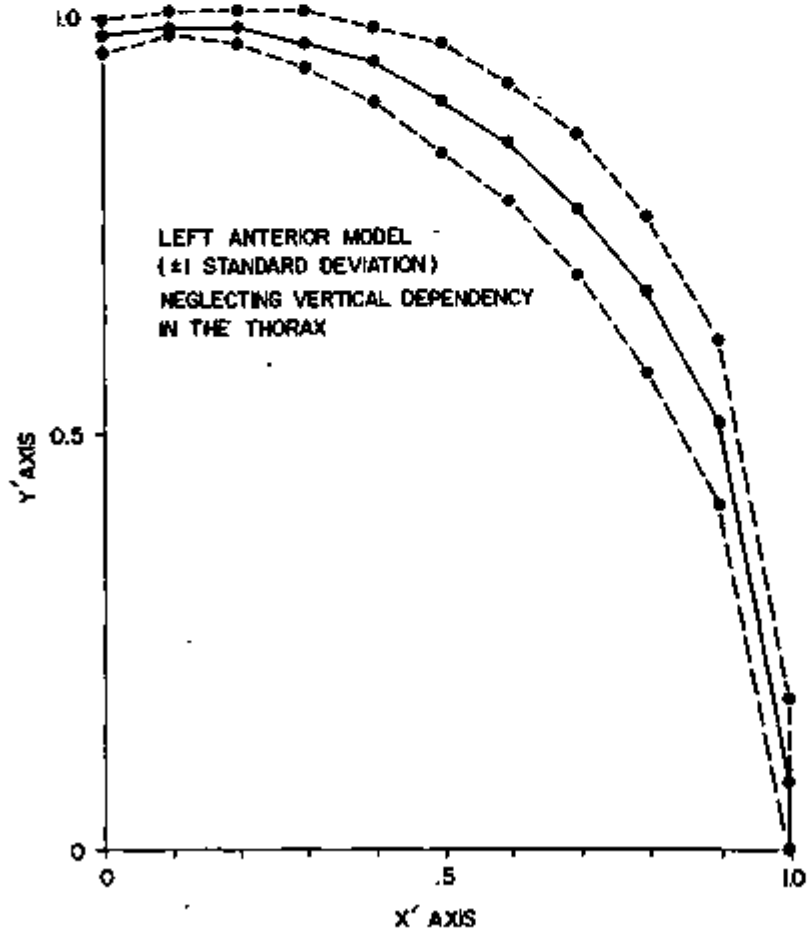

Figure 24

FROM SPEC. # 3.00TO SPEC. # 9.00
LEFT SIDE
ANTERIOR
SLICES USED IN AVERAGE= 7.00

XINT	AVG	STDEV	PRCT
0.0000	0.9796	0.0261	2.6736
0.1000	0.9951	0.0111	1.1140
0.2000	0.9989	0.0040	0.3995
0.3000	0.9849	0.0095	0.9620
0.4000	0.9644	0.0149	1.5497
0.5000	0.9370	0.0208	2.2165
0.6000	0.8897	0.0234	2.6251
0.7000	0.8160	0.0309	3.7872
0.8000	0.7075	0.0355	5.0118
0.9000	0.5268	0.0478	9.0778
1.0000	0.0623	0.0777	124.7309

FROM SPEC. # 3.00TO SPEC. # 9.00
LEFT SIDE
POSTERIOR
SLICES USED IN AVERAGE= 7.00

XINT	AVG	STDEV	PRCT
0.0000	0.0000	0.0000	0.0000
0.1000	0.1257	0.0400	31.8348
0.2000	0.5089	0.1189	23.3615
0.3000	0.8067	0.1082	13.4112
0.4000	0.9322	0.0680	7.2980
0.5000	0.9942	0.0212	2.1358
0.6000	0.9851	0.0205	2.0777
0.7000	0.9282	0.0634	6.8308
0.8000	0.7777	0.1122	14.4215
0.9000	0.5168	0.1777	34.3829
1.0000	0.0000	0.0000	0.0000

FROM SPEC. # 3.00TO SPEC. # 9.00
RIGHT SIDE
ANTERIOR
SLICES USED IN AVERAGE= 7.00

XINT	AVG	STDEV	PRCT
0.0000	0.9882	0.0106	1.0771
0.1000	0.9934	0.0058	0.5862
0.2000	0.9953	0.0078	0.7861
0.3000	0.9900	0.0110	1.1108
0.4000	0.9724	0.0185	1.9067
0.5000	0.9330	0.0237	2.5399
0.6000	0.8812	0.0273	3.1027
0.7000	0.8020	0.0380	4.7368
0.8000	0.6904	0.0551	7.9826
0.9000	0.5014	0.0651	12.9829
1.0000	0.0215	0.0367	171.1594

FROM SPEC. # 3.00TO SPEC. # 9.00
RIGHT SIDE
POSTERIOR
SLICES USED IN AVERAGE= 7.00

XINT	AVG	STDEV	PRCT
0.0000	0.0000	0.0000	0.0000
0.1000	0.0905	0.0474	52.3826
0.2000	0.4789	0.0820	17.1162
0.3000	0.8222	0.0459	5.5851
0.4000	0.9428	0.0232	2.4653
0.5000	0.9884	0.0077	0.7760
0.6000	0.9800	0.0220	2.2412
0.7000	0.9169	0.0426	4.6479
0.8000	0.7677	0.0594	7.7394
0.9000	0.5022	0.1148	22.8625
1.0000	0.0000	0.0000	0.0000

VERTICALLY DEPENDENT MODEL AT T10 REGION (LEVEL 9.0 TO 13.0)

TABLE 1

FROM SPEC. # 1.00TO SPEC. # 9.00
LEFT SIDE
ANTERIOR
SLICES USED IN AVERAGE= 9.00

XINT	AVG	STDEV	PRCT
0.0000	0.9703	0.0180	1.8602
0.1000	0.9918	0.0130	1.3139
0.2000	1.0019	0.0056	0.5564
0.3000	0.9928	0.0077	0.7748
0.4000	0.9703	0.0172	1.7728
0.5000	0.9339	0.0275	2.9398
0.6000	0.8856	0.0397	4.4808
0.7000	0.8109	0.0555	6.8409
0.8000	0.7087	0.0707	9.9781
0.9000	0.5481	0.0781	14.2568
1.0000	0.1214	0.0875	72.0709

FROM SPEC. # 1.00TO SPEC. # 9.00
LEFT SIDE
POSTERIOR
SLICES USED IN AVERAGE= 9.00

XINT	AVG	STDEV	PRCT
0.0000	0.0000	0.0000	0.0000
0.1000	0.1635	0.0495	30.2595
0.2000	0.5039	0.1058	20.9877
0.3000	0.8107	0.0790	9.7497
0.4000	0.9525	0.0353	3.7034
0.5000	0.9971	0.0075	0.7498
0.6000	0.9694	0.0097	0.9969
0.7000	0.8607	0.0315	3.6547
0.8000	0.6721	0.0698	10.3852
0.9000	0.3467	0.1070	30.8625
1.0000	0.0000	0.0000	0.0000

FROM SPEC. # 1.00TO SPEC. # 9.00
RIGHT SIDE
ANTERIOR
SLICES USED IN AVERAGE= 9.00

XINT	AVG	STDEV	PRCT
0.0000	0.9769	0.0193	1.9746
0.1000	0.9936	0.0105	1.0533
0.2000	0.9959	0.0066	0.6655
0.3000	0.9882	0.0053	0.5317
0.4000	0.9606	0.0170	1.7672
0.5000	0.9171	0.0293	3.1920
0.6000	0.8527	0.0440	5.1565
0.7000	0.7800	0.0447	5.7313
0.8000	0.6744	0.0534	7.9174
0.9000	0.4869	0.0629	12.9124
1.0000	0.0410	0.0873	213.0066

FROM SPEC. # 1.00TO SPEC. # 9.00
RIGHT SIDE
POSTERIOR
SLICES USED IN AVERAGE= 9.00

XINT	AVG	STDEV	PRCT
0.0000	0.0000	0.0000	0.0000
0.1000	0.1701	0.0273	16.0353
0.2000	0.5550	0.0868	15.6374
0.3000	0.8415	0.0573	6.8071
0.4000	0.9581	0.0419	4.3766
0.5000	0.9943	0.0094	0.9470
0.6000	0.9670	0.0214	2.2081
0.7000	0.8738	0.0391	4.4784
0.8000	0.6894	0.0628	9.1161
0.9000	0.3747	0.0799	21.3225
1.0000	0.0000	0.0000	0.0000

VERTICALLY DEPENDENT MODEL AT T6 REGION (LEVEL 3.0 TO 6.0)

TABLE 2

FROM SPEC. # 1.00TO SPEC. # 9.00
LEFT SIDE
ANTERIOR
SLICES USED IN AVERAGE=12.00

XINT	AVG	STDEV	PRCT
0.0000	0.9890	0.0151	1.5275
0.1000	0.9872	0.0153	1.5502
0.2000	0.9768	0.0260	2.6569
0.3000	0.9511	0.0383	4.0255
0.4000	0.9107	0.0482	5.2951
0.5000	0.8567	0.0566	6.6048
0.6000	0.7904	0.0628	7.9407
0.7000	0.7068	0.0693	9.8097
0.8000	0.5996	0.0754	12.5707
0.9000	0.4424	0.0781	17.6478
1.0000	0.0539	0.0891	165.3323

FROM SPEC. # 1.00TO SPEC. # 9.00
LEFT SIDE
POSTERIOR
SLICES USED IN AVERAGE=12.00

XINT	AVG	STDEV	PRCT
0.0000	0.0000	0.0000	0.0000
0.1000	0.1267	0.0517	40.8214
0.2000	0.4759	0.1042	21.9033
0.3000	0.7603	0.0913	12.0087
0.4000	0.9239	0.0557	6.0337
0.5000	0.9855	0.0237	2.4021
0.6000	0.9808	0.0155	1.5771
0.7000	0.9084	0.0451	4.9602
0.8000	0.7786	0.0895	11.5013
0.9000	0.5366	0.1686	31.4188
1.0000	0.0369	0.0870	235.9217

FROM SPEC. # 1.00TO SPEC. # 9.00
RIGHT SIDE
ANTERIOR
SLICES USED IN AVERAGE=12.00

XINT	AVG	STDEV	PRCT
0.0000	0.9853	0.0174	1.7685
0.1000	0.9824	0.0225	2.2945
0.2000	0.9695	0.0348	3.5867
0.3000	0.9453	0.0436	4.6169
0.4000	0.9077	0.0450	4.9519
0.5000	0.8611	0.0476	5.5254
0.6000	0.7986	0.0545	6.8254
0.7000	0.7200	0.0646	8.9760
0.8000	0.6182	0.0789	12.7604
0.9000	0.4661	0.1070	22.9528
1.0000	0.0782	0.1184	151.3348

FROM SPEC. # 1.00TO SPEC. # 9.00
RIGHT SIDE
POSTERIOR
SLICES USED IN AVERAGE=12.00

XINT	AVG	STDEV	PRCT
0.0000	0.0000	0.0000	0.0000
0.1000	0.1208	0.0648	53.6008
0.2000	0.4587	0.1295	28.2308
0.3000	0.7475	0.0901	12.0465
0.4000	0.9027	0.0524	5.8018
0.5000	0.9776	0.0250	2.5585
0.6000	0.9822	0.0186	1.8953
0.7000	0.9194	0.0382	4.1509
0.8000	0.7868	0.0679	8.6062
0.9000	0.5439	0.1324	24.3376
1.0000	0.0808	0.1293	159.9669

VERTICALLY DEPENDENT MODE AT T4. REGION (LEVEL -0.5 TO 3.0)

TABLE 3

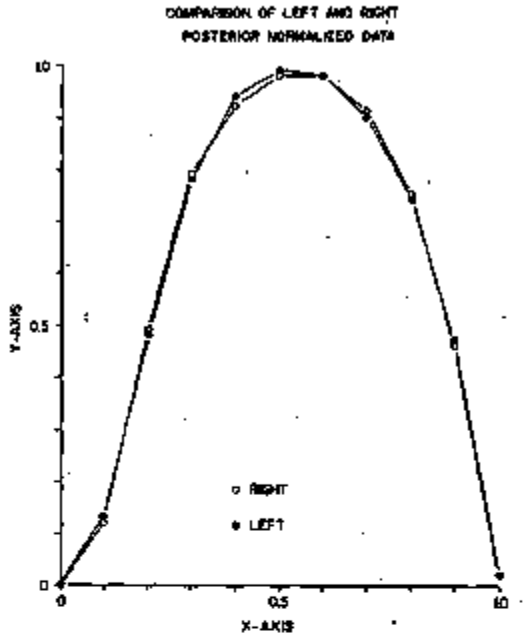

Figure 25

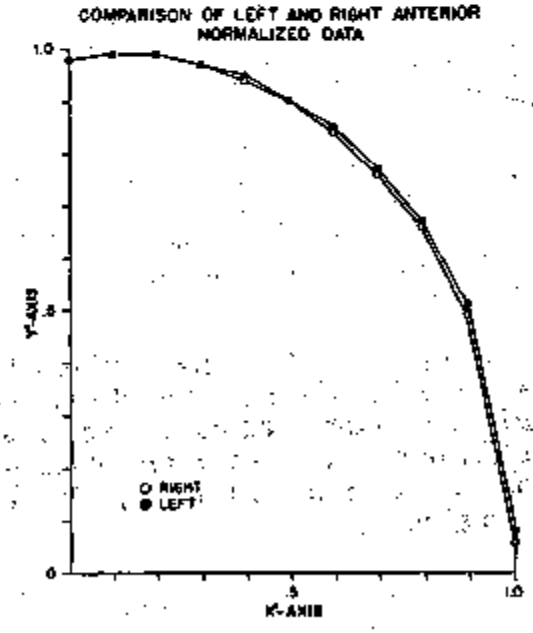

Figure 26

3.2 RADIOGRAPHIC DATA

One hundred radiographs were read and measured. Eighty of them were chosen from males and twenty from females, since comparison between the male and female chest cavity regarding the shape as well as the size was considered useful. All radiographs were obtained from outpatients of the Cleveland Clinic and were diagnosed "no findings" as far as the thorax was concerned. Their ages ranged between 40 and 55.

Figures 27 and 28 show the front and side view radiographs and the measuring points used. Appendix B gives the details of the measuring method. Approximately 80 measurements are made from each set of radiographs. Some of the data pertains to the location of the outside surface of the heart.

Several assumptions were made relative to the radiograph measurements. These assumptions were necessary to solve the problem while not compromising the results.

1. A magnification effect of 10% was assumed at all portions of the radiographs. Theoretically, it varies according to location on the body relative to the film.

2. The chest cavity is assumed symmetric on a postero-anterior radiograph. The chest is not perfectly symmetrical, as is usual in other structures of the living body. If all vertebrae clearly appear on a radiograph, a midline can be pointed out without difficulty. Very often, however, some of the thoracic vertebrae, particularly those overlapped with the heart silhouette, are not shown clearly. Therefore, a midline was obtained, not anatomically, but by dividing the width of the chest cavity by two.

3. All bones are covered with relatively radiotransparent, soft tissues. On radiographic measurements, dimensions are obtained as distances between two radiopaque bony structures. However, the mold data yields smaller inside dimensions due to the thickness of these tissues.

4. It was assumed that all patients held a deep inspiration and were standing perpendicular to the floor when the radiographs were made. This is usually the instruction given to the patient. Level of the diaphragmatic dome changes depending upon respiratory phase, while configuration of the chest changes depending upon posture. This again accounts for differences between cadavers and living patients.

At each level (where a level represents 10% of the distance between the two reference points), the average value and standard deviation was calculated. Also the standard deviation, expressed as a percent of the average, is shown. Tables 4 and 5 summarize this data for males and females, respectively. Distance between the two reference points was 16.57 ± 1.31 cm for males, and 15.77 ± .73 cm for females.

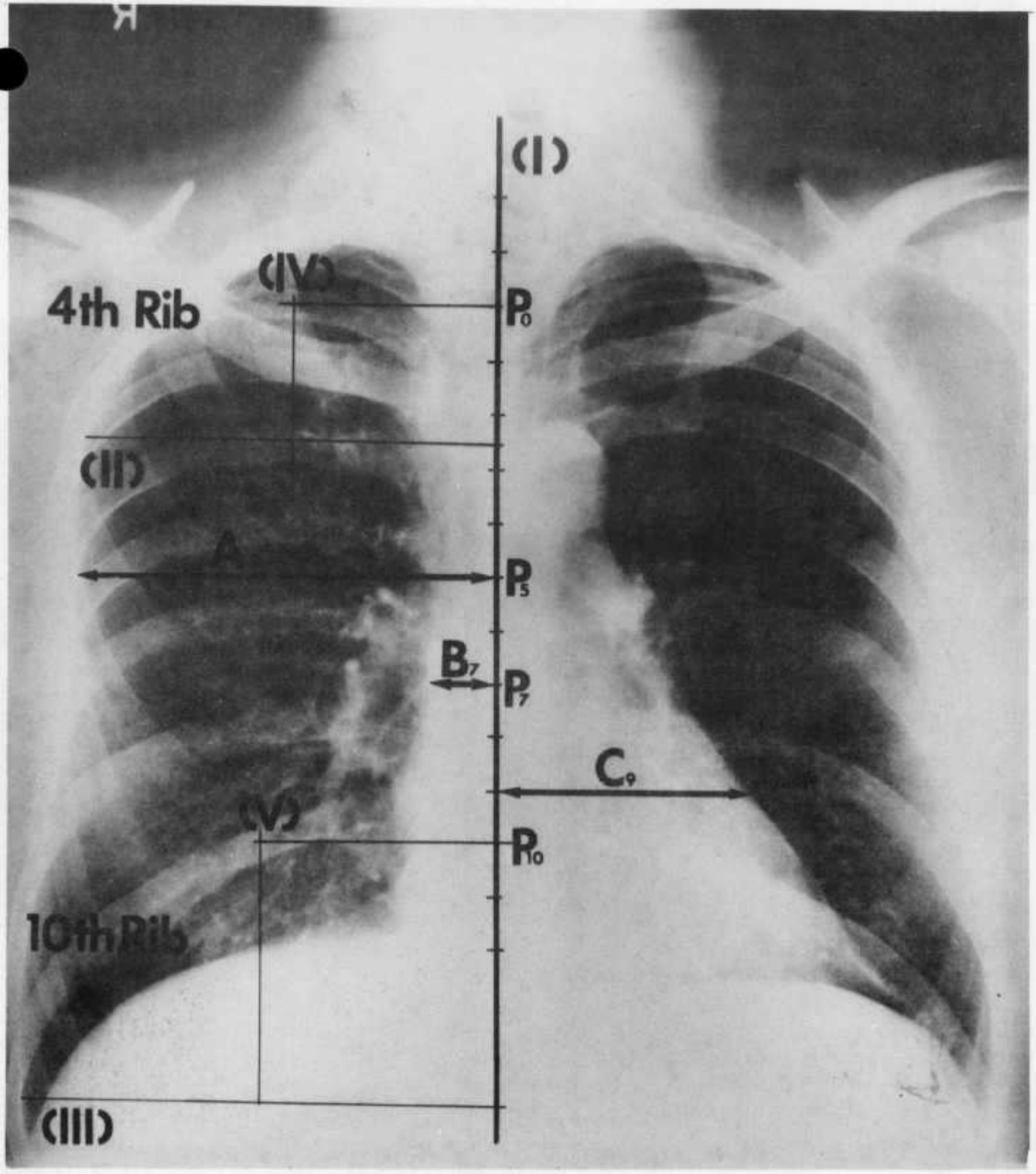

Figure 27

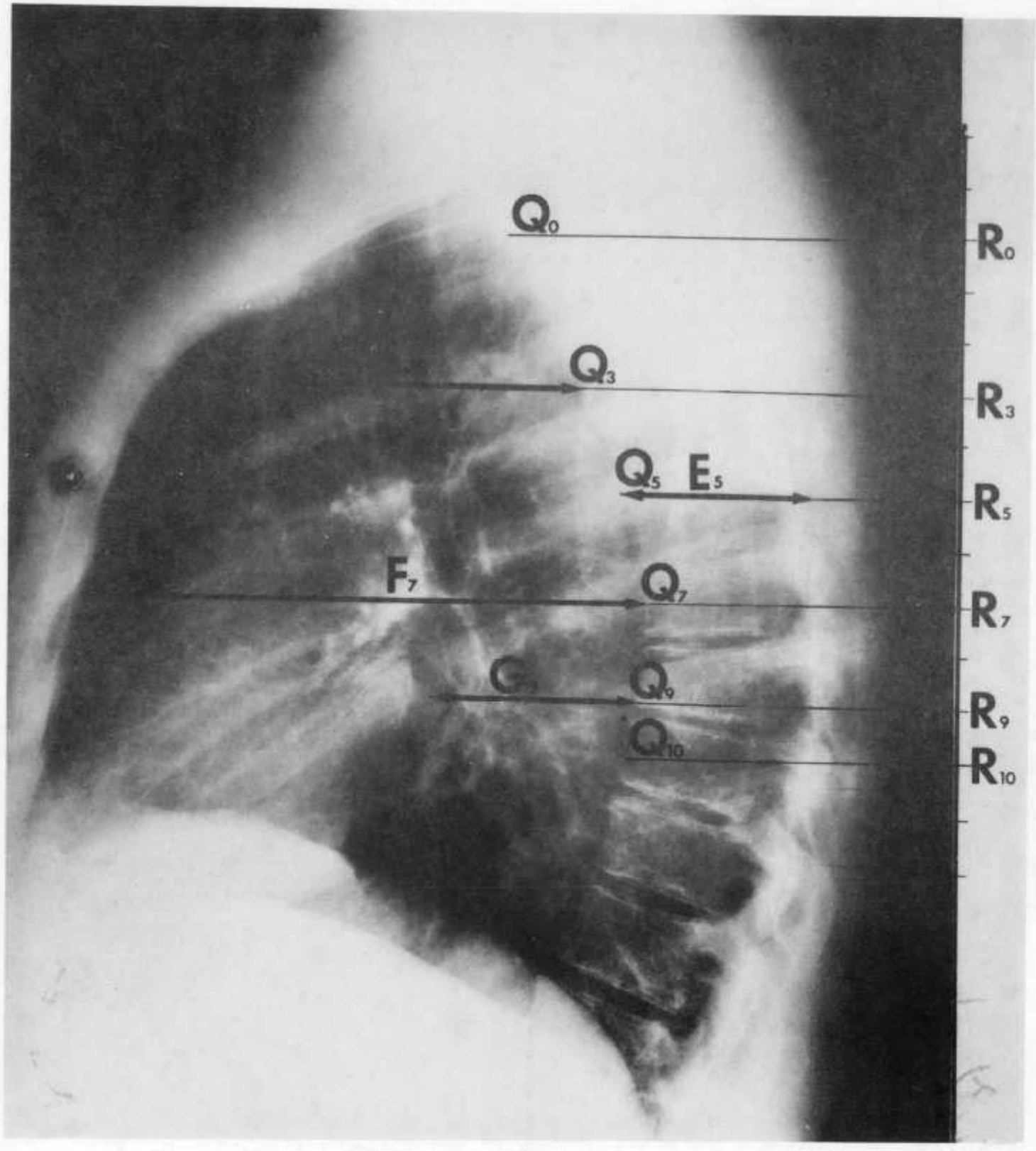

Figure 28

TABLE 4

SUMMARY OF MALE X-RAY DATA

Level	Normalizing Parameter: B			C			A		
	Avg.	σ	$\frac{\sigma}{\text{Avg.}} \times 100$	Avg.	σ	$\frac{\sigma}{\text{Avg.}} \times 100$	Avg.	σ	$\frac{\sigma}{\text{Avg.}} \times 100$
-2	4.74	0.69	14.7	1.03	0.68	66.5	1.80	0.00	0.0
-1	7.14	1.42	19.9	4.91	2.62	53.4	3.36	1.39	41.5
0 Ref	9.18	1.02	11.1	7.84	2.11	26.9	4.70	0.79	16.9
1	10.52	0.88	8.3	9.79	1.81	18.5	4.97	0.72	14.4
2	11.26	0.84	7.5	10.97	1.61	14.7	5.15	0.64	12.3
3	11.70	0.80	6.8	11.84	1.62	13.7	5.28	0.60	11.3
4	12.13	0.77	6.3	12.47	1.74	13.9	5.41	0.59	11.0
5	12.38	0.78	6.3	12.87	1.83	14.2	5.53	0.61	11.1
6	12.63	0.83	6.6	13.13	1.91	14.6	5.65	0.63	11.1
7	12.86	0.83	6.5	13.23	2.02	15.3	5.77	0.63	11.0
8	13.08	0.89	6.8	13.22	2.11	15.9	5.89	0.65	11.0
9	13.23	1.04	7.9	13.07	2.13	16.3	5.99	0.68	11.4
10 Ref	13.65	0.95	7.0	12.85	1.98	15.4	6.04	0.70	11.5
11	13.91	0.83	6.0	12.48	1.99	16.0	6.12	0.69	1.3
12	14.05	.87	6.2	12.12	1.90	15.7	6.19	0.79	12.8

TABLE 5

SUMMARY OF FEMALE X-RAY DATA

Level	Normalizing Parameter B			Normalizing Parameter C			Normalizing Parameter A		
	Avg.	σ	$\frac{\sigma}{\text{Avg.}} \times 100$	Avg.	σ	$\frac{\sigma}{\text{Avg.}} \times 100$	Avg.	σ	$\frac{\sigma}{\text{Avg.}} \times 100$
-2	3.92	0.45	11.4	0.45	0.00	0.0			
-1	6.50	1.62	15.7	2.97	1.74	58.4	1.79	0.66	36.7
0 Ref	8.52	0.83	9.7	6.32	1.80	28.4	3.31	0.48	14.6
1	9.71	0.73	7.5	8.51	1.28	15.0	3.78	0.40	10.6
2	10.33	0.73	7.0	9.63	1.33	13.8	4.12	0.44	10.7
3	10.61	0.73	6.9	10.31	1.50	14.6	4.37	0.45	10.4
4	11.00	0.75	6.9	10.91	1.48	13.5	4.58	0.46	10.0
5	11.12	0.75	6.8	11.11	1.52	13.7	4.76	0.49	10.3
6	11.22	0.79	7.1	11.13	1.44	12.9	5.00	0.51	10.3
7	11.34	0.82	7.2	11.07	1.51	13.6	5.18	0.59	11.3
8	11.45	0.89	7.7	10.86	1.53	14.1	5.28	0.64	12.1
9	11.51	0.87	7.6	10.71	1.64	15.4	5.36	0.61	11.5
10 Ref	11.58	0.87	7.5	10.16	1.65	16.2	5.42	0.62	11.4
11	11.76	1.08	9.2	9.52	0.97	10.2	5.36	0.66	12.3
12	12.13	0.70	5.8	8.69	0.28	3.2	5.57	0.59	10.6

3.3 INTEGRATION OF SHAPE MODEL AND RADIOGRAM DATA

Applying the vertically dependent model (summarized in Tables 1-3) to the X-ray data results in the statistical chest size distributions shown in Figures 29-32. These figures are to scale and represent the average X-ray parameters (plus and minus two standard deviations) for the upper, middle, and lower thorax regions. Hence, the inner and outer two dotted lines include 95% of the male adult population. Also shown are the percent values for that portion of the population smaller than the indicated curve. We anticipate that meaningful external design constraints for an artificial heart can be determined when these curves are combined with the relative location of vital soft structure.

Figure 32 shows the male thorax size distribution superimposed on the cross section of the prototype ERDA heart, at approximately the T6 region in the chest. The actual orientation and vascular connection are described later in the report, but this figure indicates the relative sizes involved.

In the case of the female thorax, a model based on two molds was obtained for levels -3 to 13. Though based on only two molds, horizontal variability was considerably less than the individual vertical variability of each mold. Model data for levels 0, 5, and 10 are shown in Tables 6-8. This model data was then combined with the X-ray data from 20 normal female radiograms (Table 5). These distributions, shown in Figures 33, 34 and 35, though based on a limited amount of data, can be compared with male distributions derived earlier, at the same levels. Note that different shapes for both left and right sides were allowed for the female model. A comparison of the male and female distributions shows considerable differences (Figures 36 and 37). Implantation of the ERDA heart within the average female chest may be more difficult than in the larger male chest. More female X-ray data must be obtained to verify this conclusively.

Patients with some form of heart disease (valvular replacement) demonstrated larger thoraxes as shown in Figures 38 and 39. These are also shown later along with pericardium information.

Validation and verification of the chest wall data is shown in Appendix C.

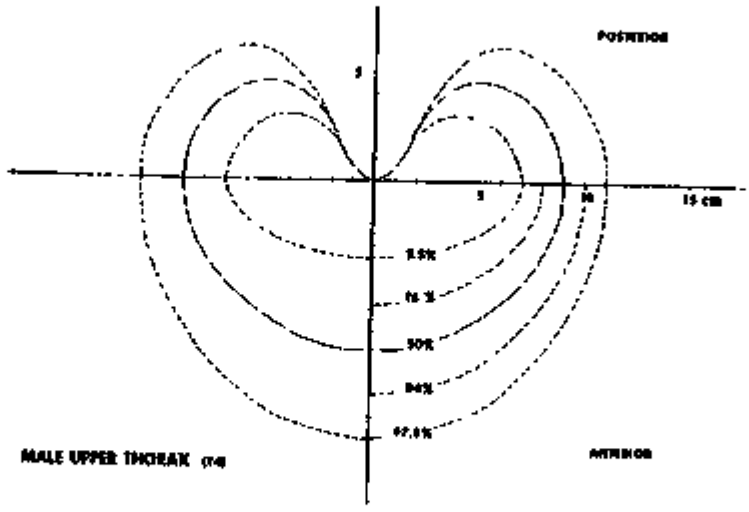

Figure 29

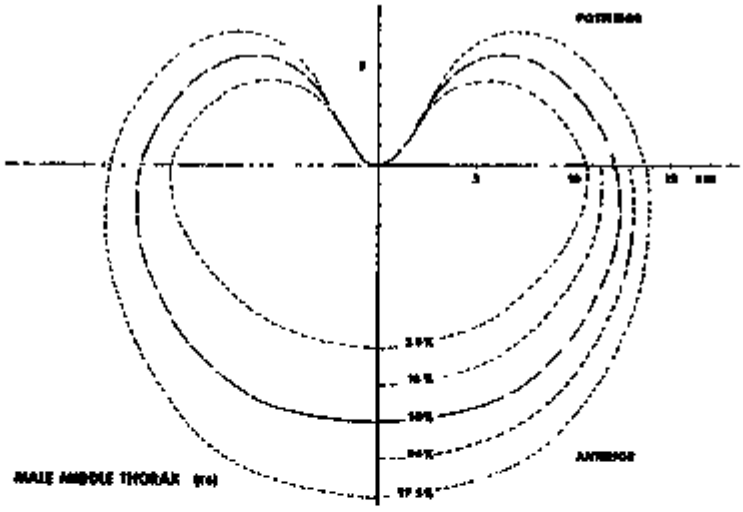

Figure 30

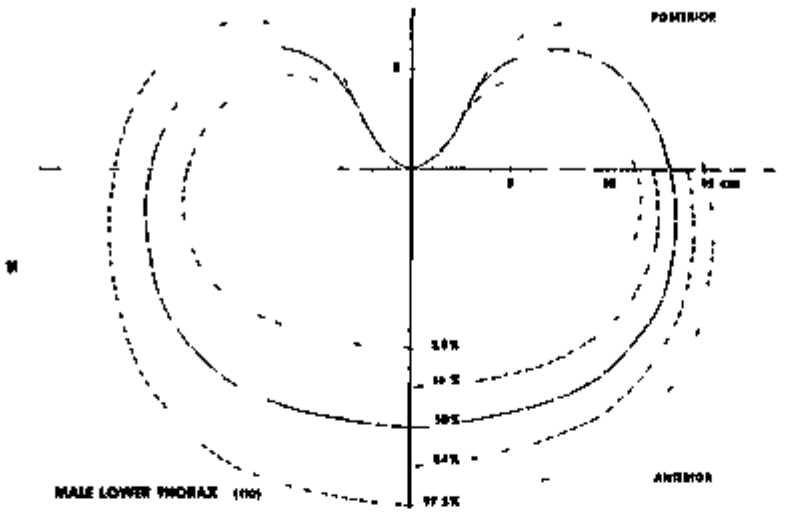

Figure 31

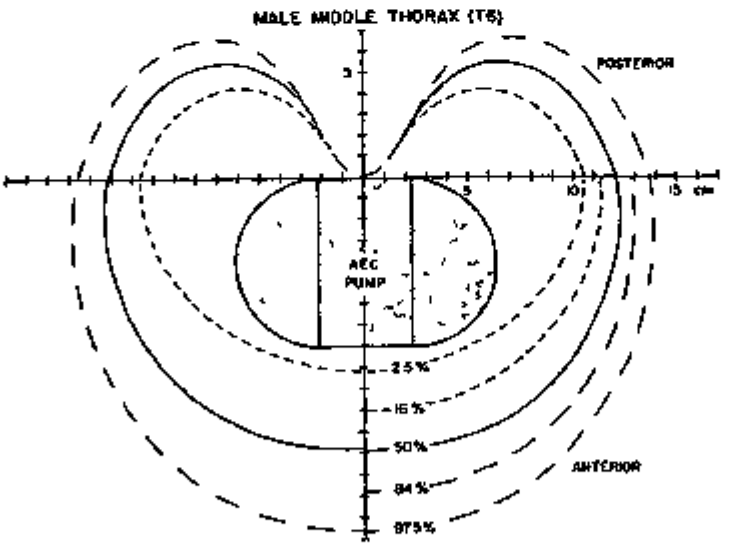

Figure 32

FROM SPEC. # 1.00TO SPEC. # 2.00
LEFT SIDE
ANTERIOR
 # SLICES USED IN AVERAGE= 2.00

XINT	AVG	STDEV	PRCT
0.0000	0.9944	0.0079	0.7901
0.1000	0.9930	0.0095	0.9567
0.2000	0.9827	0.0176	1.7915
0.3000	0.9637	0.0165	1.7079
0.4000	0.9347	0.0044	0.4710
0.5000	0.8898	0.0154	1.7325
0.6000	0.8357	0.0172	2.0589
0.7000	0.7703	0.0144	1.8753
0.8000	0.6851	0.0277	4.0391
0.9000	0.5523	0.0924	16.7224
1.0000	0.1379	0.1951	141.4214

FROM SPEC. # 1.00TO SPEC. # 2.00
LEFT SIDE
POSTERIOR
 # SLICES USED IN AVERAGE= 2.00

XINT	AVG	STDEV	PRCT
0.0000	0.0000	0.0000	0.0000
0.1000	0.1359	0.0017	1.2478
0.2000	0.4799	0.0365	7.6054
0.3000	0.8004	0.0311	3.8847
0.4000	0.9537	0.0063	0.6574
0.5000	0.9903	0.0031	0.3123
0.6000	0.9725	0.0325	3.3462
0.7000	0.8949	0.0667	7.4517
0.8000	0.7682	0.0628	8.1733
0.9000	0.5169	0.0521	10.0766
1.0000	0.0000	0.0000	0.0000

FROM SPEC. # 1.00TO SPEC. # 2.00
RIGHT SIDE
ANTERIOR
 # SLICES USED IN AVERAGE= 2.00

XINT	AVG	STDEV	PRCT
0.0000	1.0000	0.0000	0.0000
0.1000	0.9972	0.0060	0.6063
0.2000	0.9844	0.0039	0.3984
0.3000	0.9637	0.0032	0.3354
0.4000	0.9375	0.0121	1.2892
0.5000	0.9045	0.0207	2.2846
0.6000	0.8663	0.0216	2.4976
0.7000	0.8024	0.0488	6.0757
0.8000	0.7300	0.0903	12.3747
0.9000	0.6421	0.1508	23.4796
1.0000	0.1167	0.1650	141.4214

FROM SPEC. # 1.00TO SPEC. # 2.00
RIGHT SIDE
POSTERIOR
 # SLICES USED IN AVERAGE= 2.00

XINT	AVG	STDEV	PRCT
0.0000	0.0000	0.0000	0.0000
0.1000	0.1031	0.0198	19.2102
0.2000	0.4826	0.0507	10.5008
0.3000	0.8023	0.0641	7.9934
0.4000	0.9403	0.0199	2.1173
0.5000	1.0008	0.0012	0.1185
0.6000	0.9886	0.0043	0.4309
0.7000	0.9219	0.0109	1.1850
0.8000	0.8065	0.0046	0.5714
0.9000	0.5983	0.0440	7.3609
1.0000	0.1000	0.1414	141.4214

FEMALE VERTICALLY DEPENDENT MODEL (LEVEL -3.0 TO 1.0)

TABLE 6

FROM SPEC. # 1.00TO SPEC. # 2.00
LEFT SIDE
ANTERIOR
SLICES USED IN AVERAGE= 2.00

XINT	AVG	STDEV	PRCT
0.0000	0.9646	0.0125	1.2974
0.1000	0.9843	0.0001	0.0097
0.2000	1.0011	0.0011	0.1054
0.3000	0.9900	0.0060	0.6071
0.4000	0.9580	0.0073	0.7608
0.5000	0.9139	0.0091	0.9945
0.6000	0.8599	0.0280	3.2542
0.7000	0.7904	0.0548	6.9388
0.8000	0.6763	0.1103	16.3139
0.9000	0.4988	0.1997	40.0438
1.0000	0.2124	0.1752	82.4958

FROM SPEC. # 1.00TO SPEC. # 2.00
LEFT SIDE
POSTERIOR
SLICES USED IN AVERAGE= 2.00

XINT	AVG	STDEV	PRCT
0.0000	0.0000	0.0000	0.0000
0.1000	0.1703	0.0015	0.8964
0.2000	0.6651	0.0198	2.9831
0.3000	0.8923	0.0000	0.0052
0.4000	0.9850	0.0073	0.7395
0.5000	0.9955	0.0132	1.3238
0.6000	0.9320	0.0544	5.8362
0.7000	0.8145	0.0690	8.4712
0.8000	0.6230	0.0402	6.4551
0.9000	0.3148	0.1026	32.6012
1.0000	0.0000	0.0000	0.0000

FROM SPEC. # 1.00TO SPEC. # 2.00
RIGHT SIDE
ANTERIOR
SLICES USED IN AVERAGE= 2.00

XINT	AVG	STDEV	PRCT
0.0000	0.9572	0.0062	0.6433
0.1000	0.9832	0.0139	1.4137
0.2000	0.9960	0.0044	0.4383
0.3000	0.9895	0.0093	0.9402
0.4000	0.9606	0.0013	0.1394
0.5000	0.9294	0.0026	0.2745
0.6000	0.8853	0.0167	1.8850
0.7000	0.8185	0.0358	4.3694
0.8000	0.7386	0.0656	8.8755
0.9000	0.5812	0.1438	24.7431
1.0000	0.2539	0.2257	88.8747

FROM SPEC. # 1.00TO SPEC. # 2.00
RIGHT SIDE
POSTERIOR
SLICES USED IN AVERAGE= 2.00

XINT	AVG	STDEV	PRCT
0.0000	0.0000	0.0000	0.0000
0.1000	0.1788	0.0345	19.3105
0.2000	0.7796	0.0269	3.4519
0.3000	0.9281	0.0007	0.0737
0.4000	0.9871	0.0053	0.5341
0.5000	0.9838	0.0101	1.0261
0.6000	0.9320	0.0127	1.3592
0.7000	0.8300	0.0229	2.7552
0.8000	0.6332	0.0174	2.7422
0.9000	0.2879	0.0450	15.6316
1.0000	0.0000	0.0000	0.0000

FEMALE VERTICALLY DEPENDENT MODEL (LEVEL 3.5 TO 6.5)

TABLE 7

FROM SPEC. # 1.00TO SPEC. # 2.00
LEFT SIDE
ANTERIOR
 # SLICES USED IN AVERAGE= 2.00

XINT	AVG	STDEV	PRCT
0.0000	0.9713	0.0055	0.5625
0.1000	0.9939	0.0013	0.1325
0.2000	0.9985	0.0030	0.3001
0.3000	0.9909	0.0129	1.2996
0.4000	0.9825	0.0149	1.5131
0.5000	0.9514	0.0118	1.2353
0.6000	0.9019	0.0232	2.5729
0.7000	0.8414	0.0153	1.8205
0.8000	0.7475	0.0191	2.5549
0.9000	0.6030	0.0059	0.9844
1.0000	0.0407	0.0575	141.4214

FROM SPEC. # 1.00TO SPEC. # 2.00
LEFT SIDE
POSTERIOR
 # SLICES USED IN AVERAGE= 2.00

XINT	AVG	STDEV	PRCT
0.0000	0.0000	0.0000	0.0000
0.1000	0.0848	0.0093	10.9162
0.2000	0.3650	0.1450	39.7239
0.3000	0.8339	0.0118	1.4153
0.4000	0.9510	0.0115	1.2076
0.5000	0.9850	0.0024	0.2398
0.6000	0.9931	0.0000	0.0030
0.7000	0.9113	0.0011	0.1258
0.8000	0.7317	0.0257	3.5180
0.9000	0.4677	0.0189	4.0410
1.0000	0.0000	0.0000	0.0000

FROM SPEC. # 1.00TO SPEC. # 2.00
RIGHT SIDE
ANTERIOR
 # SLICES USED IN AVERAGE= 2.00

XINT	AVG	STDEV	PRCT
0.0000	0.9774	0.0063	0.6399
0.1000	0.9916	0.0124	1.2465
0.2000	0.9960	0.0039	0.3943
0.3000	0.9980	0.0131	1.3187
0.4000	0.9801	0.0068	0.6921
0.5000	0.9530	0.0107	1.1227
0.6000	0.9185	0.0097	1.0600
0.7000	0.8668	0.0101	1.1688
0.8000	0.7812	0.0078	0.9985
0.9000	0.6685	0.0012	0.1738
1.0000	0.2035	0.0307	15.0812

FROM SPEC. # 1.00TO SPEC. # 2.00
RIGHT SIDE
POSTERIOR
 # SLICES USED IN AVERAGE= 2.00

XINT	AVG	STDEV	PRCT
0.0000	0.0000	0.0000	0.0000
0.1000	0.1244	0.0501	40.2937
0.2000	0.6691	0.0432	6.4541
0.3000	0.8770	0.0216	2.4630
0.4000	0.9634	0.0121	1.2573
0.5000	0.9949	0.0007	0.0707
0.6000	0.9790	0.0077	0.7832
0.7000	0.8768	0.0384	4.3772
0.8000	0.6941	0.0879	12.6709
0.9000	0.4378	0.0794	18.1317
1.0000	0.0000	0.0000	0.0000

FEMALE VERTICALLY DEPENDENT MODEL (LEVEL 9.0 TO 13.0)

TABLE 8 38

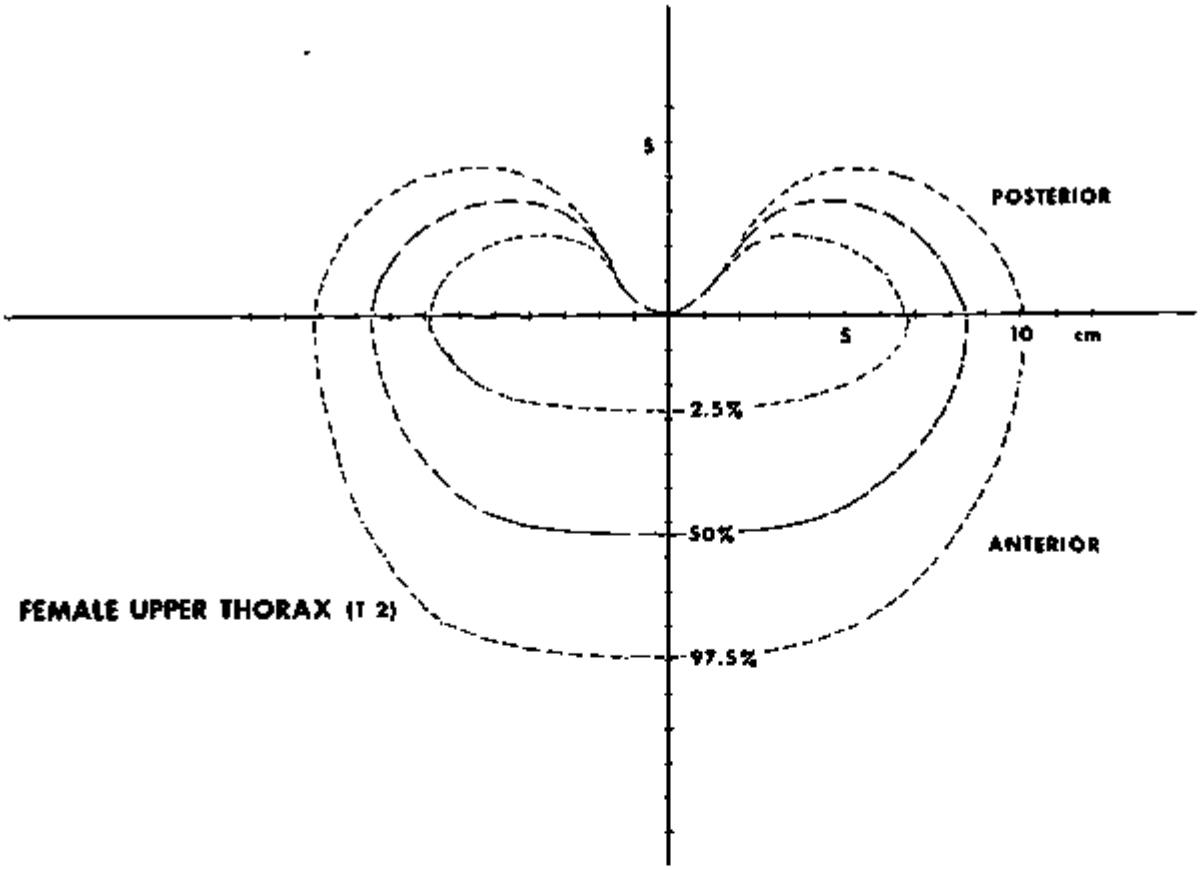

Figure 33

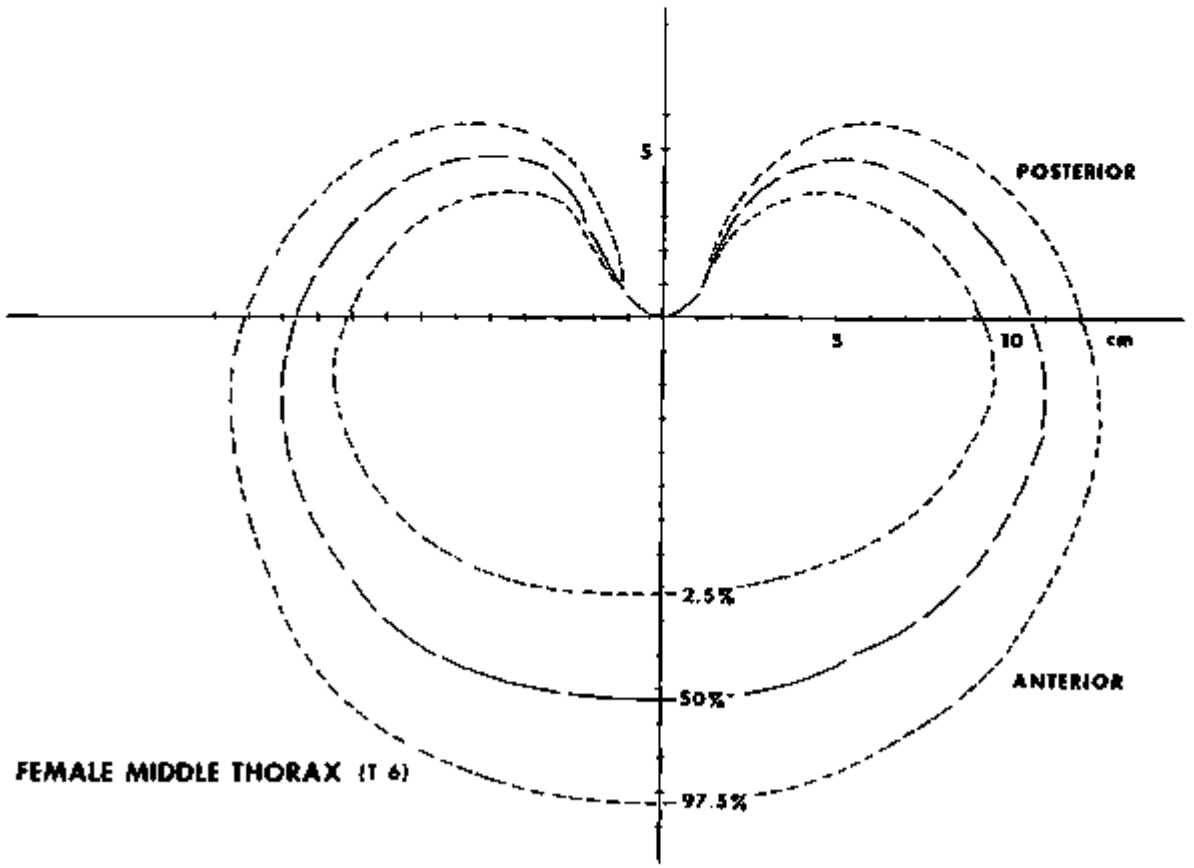

Figure 34

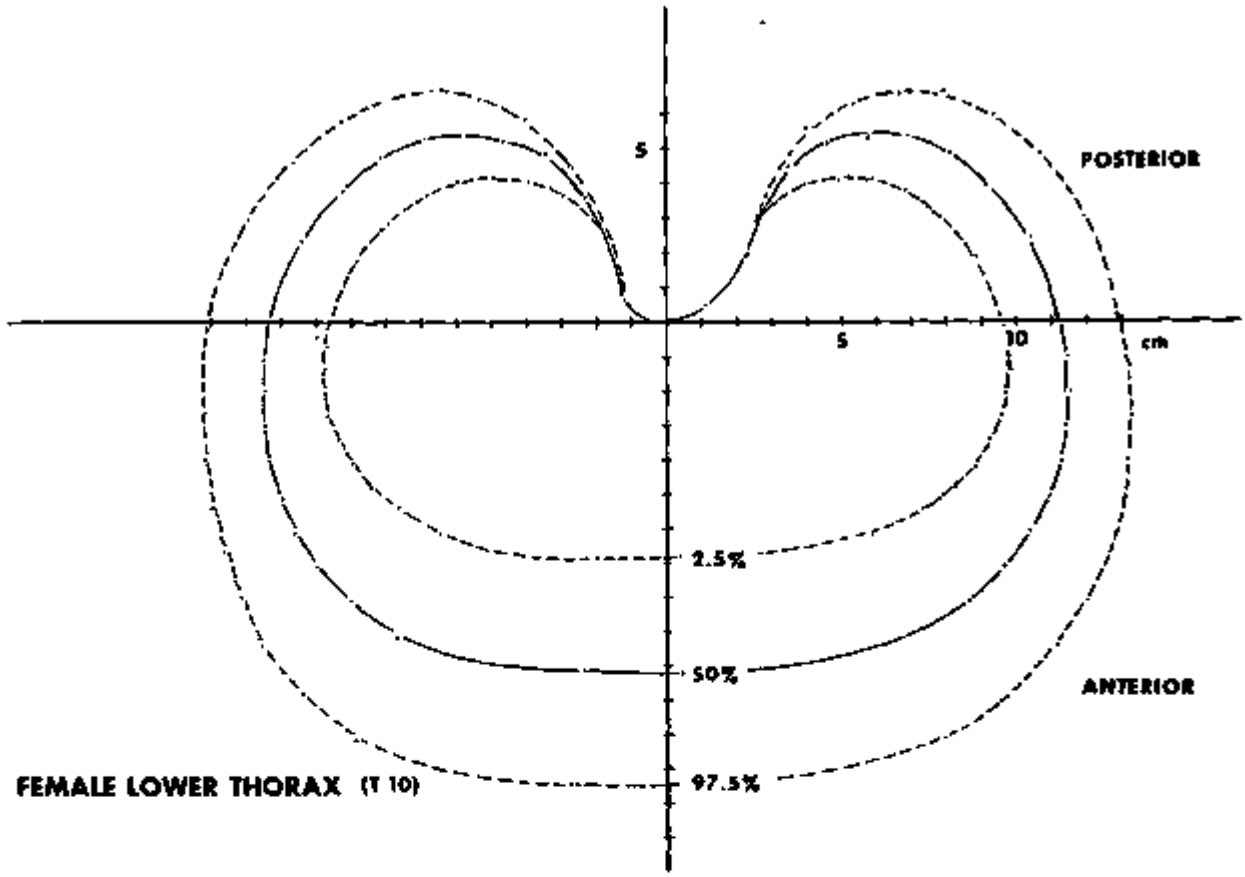

Figure 35

COMPARISON OF MALE AND FEMALE AVERAGE CHEST SIZE (MIDDLE THORAX, T6)

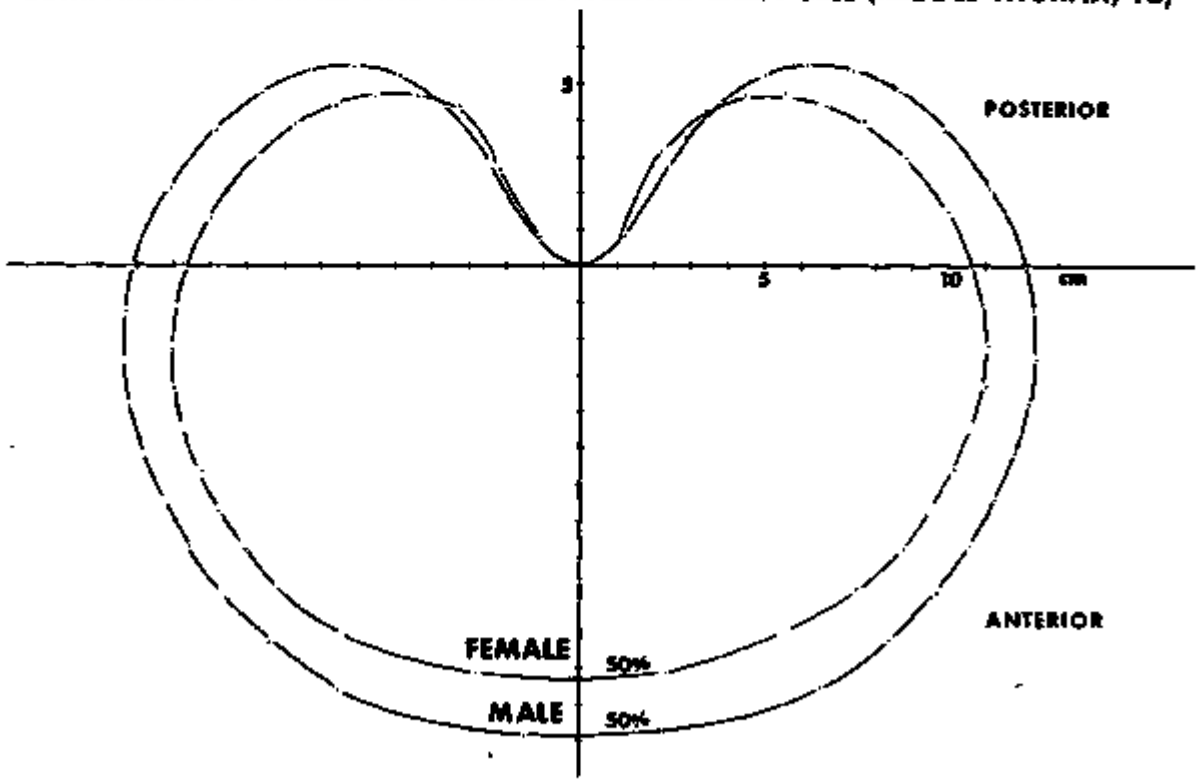

Figure 36

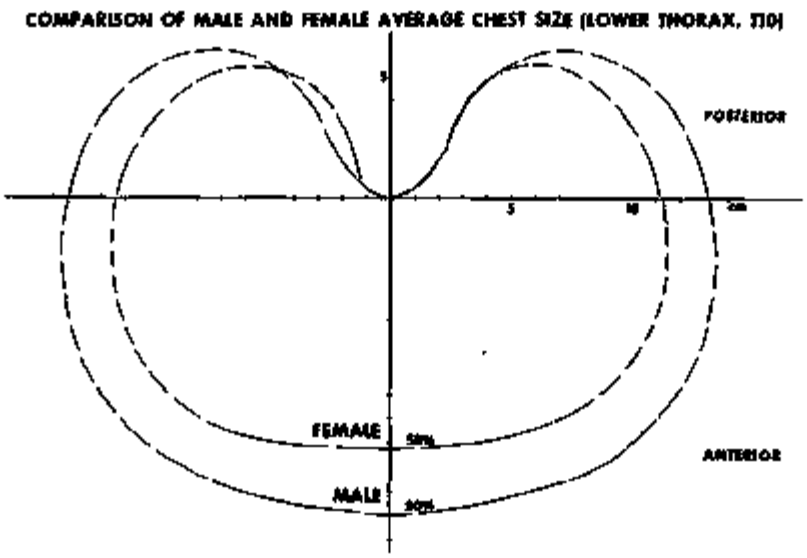

Figure 37

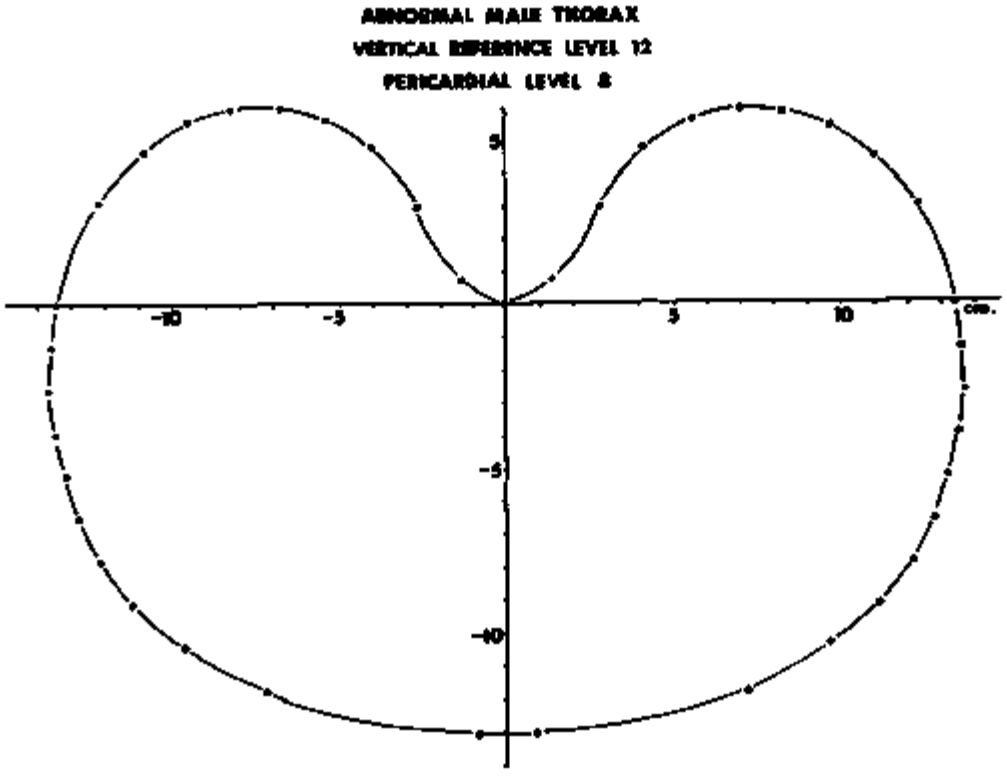

Figure 38

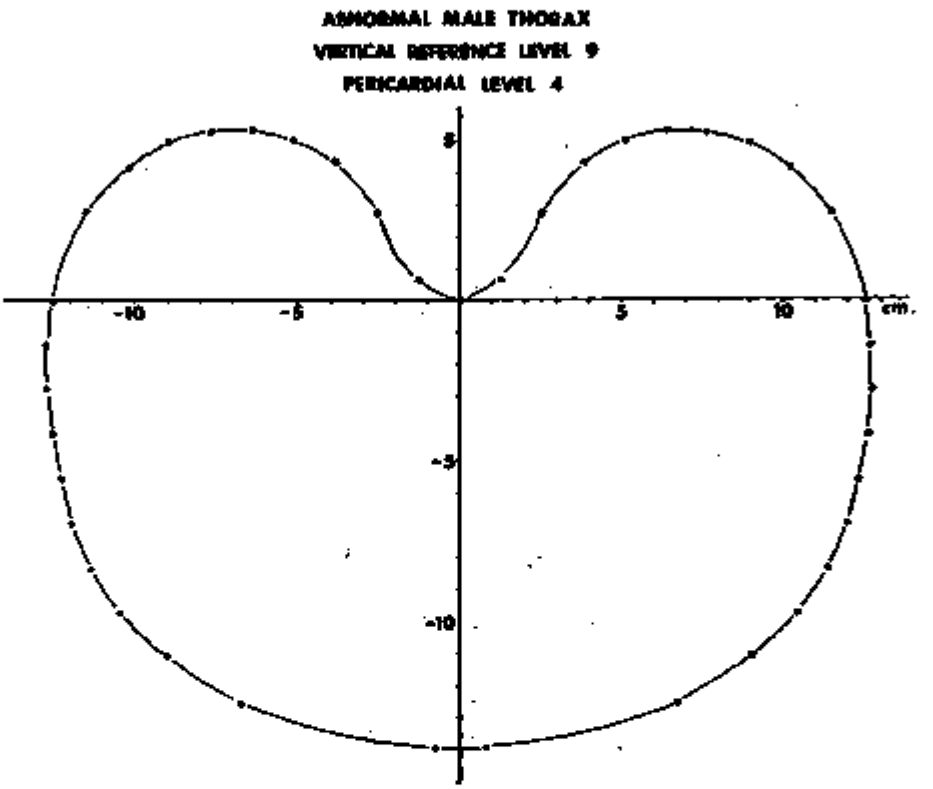
ABNORMAL MALE THORAX
VERTICAL REFERENCE LEVEL 9
PERICARDIAL LEVEL 4
5
-10
-5
5
10
cm.
-5
-10

Figure 39

4.0 DEFINITION OF PERICARDIUM

4.1 INTRODUCTION

The pericardium, though roughly ellipsoidal in shape, is unsymmetrical and with a major axis that can vary from one person to the next. As described in Section 2.2 (Current Methodology), and shown schematically in Figure 18, the approach finally selected combined shape information with two dimensional data taken from lateral and PA radiograms. Without the shape model, standard X-ray data could never be reconstructed into a three dimensional map of the pericardium and its orientation within the thorax.

The shape model, as the name implies, is a set of average dimensional data describing the pericardium after size variations have been normalized out. Consequently, data (from published sources for example) can be utilized even though the actual dimensions are unknown. Efforts to relate normalized pericardial shape to vertical levels within the overall chest coordinate system proved fruitless (44). Conclusions from these results indicated that heart height and location within the thorax did not correlate with $V_{CH\ MAX}$. The method finally chosen followed directly from this conclusion and is pictorically presented in Figure 19.

The top of the heart silhouette (cranial side of pulmonary artery) is considered as 0% and bottom of the heart as 100%, with the distance between these two points measured at V_{HMAX} (maximum heart height). A "level" is defined ; ; 10% of V_{HMAX}. The heart outline, then, has its own normalized vertical coordinate system and is referenced to the chest coordinate system by measurement V_R. Development of a pericardium shape model proceeded by searching for similarities in "shape" at identical percent distances between the top and bottom of the heart.

As with vertical normalization, it was hoped that within a given transverse section of the thorax there could be a direct correlation between the chest wall outline and the pericardial outline (i.e. a constant ratio of chest depth to pericardium depth). A cursory examination of even normal data showed that heart outline was quite independent of the chest in which it was located. Subsequently, the following referencing method was chosen and will be used in generating the pericardial shape model using data from anatomical texts, published tomographic data and actual cadavers.

Shown in Figure 40 is a transverse section at a known normalized distance between the top and bottom of the heart. A coordinate system for the pericardium with respect to the chest (X, Y) is generated by dimensions X_R and Y_R, both observable in an X-ray film (X_R = D, Y_R = F). Also observable are the extreme points of the sac, defining variables Xp_{max} and Yp_{max} (Xp_{max} = D + E, Yp_{max} = F - G). However, these points have no "tags" on them in normal radiograms and hence must be defined from the shape model. This information is provided by the ratios:

Xa/Xp_{max}
Xb/Xp_{max}
Ya/Yp_{max}
Yb/Yp_{max}

and constitutes the first component of the "shape" model.

In addition, the shape of the pericardium over each of the four regions defined by four secondary coordinate systems is normalized and constitutes the second component of the pericardial "shape" model. Each of these secondary coordinate systems is shown in Figure 40 and labeled by the section of the sac that it defines. For example, 1 LA outlines the left anterior portion of the right ventricle and is defined by a coordinate system originating at Xa/Xp_{max}. Additional sections are 2 LP which covers most of the left ventricle or left ventricle or left atrium depending on the vertical level, 3 RA which covers the remainder of the right ventricle not described by 1 LA, and 4 RP which outlines either the right atrium or right ventricle, again depending on the vertical level. Once the "shape" model is finalized, inputting the four observable data points on a radiogram, X_R, Y_R, Xp_{max}, and Yp_{max}, allows the regeneration of the pericardial outline. Hence, a combination of this model with a large array of pericardium data (X_R, Y_R, etc.) from abnormal P-A and lateral radiograms will define the space available for an artificial heart (Figure 11, shown earlier). Note that to locate this average pericardium within the thorax, which has already been defined, correlations have to be determined between thorax normalizing parameters (A, B, and C) and pericardium normalizing parameters (Xp_{max}, Yp_{max}, etc.).

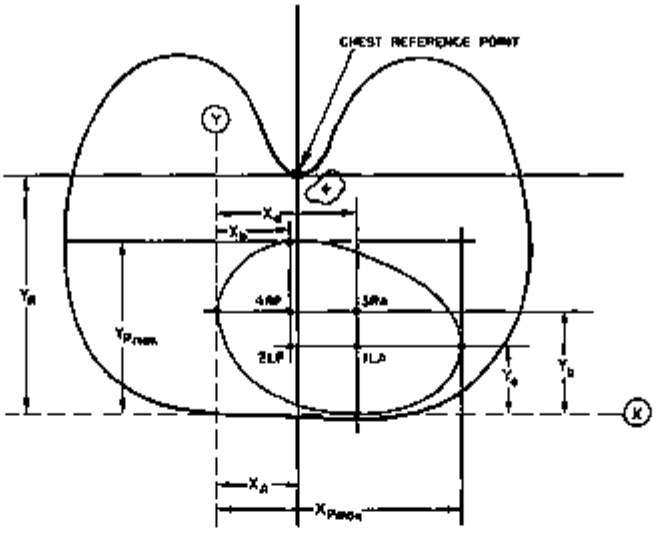

REFERENCING SYSTEM FOR PERICARDIUM MODEL

Figure 40

4.2 PERICARDIAL SHAPE MODEL RESULTS

In this section numerical results for the pericardial shape model will be presented. Sources for these results (Figure 18) include two actual cadavers and five published works based on sliced, frozen cadavers. As described above, there are two components to the shape model; ratio information for locating the secondary axis and shape information for each quadrant of the pericardium.

All the ratio data is included in Table 1 of Appendix D. X_a for example, at Level 3, would just be the product of Xp_{max} and .548. Y_a would equal .492 times Yp_{max}. X_b and Y_b are determined in a similar manner.

The second component, shape data, is included in Tables 2-5 and Figures 1-16 of Appendix D. To generate the perimeter of the left anterior quadrant of the pericardial sac, 1 LA, XINT would vary from 0.0 to $(Xp_{max} - X_a)$, while YINT varies correspondingly from $(Yp_{max} - Y_a)$ to 0.0. At level 3 then, per table 21 in Appendix D, the second data point for 1LA would be:

$$(XINT_2, YINT_2) = [.1\ (Xp_{max} - X_a), .987\ (Yp_{max} - Y_a)] \qquad [1]$$

Because of the minimal number of sources for this shape information (data from Delta scanner has not been incorporated yet), male and female were averaged together.

4.3 PERICARDIUM RADIOGRAPHIC DATA

Still not presented for the pericardium definition are the values for Xp_{max} and Yp_{max} necessary to complete the calculations in Equation 1 above. Additional necessary data include the variables Y_Q, Y_R, A, B, and C. These "absolute" measurements are summarized in Tables 9 and 10 and represent data averaged from patients with some form of heart disease. Table 9 includes both male and female results, while Table 10 is male data only. Note that some actual cadaver data has also been included. NDAPTS refers to the number of data points.

4.4 INTEGRATION OF PERICARDIAL SHAPE MODEL AND RADIOGRAPHIC DATA

Using Equation 1 above, shape information in Section 4.2 was combined with the dimensional data in 4.3 to proeuce outlines of the pericardium within the human thorax. Some results are displayed in Figures 41 and 42. Variability of the curves in these figures includes only the standard deviations of Xp_{max} and Yp_{max}. Shape model variations were excluded.

However, Xp_{max} and Yp_{max} must be correlated with each other in order to show pericardial variability correctly. That is, a wider heart must also be a deeper heart. If it was found that a wide heart did not correspond to a deep heart, then Figures 41 and 42 would be invalid as a representation of pericardial variability. This was checked using data from X-rays of heart diseased patients and simply plotting Xp_{max} vs. Yp_{max} at pericardial levels

4 and 8. The graphs are shown in Figures 43 and 44. The correlations at both levels are found to be significant. Therefore, a wider heart does tend to be a deeper heart at levels 4 and 8. Thus, the method for determining pericardial variability is correct. In Section 8.0 of this report, pericardial results are displayed in perspective with the other components of the human thorax.

Table 9

Pericardium Radiographic Data

(Male + Female + two cadavers and reflects some form of heart disease)

Pericardial Level	$X_{P_{Max}}$		$Y_{P_{Max}}$		X_R		Y_R		Right B		Left B		C		NDAPTS
	Mean	S.D.	Mean	S.D.	Mean	S.D.	Mean	S.D.	Mean	S.D.	Mean	S.D.	Mean	S.D.	
0	6.11	1.03	.642	.45	-2.35	.65	7.38	1.38	11.56	1.36	11.37	.995	12.07	1.61	26
2	8.77	1.89	9.81	1.20	-3.20	.82	12.69	1.69	11.83	1.04	11.86	1.06	13.30	1.72	27
4	12.32	1.88	11.65	1.48	-4.43	1.15	13.69	1.73	12.29	1.18	12.31	1.31	13.69	1.74	27
6	14.31	1.88	11.45	1.65	-4.63	1.25	13.44	1.72	12.79	1.27	12.94	1.70	13.44	1.72	27
8	13.41	2.09	9.63	1.92	-3.36	1.30	12.75	1.70	13.13	1.29	13.10	1.44	12.75	1.70	27
10	2.14	1.09	.623	.93	+2.66	1.32	11.21	2.04	13.28	1.32	13.34	1.55	11.40	1.95	26

Table 10

Pericardium Radiographic Data

(Male + one cadaver and reflects some form of heart disease)

Pericardial Level	$X_{P_{Max}}$		$Y_{P_{Max}}$		X_R		Y_R		Right B		Left B		C		NDAPTS
	Mean	S.D.	Mean	S.D.	Mean	S.D.	Mean	S.D.	Mean	S.D.	Mean	S.D.	Mean	S.D.	
0	6.37	.91	.66	.43	-2.51	.61	7.46	1.60	11.74	.75	11.71	.86	12.18	1.75	19
2	9.01	1.77	9.70	1.25	-3.34	.87	12.82	1.79	12.23	.82	12.23	.92	13.37	1.79	20
4	12.51	1.79	11.57	1.50	-4.53	1.27	13.81	1.86	12.73	.98	12.75	1.12	13.81	1.86	20
6	14.76	1.61	11.35	1.66	-4.78	1.26	13.60	1.85	13.29	.97	13.24	1.19	13.59	1.86	20
8	13.97	1.78	9.61	1.79	-3.50	1.2	12.92	1.85	13.64	.96	13.61	1.20	12.92	1.85	20
10	2.45	1.00	.53	.94	+2.38	1.68	11.38	2.25	13.81	.96	13.89	1.24	11.59	2.2	19

MALE PERICARDIAL VARIABILITY AT
PERICARDIAL LEVEL 4

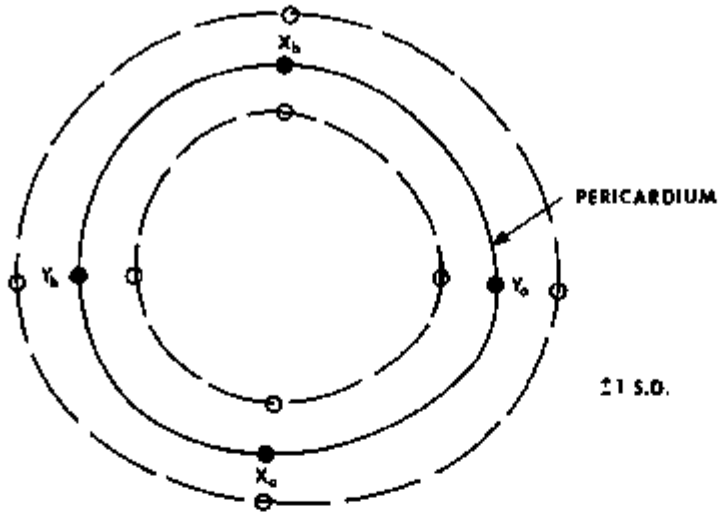

Figure 41

MALE PERICARDIAL VARIABILITY AT
PERICARDIAL LEVEL 8

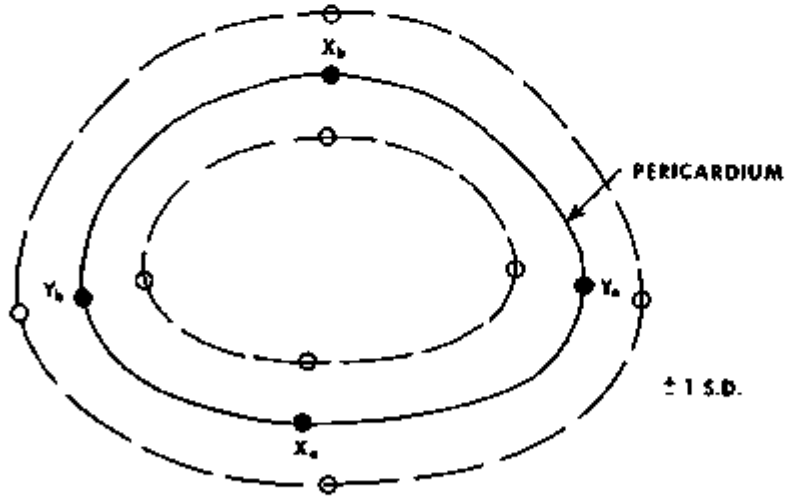

Figure 42

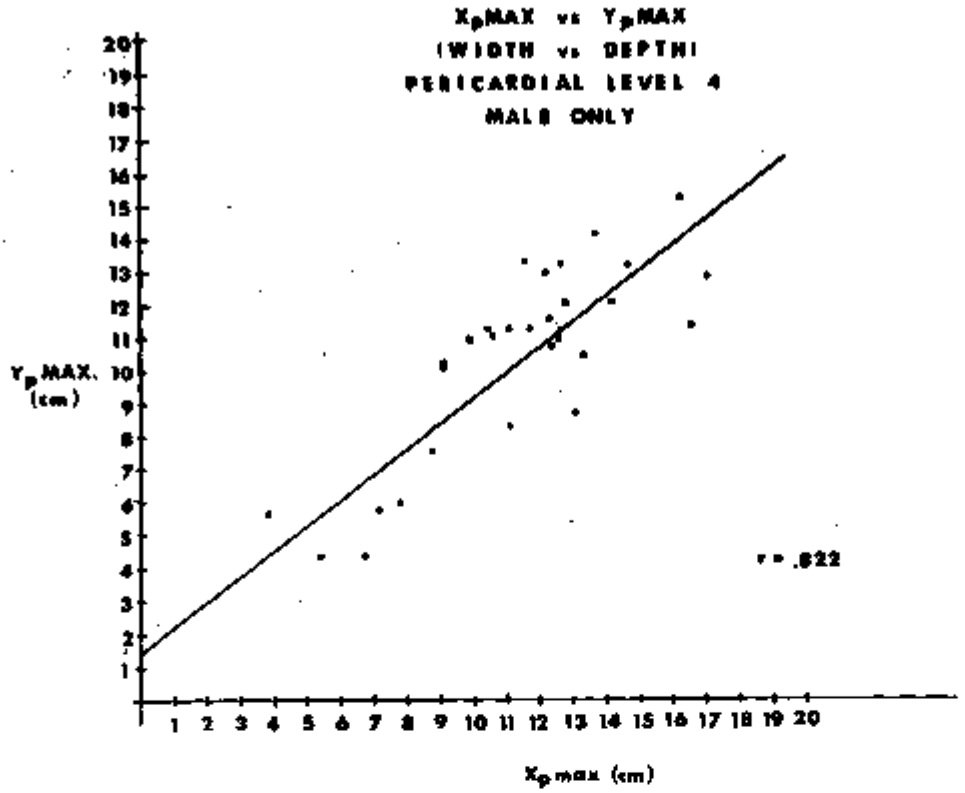

Figure 43

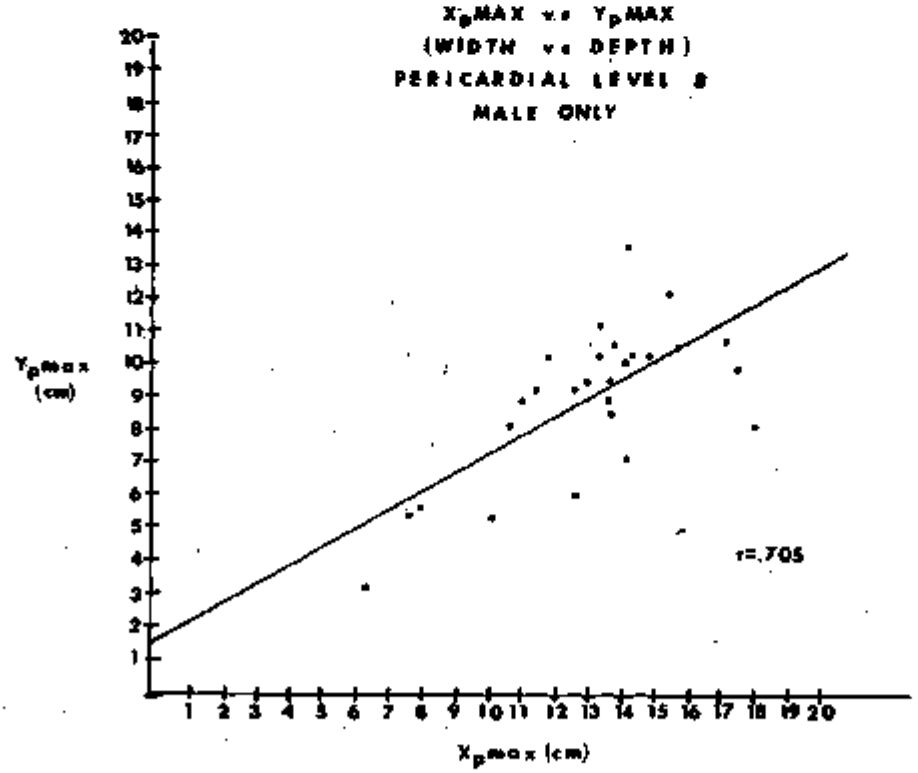

Figure 44

5.0 VASCULAR CONNECTION POINT DEFINITION

Because the anastamosis points for TAH implantations will most likely be just distal to the natural valves, it is extremely important to identify these locations precisely. An overly large artificial heart that extended beyond the boundary imposed by these points and the thoracic wall would obviously compress sensitive venous structures (Figures 2-4, shown earlier). To insure reliability of this data, measurements were taken from different kinds of sources and then compared.

5.1 METHODS AND DATA SOURCES

A general description of data sources and the recorded variables was presented in Section 2.4. Specifically, Figures 18-20 summarize the coordinate systems used along with a breakdown of the data sources. Measurements were gathered from 30 radiograms of adult patients with one or more prosthetic valves, two actual cadavers and five textbooks of frozen cadaver slices. The radiograms and two cadavers provide a source of dimensional data that is correct in an absolute sense (ABS); that is, the absolute value of the numbers are correct. The third source (published sections of cadavers), however, because the photographs have not been scaled, provide only ratio information and will be labeled as non-absolute (NABS) in this report. Referring to Figure 20, a typical absolute measurement would be N_{CHMID}, the measured distance from the mitral valve (center of orifice) to the chest midline.

A typical ratio measurement taken off a NABS source would be X_M/X_{PMAX}, the ratio of the distance from right margin of the pericardium to the mitral valve divided by the total width of the pericardial sac at that level in the thorax.

Ratios were calculated for a number of reasons. Valve measurements referenced to pericardial width for example, hopefully would be independent of size variations and also could be determined from either ABS or NABS type sources. In some cases where the pericardium was not clearly defined, valve distances to chest midline were referenced to thorax wall dimensions; i.e. A_{CHMID}/B, or in the Y direction, Y_M/C. Such ratio measurements were then compared with ABS data, such as the direct distance to chest wall or the actual distance between valves. All of these calculations, using numbers derived from the three main types of data banks, constitute a direct approach for determining vascular connection point locations (see Figure 45).

Because very few radiograms of patients with pulmonary or tricuspid valve replacements are available, a supplementary indirect method was devised to predict their location. An explanation of the method along with results are presented in Appendix E. However, for comparison purposes, some of these results are displayed in Figure 46 (discussed in the text below).

5.2 RESULTS OF DIRECT METHOD

Overall results for ratios referenced to the pericardium from the direct approach are shown in Table 11 for each of the four valves and in all three dimensions. In Table 12, ratio values are shown referenced to the chest wall (dimension B and C). In Figure 46, three of these sets of data are compared

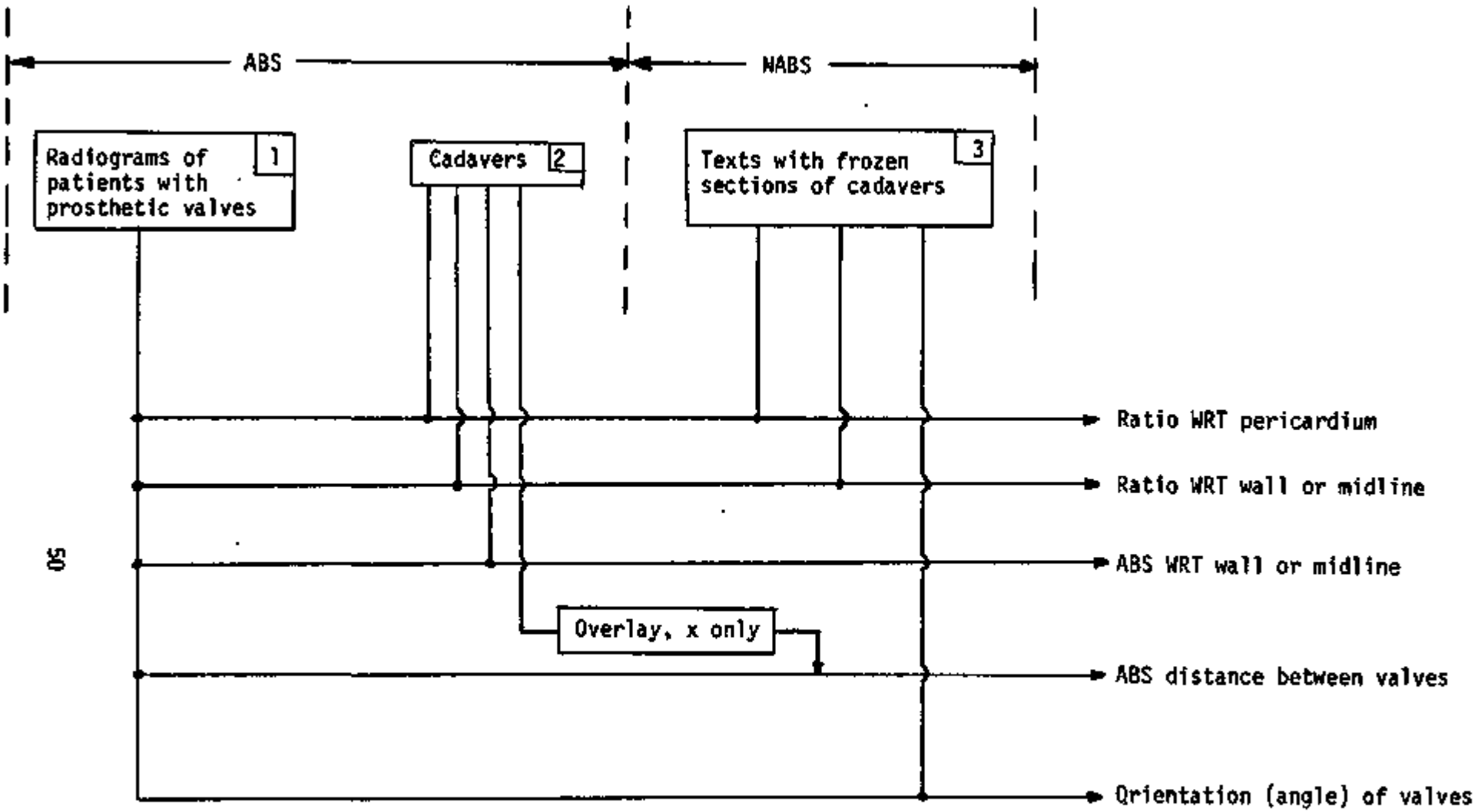

DIRECT APPROACH FOR ESTABLISHING
VASCULAR CONNECTION POINT LOCATION

Figure 45

Table 11

Valve Data Referenced to Pericardium

(Males only)

Pulmonary Valve				
Variables		$\frac{X_P}{X_P MAX}$	$\frac{Y_P}{Y_P MAX}$	$\frac{P_H}{V_H MAX}$
NABS*	MEAN	.689	.335	.291
	S.D.	.087	.061	.041
	NDAPTS	9	5	4

Tricuspid Valve				
Variables		$\frac{X_T}{X_P MAX}$	$\frac{Y_T}{Y_P MAX}$	$\frac{T_H}{V_H MAX}$
NABS	MEAN	.353	.389	.730
	S.D.	.070	.047	.053
	NDAPTS	10	7	5
ABS**	MEAN	.353	.420	.650
	S.D.	---	---	---
	NDAPTS	1	1	1
NABS + ABS	MEAN	.353	.393	.717
	S.D.	.066	.045	.058
	NDAPTS	11	8	6

* NABS = non absolute

** ABS = absolute

Table 11 (continued)

Mitral Valve							
Variables		X_A in cm	$\frac{X_A}{X_P MAX}$	Y_A in cm	$\frac{Y_A}{Y_P MAX}$	A_H in cm	$\frac{A_H}{V_H MAX}$
NABS	MEAN	----	.563	----	.726	----	.554
	S.D.	----	.065	----	.036	----	----
	NDAPTS	----	6	----	5	----	1
ABS	MEAN	8.03	.520	7.03	.593	8.29	.514
	S.D.	1.38	.048	1.33	.084	.094	.057
	NDAPTS	11	11	11	11	11	11
NABS + ABS	MEAN	8.03	.535	7.03	.634	8.29	.518
	S.D.	1.38	.057	1.33	.095	.094	.056
	NDAPTS	11	17	11	16	11	12

Aortic Valve							
Variables		X_A in cm	$\frac{X_A}{X_P MAX}$	Y_A in cm	$\frac{Y_A}{Y_P MAX}$	A_H in cm	$\frac{A_H}{V_H MAX}$
NABS	MEAN	----	.484	----	.457	----	.443
	S.D.	----	.050	----	.080	----	.041
	NDAPTS	----	6	----	7	----	3
ABS	MEAN	6.07	.466	5.12	.443	6.01	.386
	S.D.	1.85	.066	.570	.053	1.07	.069
	NDAPTS	13	13	13	12	13	13
NABS + ABS	MEAN	6.07	.471	5.12	.449	6.01	.397
	S.D.	1.85	.060	.570	.063	1.07	.068
	NDAPTS	13	19	13	19	13	16

Table 12

Valve Data Referenced to Chest

(males only)

Aortic Valve					
Variables		A_{WY} in cm	$\frac{A_{WY}}{C}$	A_{CHMID} in cm	$\frac{A_{CHMID}}{B}$
NABS	MEAN	----	.336	----	.098
	S.D.	----	.019	----	----
	NDAPTS	0	3	0	1
ABS	MEAN	5.12	.367	1.3	.120
	S.D.	.795	.040	1.24	.086
	NDAPTS	13	13	14	13
NABS ABS	MEAN	5.12	.361	1.3	.111
	S.D.	.795	.039	1.24	.081
	NDAPTS	13	16	14	14

Mitral Valve					
Variables		M_{WY} in cm	$\frac{M_{WY}}{C}$	M_{CHMID} in cm	$\frac{M_{CHMID}}{B}$
ABS	MEAN	7.03	.529	2.69	.207
	S.D.	1.33	.073	.452	.043
	NDAPTS	11	13	11	11

Tricuspid Valve		
Variables		T_{CHMID} * in cm
ABS	MEAN	-.333
	S.D.	1.007
	NDAPTS	3

* male and female

in the P-A view only. As would be expected, the scatter for the aortic and mitral valves is considerably smaller than that for the tricuspid and pulmonary valves. More accurate data for the latter two might reduce this dispersion.

Figure 46

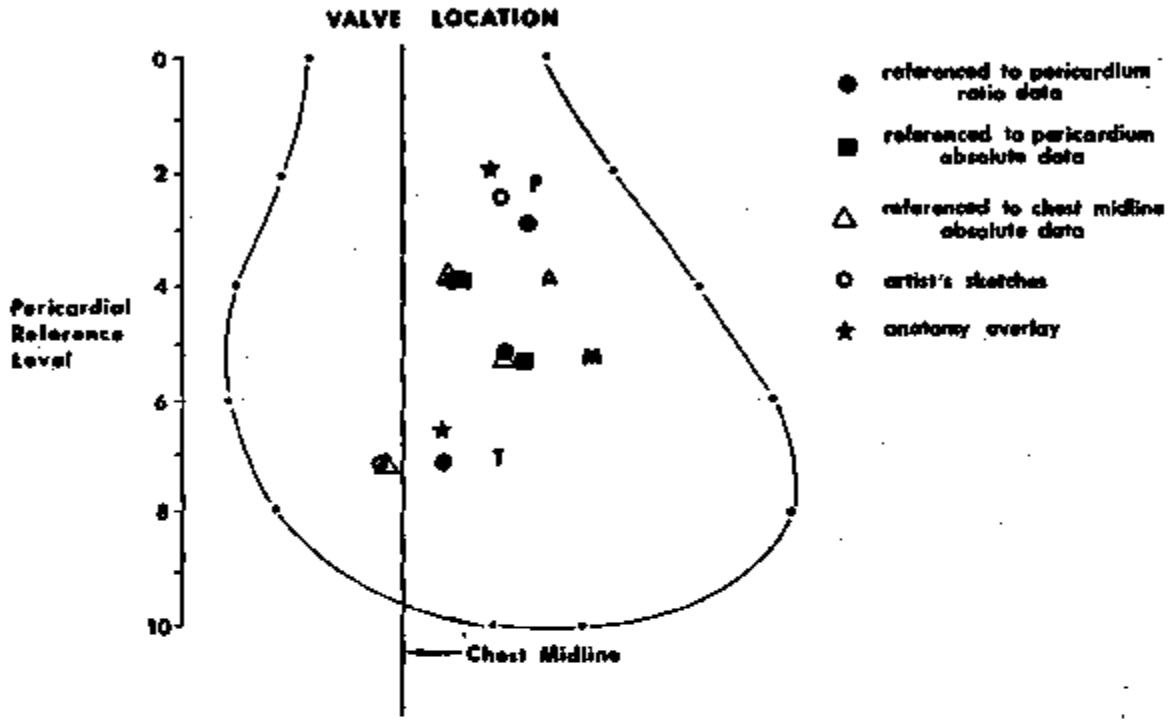

5.3 RESULTS OF INDIRECT METHOD

The open circle and star (artist's sketches of cadavers and anatomy overlay) refer to ratio information used in the indirect method described in Appendix E. Integrated results showing the relative location of the valves to other structures in the human thorax are discussed in Section 8.0.

5.4 VALVE VARIABILITY

The data spread is shown in the P-A view Figure 47. This picture gives a measure of variability in the vertical (Z) and width (X) dimensions and is derived from Tables 11, 12 and Appendix E. Anatomy overlay deviation is valid only in the X dimension because of lack of data in the Z dimension.

Transverse slices at pericardial levels 4 and 8 show valve variability in the width (X) and depth (Y) dimensions (Figures 48 and 49). Anatomy overlay and the artist's sketches variability (indirect approach) is valid in the X-dimension only because of lack of data in the Y dimension. Chest midline variability is valid only in the X dimension.

Figure 47

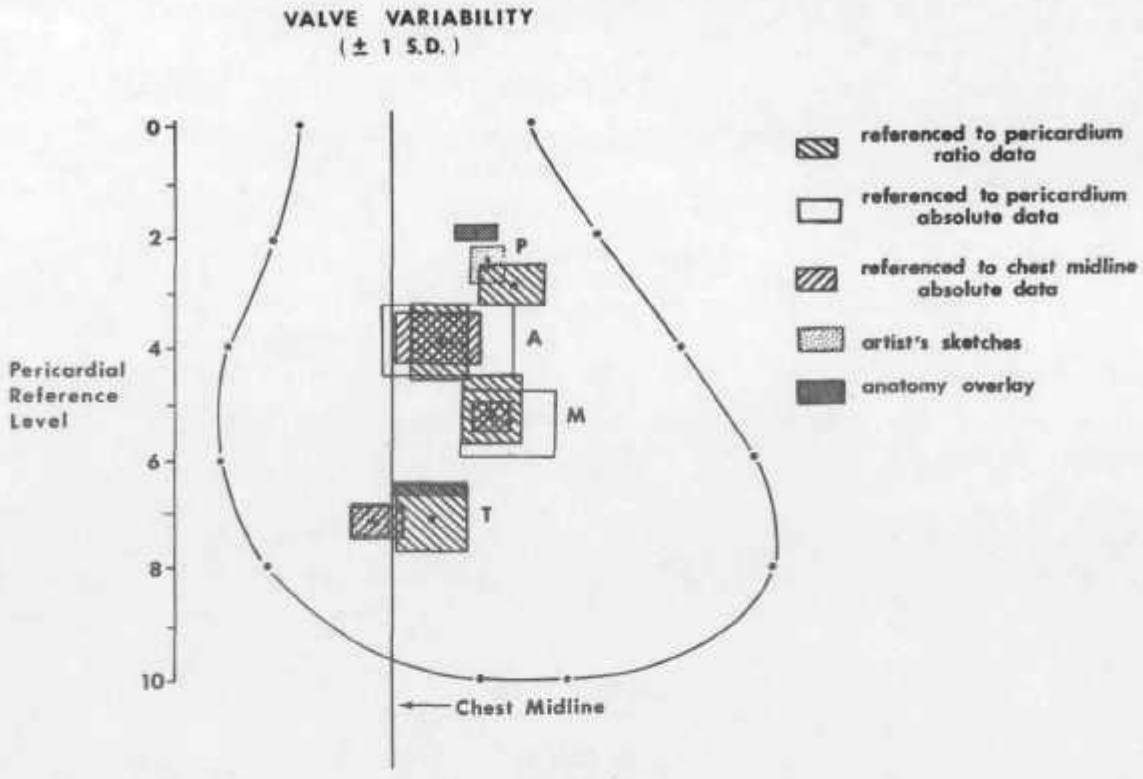

Figure 48

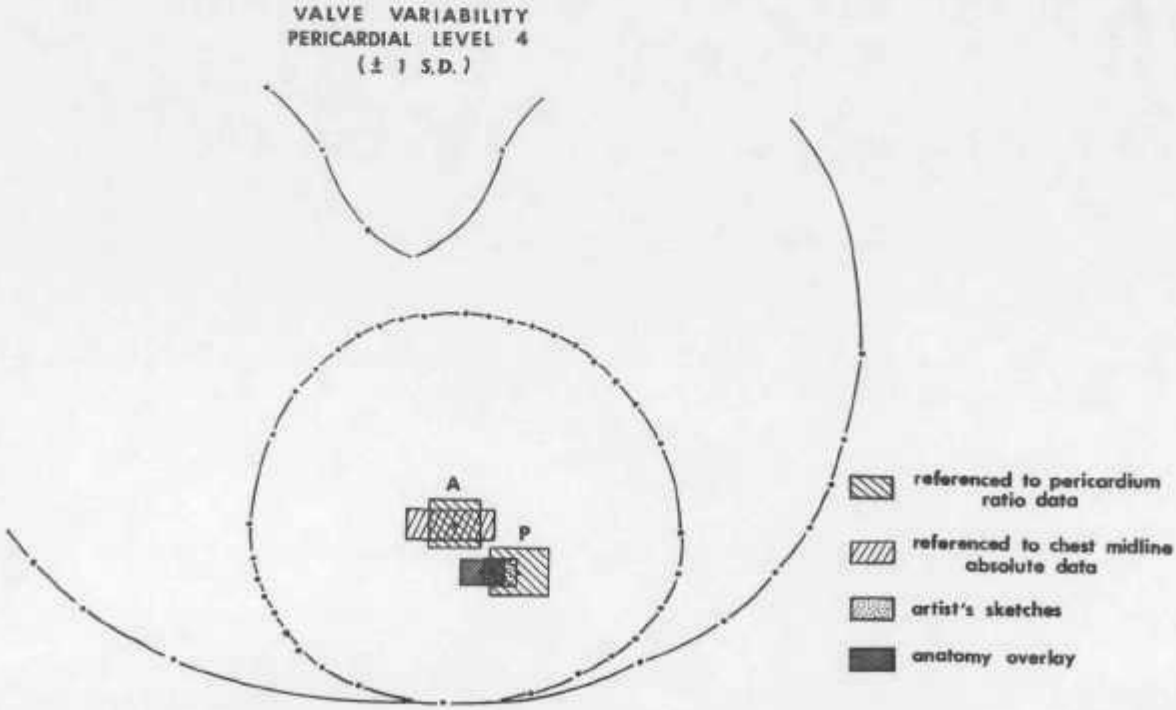

Figure 49

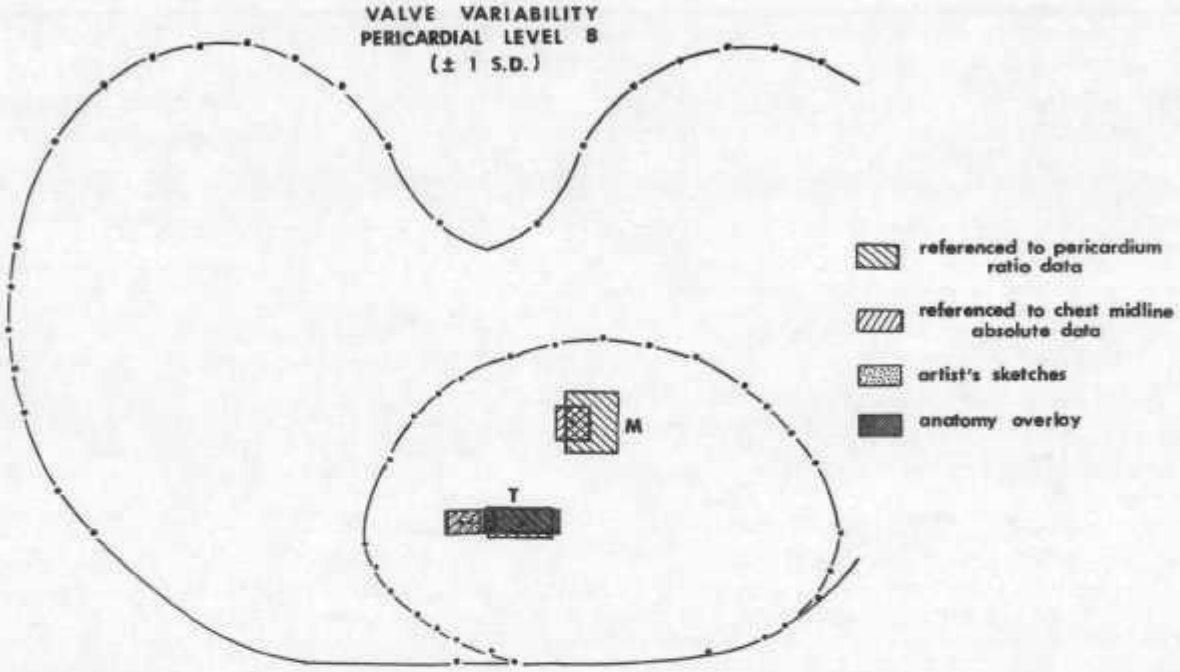
VALVE VARIABILITY
PERICARDIAL LEVEL B
(± 1 S.D.)
M
T
referenced to pericardium ratio data
referenced to chest midline absolute data
artist's sketches
anatomy overlay

6.0 GREAT VESSEL DEFINITION

Data relevant to the problem of defining the great vessels is derived from seven published anatomy texts of cadaver slices and two sliced cadavers obtained by us. Ratio methods were used because they enable both absolute (two cadavers) and non-absolute (seven anatomy text cadavers) to be combined. Likewise male and female ratio information can be mixed assuming there are no significant differences between male and female internal thoracic cavity shapes.

As in valve locations, two referenceing systems (for checking validity of the data) were employed to locate great vessels. Ratios referenced to both the pericardium and chest allowed location of a vessel within the vertical referencing system. For each slice in which a particular great vessel was present, various parameters were measured with respect to both the chest and the pericardium. For example, in order to locate the descending aorta at a certain vertical level, the parameters DA^C_X, DA^C_Y, DA^P_X, and DA^P_Y were measured along with B, C, XpMAX, and YpMAX. With respect to the chest at this particular vertical level, ratios DA^C_X/B and DA^C_Y/C locate the descending aorta in two dimensions. Ratios $DA^P_X/XpMAX$ and $DA^P_Y/YpMAX$ locate the descending aorta in two dimensions with respect to the pericardium at this level. Using the same procedure, superior and inferior vena cavae and the ascending aorta were defined at any desired vertical level.

Each slice has been tagged with a certain pericardial number. This number, between 0 and 10 inclusive, represents the % distance between the top and the bottom of the heart (V_HMAX). Pericardial reference level 1 means this slice is at 10% of the total distance between the upper pericardial reference point (top of the pulmonary artery) and the lower pericardial reference point (bottom of the heart) measured from the upper pericardial reference point. In addition, negative levels have been used where great vessels extend above the heart and level numbers greater than ten are slices below the pericardial reference point.

The ratios mentioned above have been tabulated along with their corresponding pericardial reference level number. All the data for each ratio has been plotted vs. the pericardial reference number corresponding to that data point. These graphs are shown in Appendix G. The points have been curve fitted by estimation. From these curves, ratios have been obtained at each integral pericardial reference level. The data is displayed in Table 13.

Data from this table has been used to locate great vessels in P-A and lateral views (Figures 50 and 51). From these figures results of the two referencing systems, chest and pericardial, can be observed. The pericardial reference locations are generally to the left of the chest reference locations in the P-A view. This can be partially explained by the fact that this figure represents an abnormally sized heart within a normal chest. Thus XpMAX is proportionally greater than B, hence increasing DA^P_X. This will tend to push the pericardial referencing system to the left producing the difference between the two points. Consequently, data with respect to chest was used in the integrated results (Section 8.0).

Table 13

Great Vessel Location Data

	Pericardial Level	Sup. $\frac{VC_X^C}{B}$	Sup. $\frac{VC_Y^C}{C}$	Sup. $\frac{VC_X^P}{XpMAX}$	Sup. $\frac{VC_Y^P}{YpMAX}$
Superior Vena Cava	-5	.27	.63		
	-4	.28	.59		
	-3	.3	.57		
	-2	.29	.56		
	-1	.28	.56		
	0	.27	.54	.16	.54
	1	.24	.52	.16	.66
	2	.2	.48	.145	.74
	3	.16	.44	.12	.79
		Inf. $\frac{VC_X^C}{B}$	Inf. $\frac{VC_Y^C}{C}$	Inf. $\frac{VC_X^P}{XpMAX}$	Inf. $\frac{VC_Y^P}{YpMAX}$
Inferior Vena Cava	7	.19	.39	.18	.85
	8	.18	.37	.14	.94
	9	.19	.33	.09	1.07
	10	.19	.31		
	11	.19	.26		
	12	.2	.22		
	13	.21	.17		
		$\frac{DA_X^C}{B}$	$\frac{DA_Y^C}{C}$	$\frac{DA_X^P}{XpMAX}$	$\frac{DA_Y^P}{YpMAX}$
Descending Aorta	-4	.12	-.29		
	-3	.15	-.19		
	-2	.16	-.13		
	-1	.19	-.07		
	0	.195	-.02	.67	1.6
	1	.19	.005	.67	1.45
	2	.18	.01	.66	1.33
	3	.17	.01	.64	1.21
	4	.16	.01	.62	1.14
	5	.16	0	.59	1.11
	6	.14	0	.55	1.14
	7	.14	0	.5	1.2
	8	.12	-.02	.44	1.3
	9	.11	-.03	.36	1.62
	10	.09	-.05		
	11	.07	-.07		
	12	.06	-.08		
	13	.05	-.09		

Table 13 (con't.)

	Pericardial Level	$\frac{A_X^C}{B}$	$\frac{A_Y^C}{C}$	$\frac{A_X^P}{XpMAX}$	$\frac{A_Y^P}{YpMAX}$
Ascending Aorta	-5	.11	.72		
	-4	.05	.67		
	-3	0	.64		
	-2	-.05	.625		
	-1	-.03	.61		
	0	.02	.61	.43	.53
	1	.07	.62	.46	.47
	2	.12	.65	.48	.43
	3	.16	.7	.5	.45

Figure 50

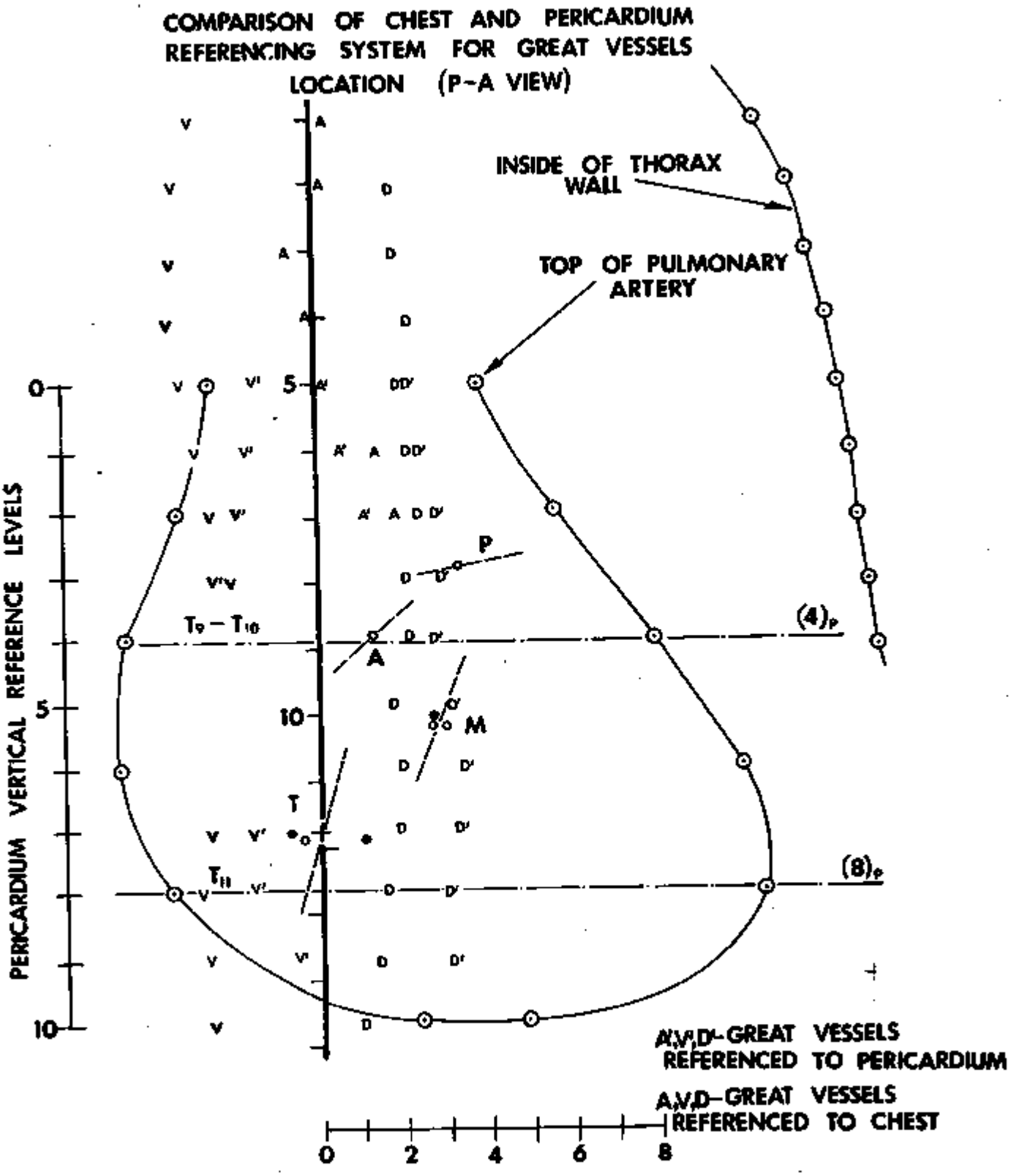
COMPARISON OF CHEST AND PERICARDIUM REFERENCING SYSTEM FOR GREAT VESSELS LOCATION (P-A VIEW)
INSIDE OF THORAX WALL
TOP OF PULMONARY ARTERY
PERICARDIUM VERTICAL REFERENCE LEVELS
0
5
10
$T_9 - T_{10}$
T_{11}
T
P
A
M
$(4)_p$
$(8)_p$
A,V,D'-GREAT VESSELS REFERENCED TO PERICARDIUM
A,V,D-GREAT VESSELS REFERENCED TO CHEST
0
2
4
6
8

Figure 51

COMPARISON OF CHEST AND PERICARDIUM REFERENCING SYSTEMS FOR GREAT VESSELS LOCATION (LATERAL VIEW)

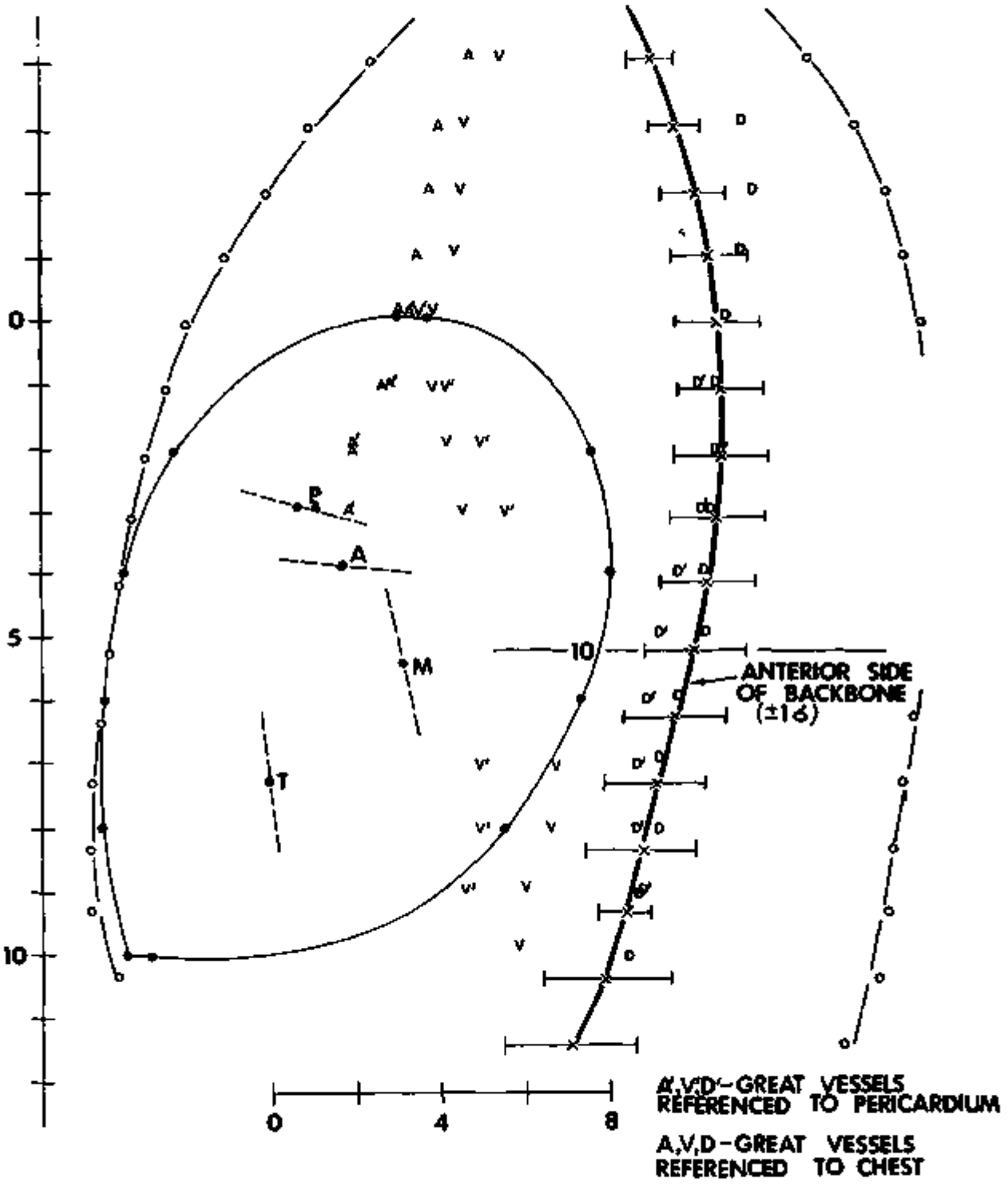

7.0 VERTEBRAL COLUMN DEFINITION (MALE)

Nineteen male lateral X-rays (absolute data) were used. The most ventral point on the backbone between the reference point and the 12th reference level was used as the baseline. Measurements were taken at each vertical reference level. The numbers tabulated are with 10% taken off for X-ray magnification. See Figure 52 for method of referencing.

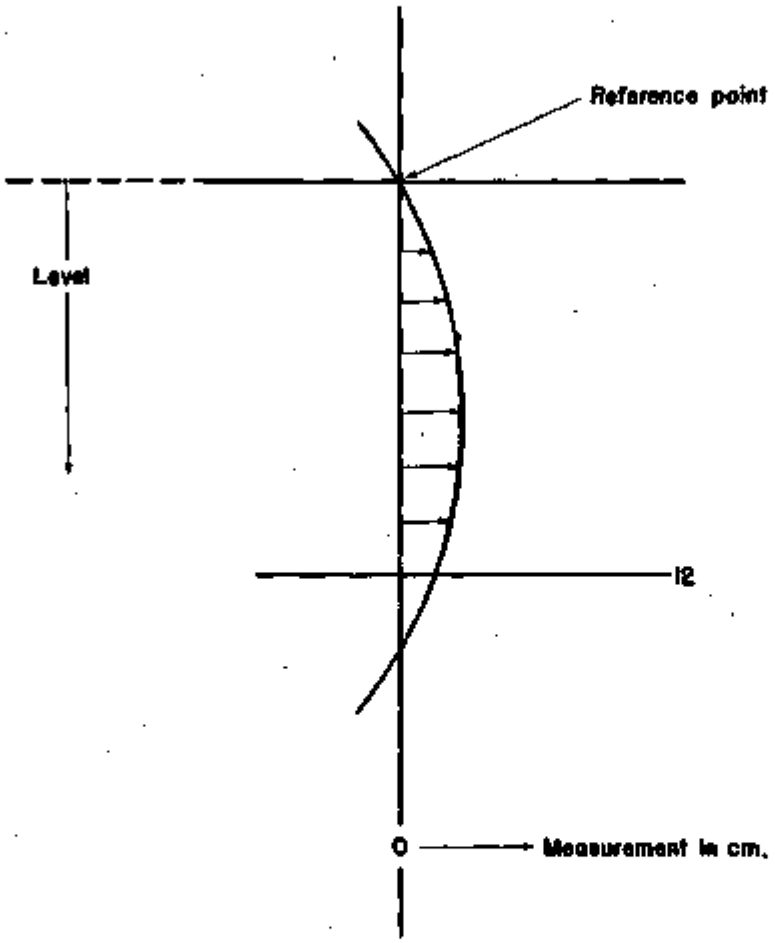

Figure 52

A summary of the results is displayed in Table 14. Also included is the average $V_{CH_{Max}}$ variable, the distance in cm between the upper and lower reference points of the chest.

Table 14

Backbone Curvature Data

(V_{CH_4ax} = 15.9 ± 1.2 cm)

Level	Average distance (cm)	Standard deviation (cm)
-2	-0.81	0.0
-1	-0.6	0.527
0	0.233	0.45
1	0.952	0.577
2	1.525	0.617
3	1.956	0.779
4	2.28	0.905
5	2.52	0.995
6	2.62	1.04
7	2.63	1.10
8	2.49	1.12
9	2.27	1.16
10	1.98	1.22
11	1.53	1.23
12	1.03	1.28
13	0.769	1.27
14	0.36	0.61
15	-0.135	1.53

8.0 INTEGRATED RESULTS

8.1 RESULTS

Using the data presented in the earlier sections of this report, a composite integrated thorax can be defined. Features include chest wall, pericardium outline, vascular connection points represented by the natural valve locations, and the aorta and vena cava. The results have been shown to be quantitative and generally enough data has been processed to allow a statistical distribution of feature sizes as a function of the percentage of the human population.

In order to generate either the lateral or P-A view of the human thorax, certain overall measurements are necessary. On both the 80 normal male and 20 abnormal male radiograms, $V_{CH_{Max}}$ was measured. This is the distance between the upper and lower chest reference points as determined from the P-A skeletal structure. V_R, the distance from the lower chest reference point to the bottom of the pericardial outline, is necessary to locate the heart within the chest. This has only been measured on the 20 abnormal radiograms. A third dimension, $V_{H_{Max}}$, is the heighth of the heart and locates the top of the pericardium (which in this report is defined as the top of the pulmonary artery). All three variables are summarized in Table 15.

Table 15

*Dimensions Necessary to Locate Pericardium within the Thorax**
(Abnormal male X-rays + 2 cadavers)

	$V_{CH_{Max}}$	V_R	$V_{H_{Max}}$
Mean	15.94 cm	7.39 cm	15.37 cm
Standard deviation	1.03 cm	2.14 cm	1.79 cm
Number of data points	19	19	20

*Abnormal male X-rays + 2 cadavers.

An example of the definition in three dimensions is shown in Figures 53 through 56 for the fiftieth percentile (average) adult male. Superimposed on Figure 53 is the outline of the ERDA pump. Two transverse sections through the thorax are shown in Figures 54 and 55 showing the sections of the pump in these planes. As observed, the current pump configurations fits easily into the fifty percentiles adult male. Comparisons with thoracic representations of smaller segments of the population have not been performed as yet. Figures 57 to 60 show similar data except that the thoracic wall was determined using measurements from heart disease patients only. (Figures 53-56 are similar except chest wall dimensions were derived from patients with no heart disease).

Figure 53

P-A VIEW OF AVERAGE MALE THORAX

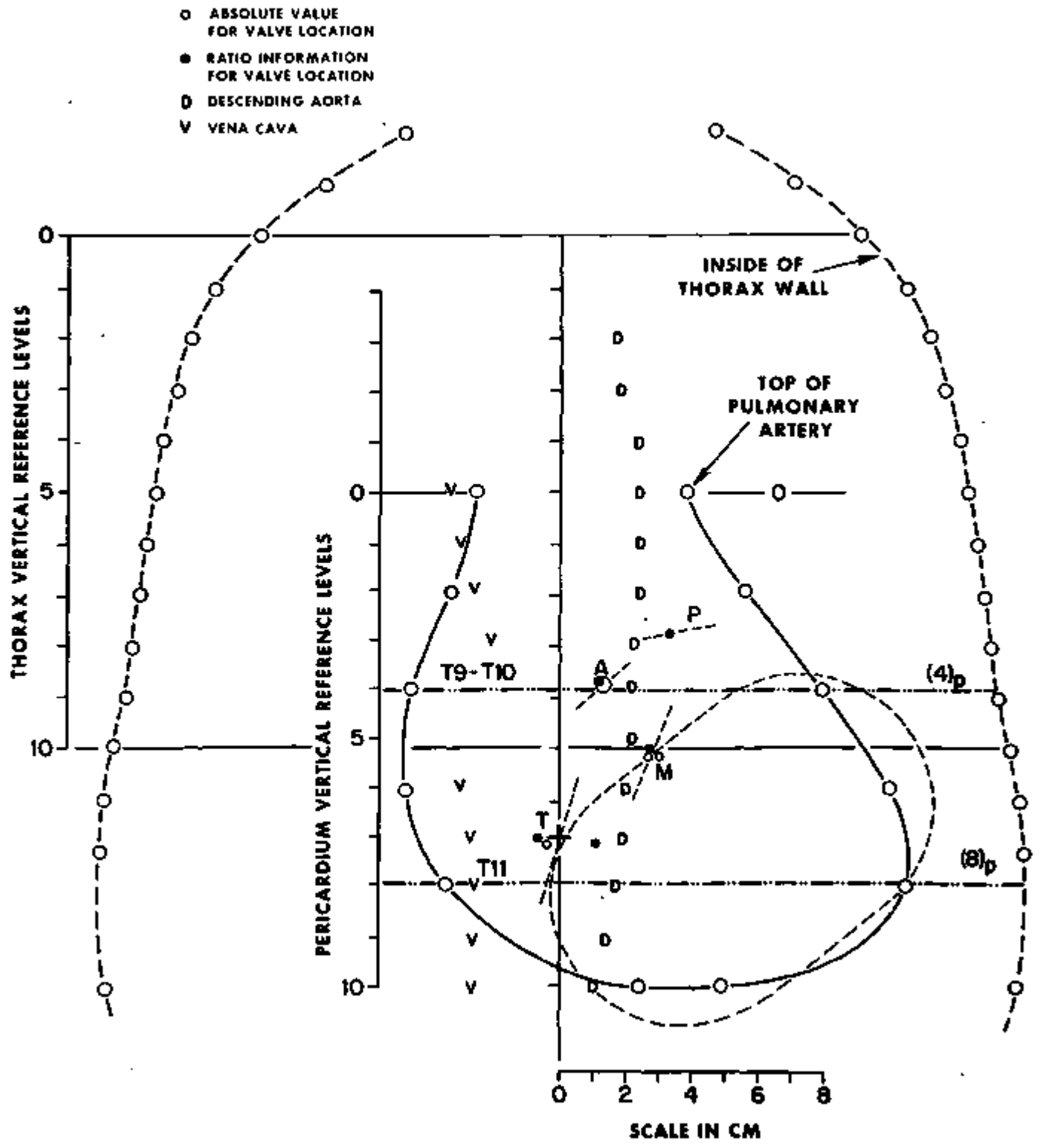

Figure 54

MALE THORAX AT VERTICAL REFERENCE LEVEL 9 $(4)_p$

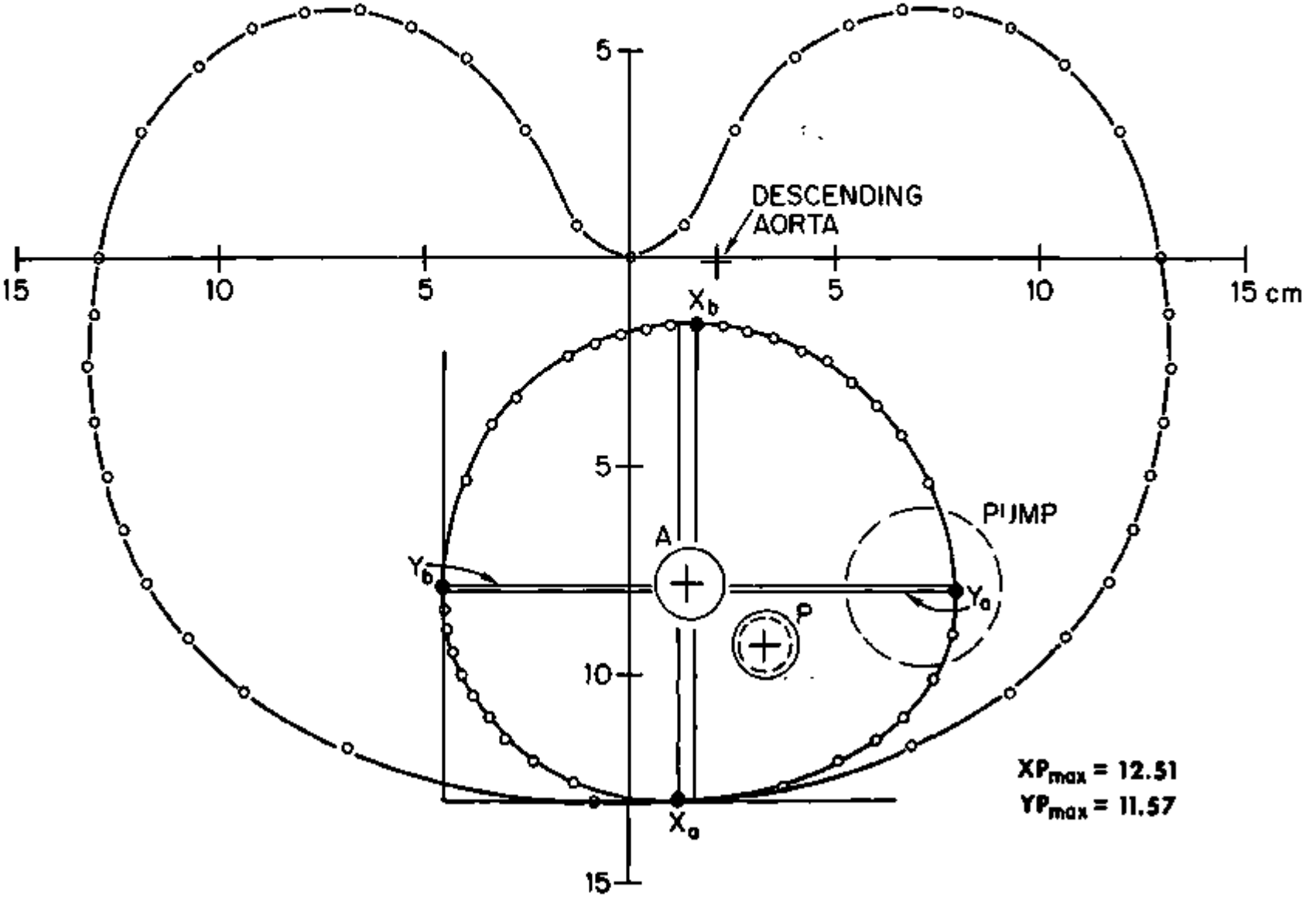

Figure 55

MALE THORAX AT VERTICAL REFERENCE LEVEL 12 $(8)_p$

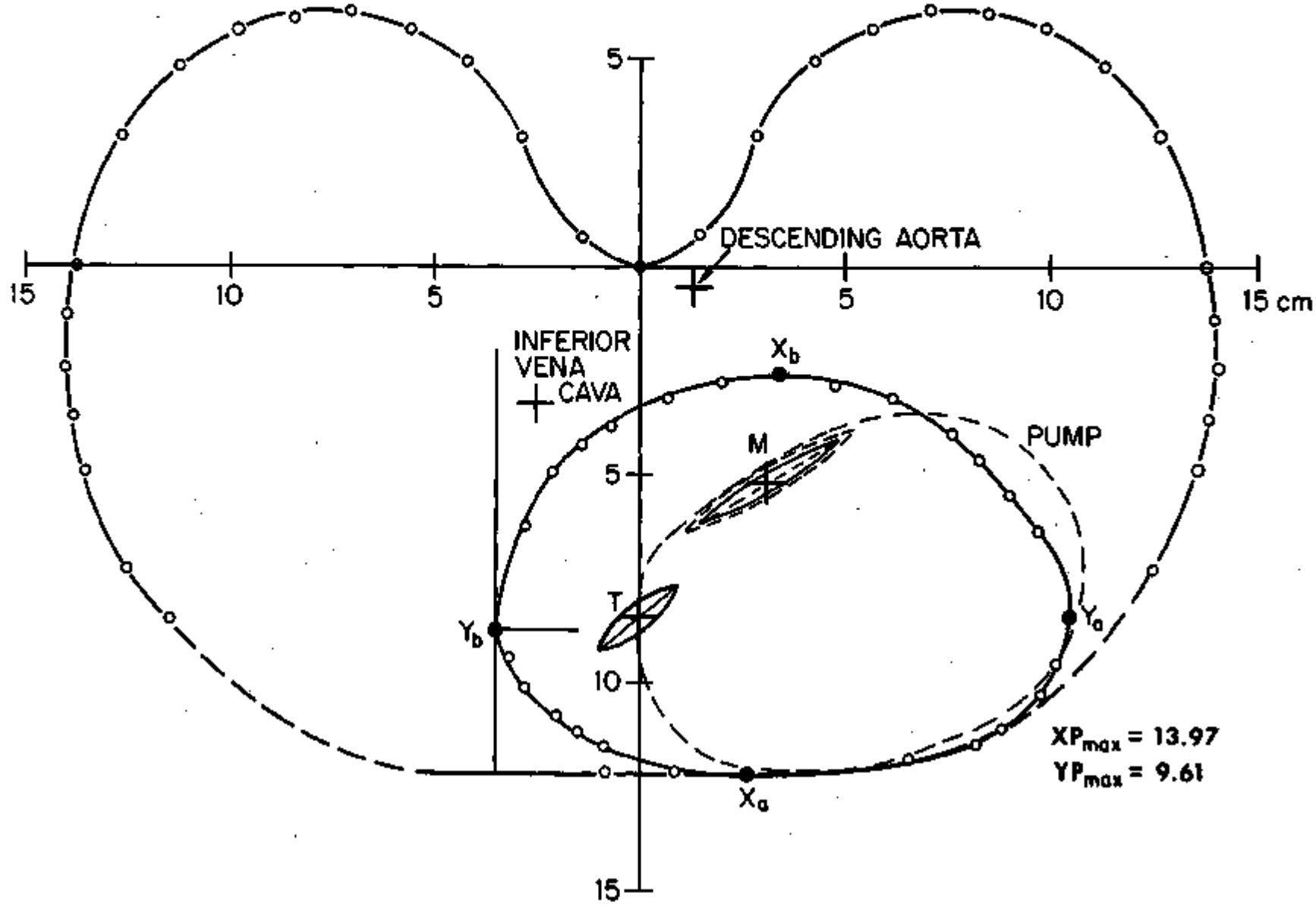

Figure 56

LATERAL VIEW OF AVERAGE MALE THORAX (REFLECTS DATA OF HEART DISEASE PATIENTS)

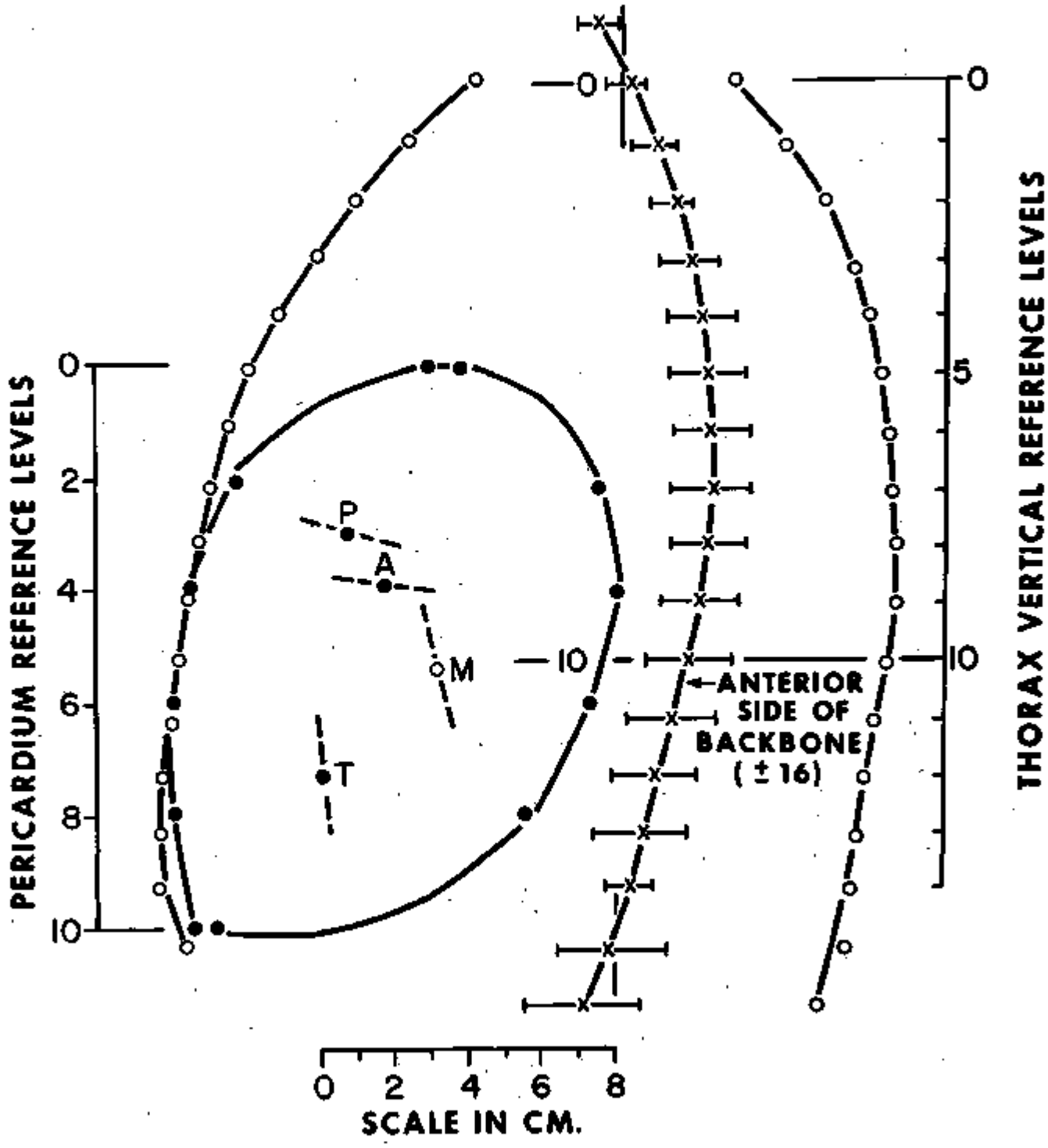

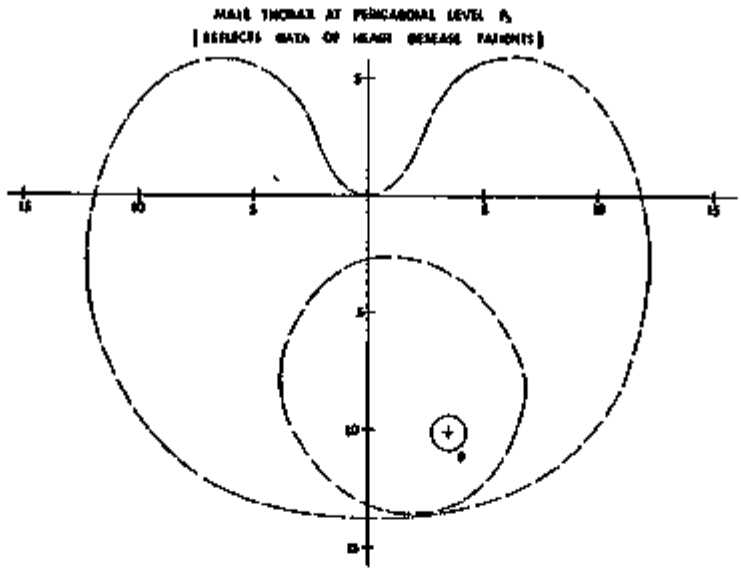

Figure 57

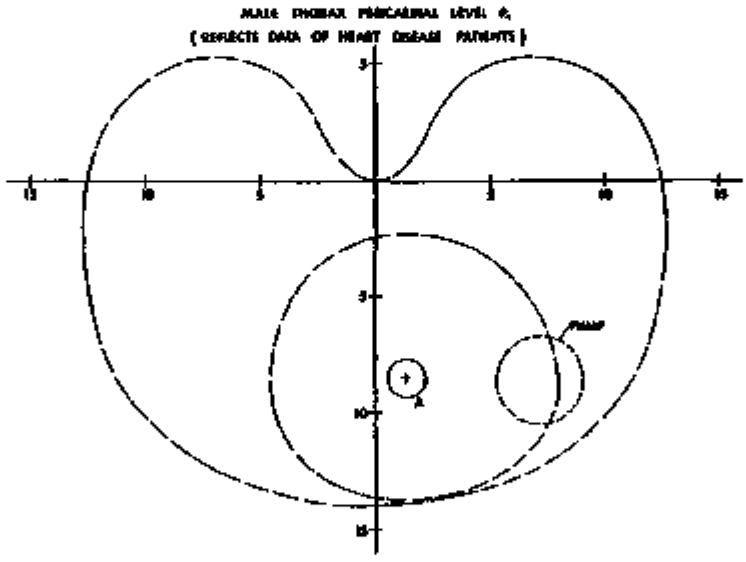

Figure 58

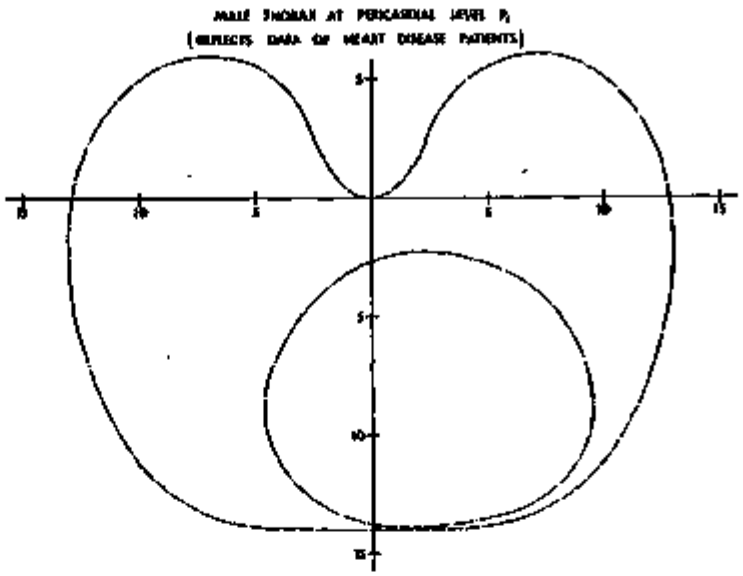

Figure 59

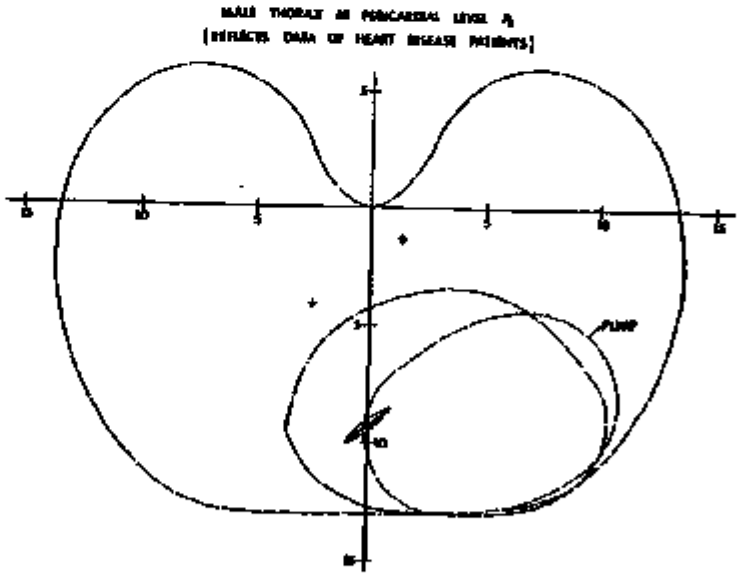

Figure 60

8.2 DISCUSSION

Until more data is gathered, a detailed comparison of our results with the literature would not be relevant. However, it should be pointed out that comparison of this data with cadaver data will demonstrate a definite difference. For example, Eycleshymer (4) places the bottom of the heart at the junction between T10 and T11, while our data shows it to be closer to T12. This is understandable since the key dimension for placement is V_R, which we derived from radiograms of living patients during the inspiratory phase of breathing. Radiographic data from other sources also indicate large variations in overall placement of the heart within the thorax. Kaneko et al (32) demonstrated a maximum difference of 10 cm between heart placement in the vertical direction based on 140 cases. Heart width from his results were 14.55 cm $\pm$ a standard deviation of 2.05 cm, which agrees quite well with our width of 14.76 $\pm$ 1.61 cm.

The present shape model and bank of statistical measurements is continually being updated, most recently by using data obtained on a total body scanner from living patients at the Cleveland Clinic. This new technique will be the most accurate data obtainable and is applicable to all the connection points except vascular.

APPENDIX A

EXAMPLE OF MODEL USE AND COMPARISON WITH SOME CLASSICAL DATA

Assume that the Atlas projections shown in Figures A1 and A2 represent the actual structure of a patient under investigation for a possible prosthesis. The transverse section shown in Figure A1 is labeled with a set of axes determined by one reference point on the vertebral column and another on the distal point of the inner side of the sternum. The dimensions A, B, and C represent those measurements of the chest cavity visible on the radiogram (Figure A3). These simulated X-ray dimensions are shown at the top of Table A1 as A', B', and C'. Assuming T10 region of the symmetrical model is used, x-y coordinates of the predicted thorax are generated by simple multiplication; i.e., for the left anterior quadrant, the normalized x values (X_n) are multiplied by C'. The total predicted curve for this simulated patient is shown in black squares in Figure A2.

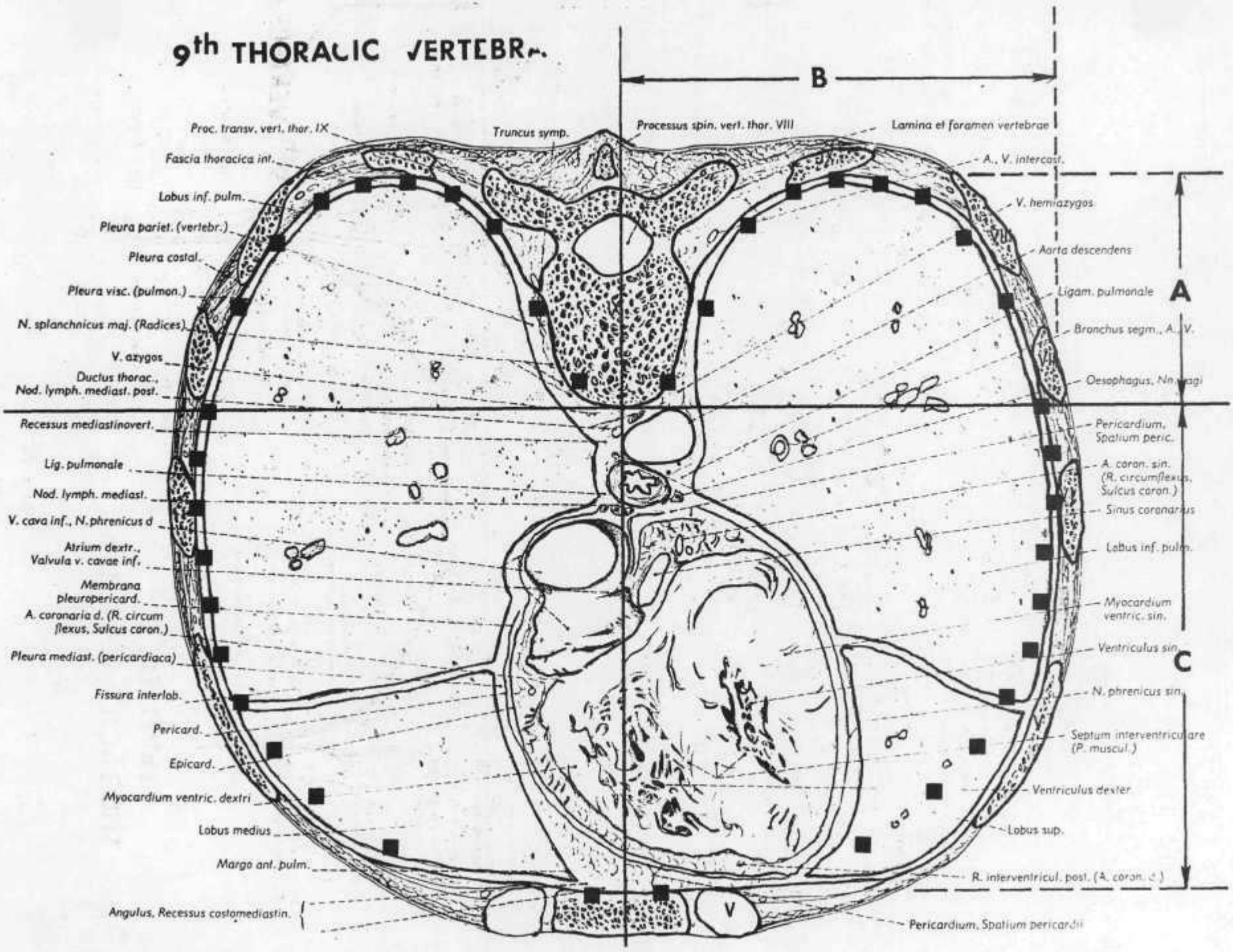
9th THORACIC VERTEBRA
B
A
C
Proc. transv. vert. thor. IX
Truncus symp.
Processus spin. vert. thor. VIII
Lamina et foramen vertebrae
Fascia thoracica int.
A., V. intercost.
Lobus inf. pulm.
V. hemiazygos
Pleura pariet. (vertebr.)
Aorta descendens
Pleura costal.
Pleura visc. (pulmon.)
Ligam. pulmonale
N. splanchnicus maj. (Radices)
Bronchus segm., A., V.
V. azygos
Ductus thorac.
Oesophagus, Nn. vagi
Nod. lymph. mediast. post.
Recessus mediastinovert.
Pericardium, Spatium peric.
Lig. pulmonale
A. coron. sin. (R. circumflexus, Sulcus coron.)
Nod. lymph. mediast.
Sinus coronarius
V. cava inf., N. phrenicus d
Lobus inf. pulm.
Atrium dextr., Valvula v. cavae inf.
Membrana pleuropericard.
Myocardium ventric. sin.
A. coronaria d. (R. circum flexus, Sulcus coron.)
Ventriculus sin.
Pleura mediast. (pericardiaca)
N. phrenicus sin.
Fissura interlob.
Septum interventriculare (P. muscul.)
Pericard.
Epicard.
Ventriculus dexter
Myocardium ventric. dextri
Lobus sup.
Lobus medius
R. interventricul. post. (A. coron. d.)
Margo ant. pulm.
Angulus, Recessus costamediastin.
V
Pericardium, Spatium pericardii

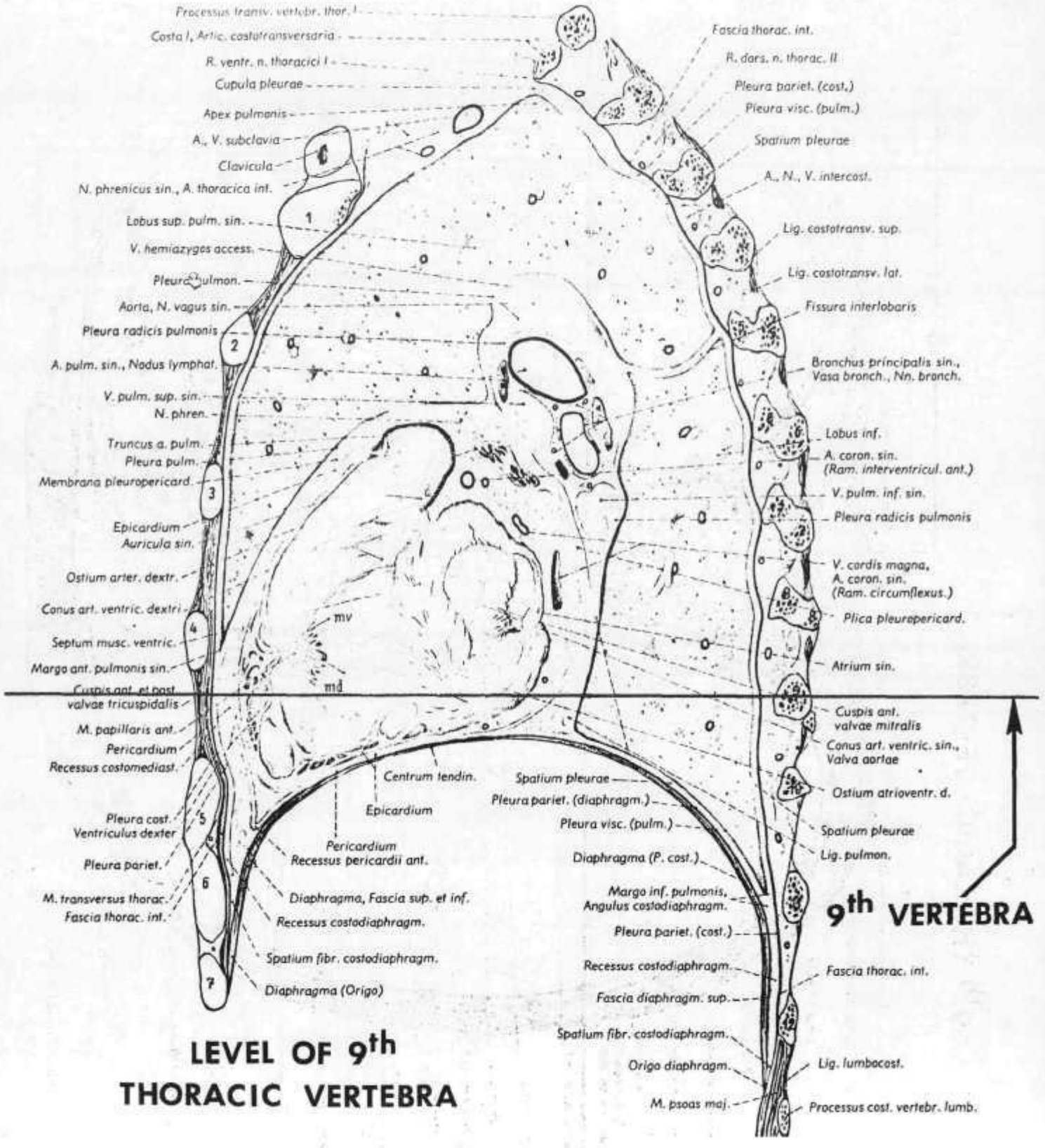
Processus transv. vertebr. thor. I
Costa I, Artic. costotransversaria
R. ventr. n. thoracici I
Cupula pleurae
Apex pulmonis
A., V. subclavia
Clavicula
N. phrenicus sin., A. thoracica int.
Lobus sup. pulm. sin.
V. hemiazyges access.
Pleura pulmon.
Aorta, N. vagus sin.
Pleura radicis pulmonis
A. pulm. sin., Nodus lymphat.
V. pulm. sup. sin.
N. phren.
Truncus a. pulm.
Pleura pulm.
Membrana pleuropericard.
Epicardium
Auricula sin.
Ostium arter. dextr.
Conus art. ventric. dextri
Septum musc. ventric.
Margo ant. pulmonis sin.
Cuspis ant. et post. valvae tricuspidalis
M. papillaris ant.
Pericardium
Recessus costomediast.
Pleura cost.
Ventriculus dexter
Pleura pariet.
M. transversus thorac.
Fascia thorac. int.
Centrum tendin.
Epicardium
Pericardium
Recessus pericardii ant.
Diaphragma, Fascia sup. et inf.
Recessus costodiaphragm.
Spatium fibr. costodiaphragm.
Diaphragma (Origo)
mv
md
Fascia thorac. int.
R. dors. n. thorac. II
Pleura pariet. (cost.)
Pleura visc. (pulm.)
Spatium pleurae
A., N., V. intercost.
Lig. costotransv. sup.
Lig. costotransv. lat.
Fissura interlobaris
Bronchus principalis sin., Vasa bronch., Nn. bronch.
Lobus inf.
A. coron. sin. (Ram. interventricul. ant.)
V. pulm. inf. sin.
Pleura radicis pulmonis
V. cordis magna, A. coron. sin. (Ram. circumflexus.)
Plica pleuropericard.
Atrium sin.
Cuspis ant. valvae mitralis
Conus art. ventric. sin., Valva aortae
Ostium atrioventr. d.
Spatium pleurae
Lig. pulmon.
Spatium pleurae
Pleura pariet. (diaphragm.)
Pleura visc. (pulm.)
Diaphragma (P. cost.)
Margo inf. pulmonis, Angulus costodiaphragm.
Pleura pariet. (cost.)
Recessus costodiaphragm.
Fascia diaphragm. sup.
Spatium fibr. costodiaphragm.
Origo diaphragm.
M. psoas maj.
Lig. lumbocost.
Processus cost. vertebr. lumb.
9th VERTEBRA
LEVEL OF 9th THORACIC VERTEBRA

Figure A2

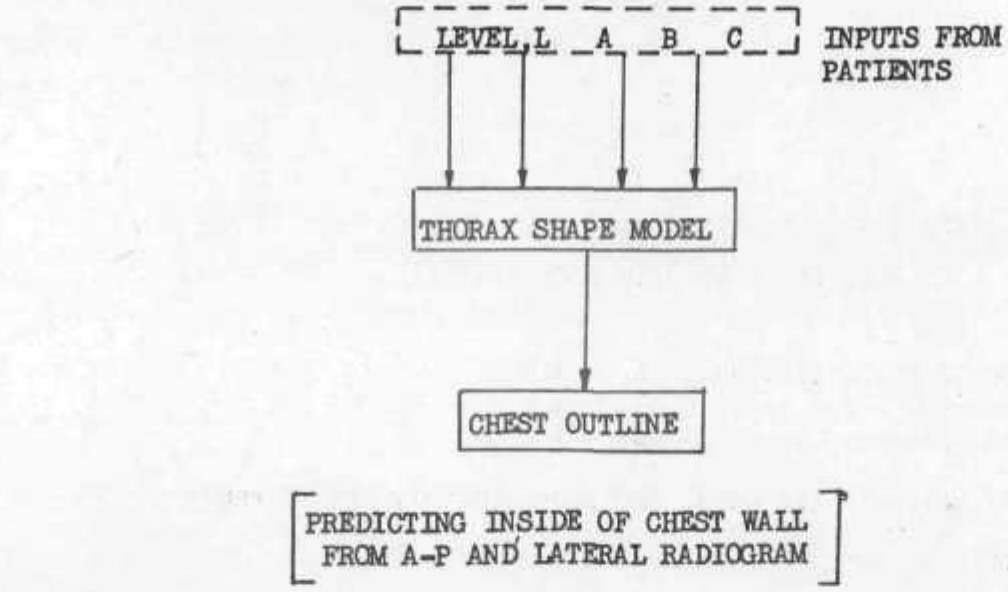

FIGURE A3

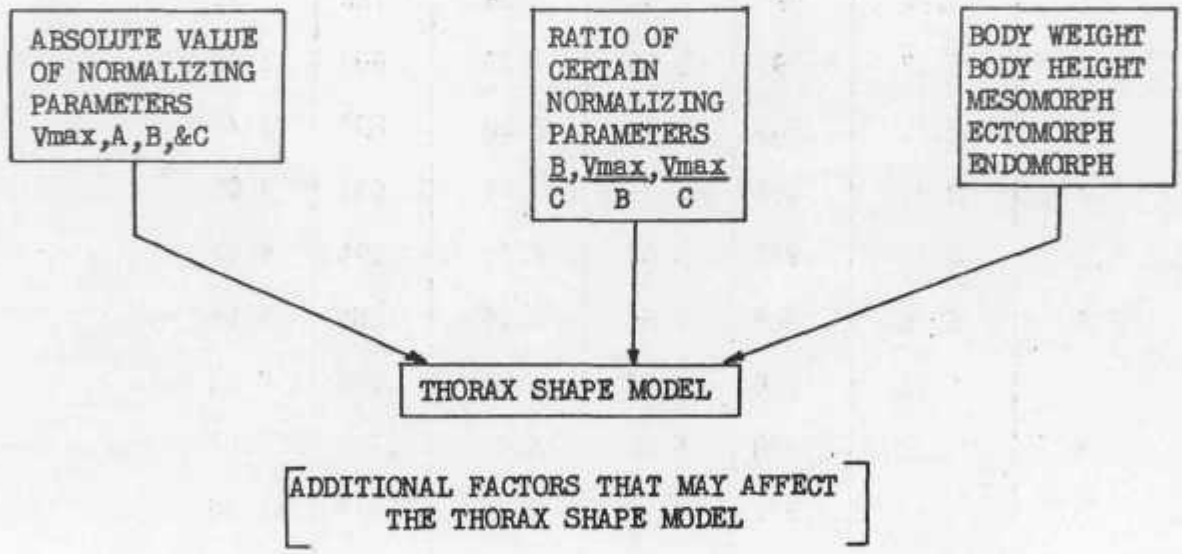

Figure A4

Table A1

TRANSFORMATION OF SIMULATED X-RAY MEASUREMENTS FROM FIGURE 21 INTO THE PREDICTED THORAX CAVITY

Simulated X-ray Dimensions: $A_1' = 4.6$ cm
$B_1' = 8.6$ cm
$C = 9.6$ cm

Note: Y_n below is the model for approximately the T9 region

	Left Anterior			Left Posterior		
X_n	$X_n \cdot C'$	Y_n	$Y_n \cdot B'$	$X_n \cdot B'$	Y_n	$Y_n \cdot A'$
0	.0	.979	8.42	0.0	0.0	0.0
.1	.96	.995	8.56	.86	.126	.58
.2	1.92	.999	8.60	1.72	.509	2.34
.3	2.88	.985	8.47	2.58	.807	3.71
.4	3.84	.964	8.29	3.44	.932	4.29
.5	4.8	.937	8.06	4.30	.994	4.57
.6	5.76	.889	7.64	5.16	.985	4.53
.7	6.72	.816	7.02	6.02	.928	4.27
.8	7.68	.708	6.09	6.88	.777	3.57
.9	8.64	.527	4.53	7.74	.517	2.38
1.0	9.6	.062	.53	-	-	-

APPENDIX B

RADIOGRAPH MEASUREMENT TECHNIQUE
(Chest Wall Data)

MEASUREMENTS ON POSTERO-ANTERIOR RADIOGRAPHS (Figure B1)

1. Define the median line (I), assuming that the chest is symmetric.

2. Locate the fourth and tenth ribs of both sides.

3. Draw the lines, which cross perpendicularly to (I) and pass through the points at which the fourth (II) and tenth rib (III) is farthest from line (I).

4. Draw a line from the midpoint of Line II, parallel to (I), to Point (IV) on the dorsal shadow of the fourth rib. Do the same and obtain Point (V) on the tenth rib.

5. Define the upper reference point (P_0) on Line (I) where a line perpendicular to Line (I) passes through Point (IV). Define the lower reference point (P_{10}) on Line (I) from Point (V).

6. Measure the distance between Point (P_0) and (P_{10}). This is V_{Chmax}

7. Divide V_{Chmax} into ten divisions and name divisional points in an order of P_0, P_1, P_2 ... P_{10} and extend these points on Line (I) upward to P_1, P_2... and downward to P_{11}, P_{12} with the same divisional distance.

8. Measure distances B_0, B_1, B_2 ... B_{10} and B_{-1}, B_{-2} ... B_{11}, B_{12} ... as many as exist in such a manner as B_n is a distance between Point (P_n) and a point at which a perpendicular to Line (I), passing through P_n, crosses the internal margin of the chest cavity on a radiograph.

9. Measure distances D_0, D_1, D_2 ... which are defined by the distances from P_0, P_1, P_2 ... to points at which lines perpendicular to Line (I) and passing through P_0, P_1, P_2 ... cross the right margin of the heart silhouette.

10. Measure E_0, E_1, E_2 ... which are defined as the same as D_0, D_1, D_2 ... but to the left margin of the heart silhouette. An upper and lower limitation of the pericardial cavity are confirmed on a corresponding lateral view of chest radiograph.

If any upper and/or lower limitation of structures to be measured are not on exact divisions, half the divisional scale is set and indicated on a chart. (For example (3.5) in Column D in Table B1). The level of each side of the diaphragm is individually noted in Table B1 since very often it differs.

Figure B1

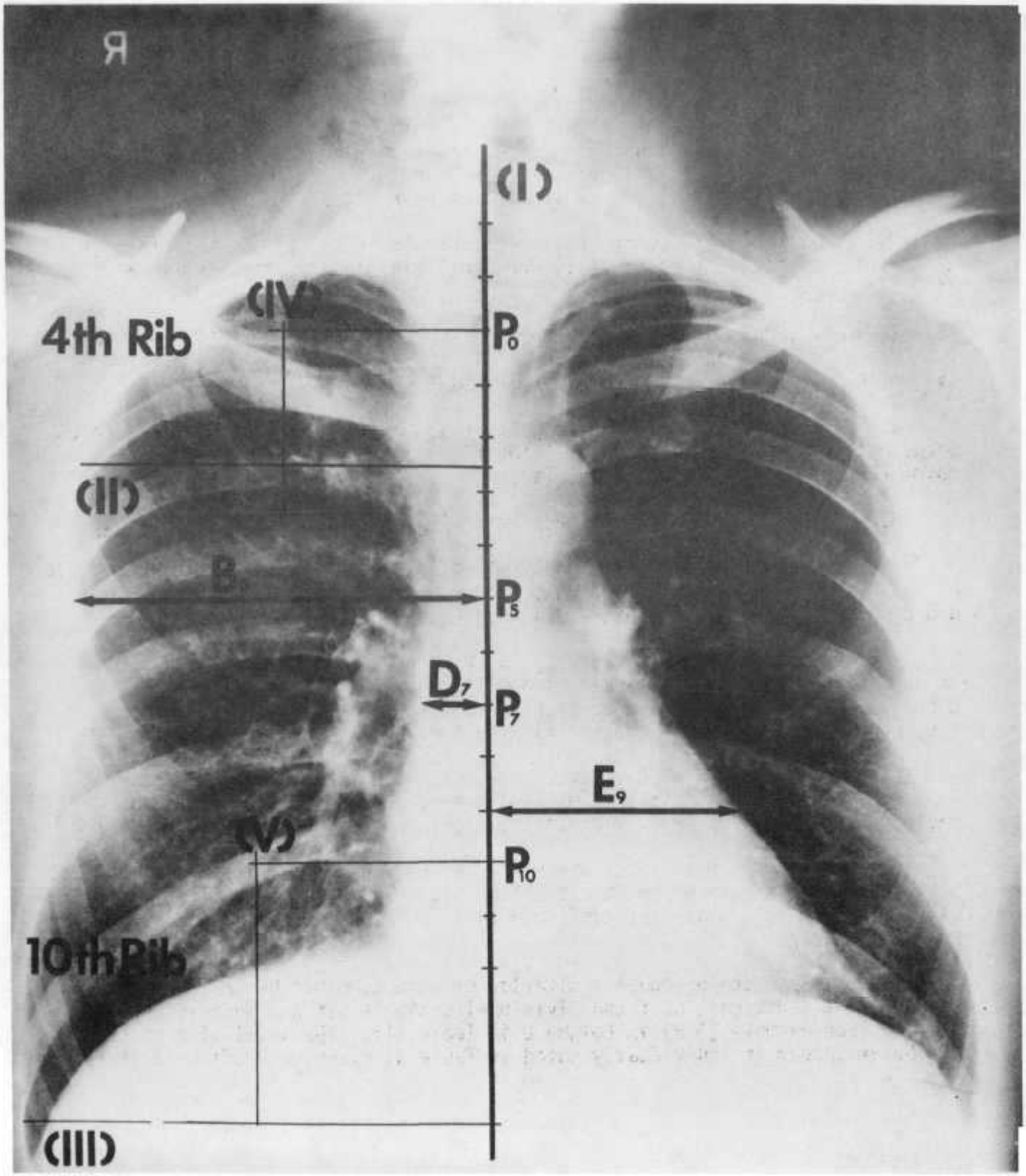

MEASUREMENTS ON LATERAL RADIOGRAPHS (Figure B2)

1. Locate and define the reference point (Q_0) on the anterior line of the vertebral column which has already been determined as the corresponding point (P0) on the posteroanterior view. Point ($P_0 = Q_0$) usually positions itself at a lower rim of the third thoracic vertebra.

2. Define point (R_0) which is marked on a posterior edge of the film and at the same horizontal level to (Q_0).

3. Make point (R_{10}) on a posterior edge of the film with a distance of V_{Chmax} from R_0. Q_{10} can be marked by tracing a horizontal line passing through R_{10} on the anterior line of the vertebral column.

4. Divide the distance between R_0 and R_{10} into ten divisions and name divisional points in an order of R_0, R_1, R_2 ... R_{10} and extend these points upward to R_{-1}, R_{-2} ... and downward to R_{11}, R_{12} ... with the same divisional distance.

5. Mark Q_1, Q_2 ... Q_9 on the anterior line of the vertebral column so as to be at the same horizontal level to the corresponding points of R_1, R_2 ... R_9.

6. Measure distances C_0, C_1 ... C_{10} in such a manner as C_n is defined by a horizontal distance between Q_n and the anterior internal margin of the chest cavity.

7. Measure distances A_0, A_1 ... A_{10} and A_{-1}, A_{-2} ... A_{-11}, A_{-12} ... in such a manner as A_n is defined by a horizontal distance between Q_n and the posterior internal margin of the chest cavity.

8. Measure distances ... F_2, F_3 ... F_5, F_6 ... in such a manner as F_n is defined by a distance between Q_n and the point where a horizontal line through Q_n crosses an anterior line of the heart silhouette.

9. Measure distances ... G_2, G_3 ... G_5, G_6 ... in such a manner as G_n is defined by a distance between Q_n and the point where a horizontal line through Q_n crosses a posterior line of the heart silhouette. A typical case of the measurements is presented in Table B1.

Figure B2

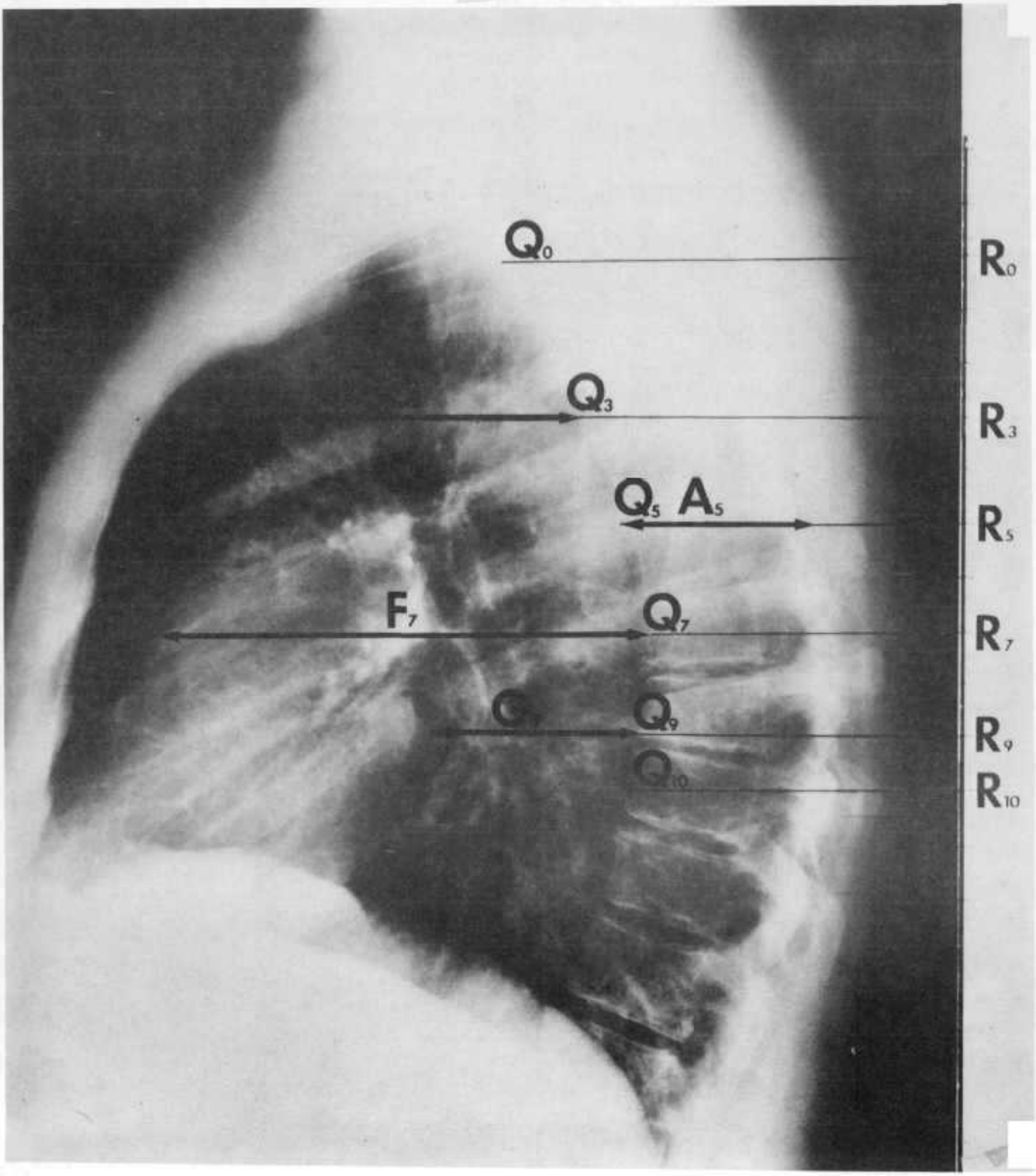

Table B1

NO. 74 NAME: B.J.R. SEX: Male
AGE: 54

	A	B	C	D	E	F	G
-5							
-4							
-3							
-2		(-1.5) 4.4	(-1.5) 0.5				
-1	3.0	6.8	8.0				
0	5.0	9.6	10.1				
1	5.4	11.6	13.2				
2	5.6	12.7	13.6				
3	5.8	13.3	13.6	(3.5) 2.0	(3.5) 2.2	(3.5) 7.8	(3.5) 7.8
4	6.1	14.0	13.8	2.6	2.2	10.8	6.5
5	6.5	14.1	13.5	3.0	2.4	12.5	4.1
6	7.2	14.6	13.2	3.4	3.1	13.2	3.1
7	7.5	14.7	12.9	3.6	4.2	12.9	2.8
8	7.5	14.8	12.5	4.3	6.1	12.5	2.5
9	7.6	14.8	12.4	4.5	8.0	12.4	2.5
10	7.6	15.4	12.4	4.5	9.0	12.4	3.2
11	7.6	15.4	12.4	4.5	10.0	12.4	5.0
12	7.6	R L (12.0) (12.0) 9.0 11.0	R L (12.0) (12.0) 7.0 7.0	4.5	10.5		
13							
14							
15							
16							
Vmax	18.0						

( ) indicates a divisional scale.

Numbers indicate actual distance in cm.

APPENDIX C

VALIDATION AND VERIFICATION OF CHEST WALL DATA

Comparison of X-ray and Mold Data

To check the assumption of dimensional symmetry in the thorax, as opposed to the symmetry of "shape" described earlier, left and right measurements for the normalizing parameters A and B were taken from the mold data and plotted against each other in Figures C1 and C2. Regression lines (solid) were calculated and are shown compared with the dotted identity line. Slopes of these regressions were .92 for A (y intercept = .51) and .83 for B (y intercept = 1.85). Perfect symmetry would have resulted in a slope of 1 and y intercept values of 0. This minor lack of symmetry, however, besides being within the expected error in the process of generating molds (they are used primarily for "shape" information rather than absolute measurements), would result in a negligible error in the overall predicted distributions.

Besides the dimensional symmetry check on the raw mold data, comparisons were made between X-ray and mold data at various vertical levels in the chest. The mold measurements should be approximately from the same statistical distribution as the X-ray data. Parameters A and B showed very close correlations between mold and X-ray data, although on the whole, mold dimensions were slightly less than corresponding radiogram measurements. This discrepancy probably reflects the fact that soft tissue between the actual chest cavity and the rib cage does not show up on X-ray film. Parameter C, shown in Figure C3, showed the largest difference (again the mold data smaller than X-ray data). The difference could be due to the fact that X-rays are taken during inspiration, while cadavers represent practically full expiration. Considering the "pump handle" action of the ribs during respiration, the somewhat larger difference is not surprising. Figures C4 through C6 demonstrate the quite marked difference between male and female chest dimensions. The smaller size, especially in the heart region, could be a limiting factor in the design of a universal cardiac prosthesis.

Checking of Shape Model

Additional comparisons of the model with some classical transverse thorax sections (3) are shown in Figures C7 through C9. Greatest errors are in the anterior region of the chest, on either side of the sternum. Fortunately, it results in an underestimation rather than an overestimation of available space. Source of the error probably stems from the fact that this is precisely the region where the cadaver chest wall section was removed in order to empty the thorax and pour in the silastic. Even though the section was replaced during curing, some error could be present in repositioning the section.

Additional factors that may affect the standard deviation of the thorax model are illustrated in Figure A4. These include absolute values of the normalizing parameters, ratio of certain normalizing parameters, and qualitative data, such as mesomorph or ectomorph designations. These correlations have not been pursued, since pericardium and valve data were considered more important.

Examination of Correlation between Normalizing Parameters (A, B, and C) Obtained from 80 Male X-Rays.

In these final results, terms A+ 2σ, B + 2σ, and C + 2σ are combined. Similarly, points A - 2σ, B - 2σ, and C - 2σ are also connected. This implies that there is a direct correlation between these three parameters; and hence the "shapes" outlined by these curves indicate actual statistical distributions. If there is no correlation between these parameters (and the data is normal), then the standard deviation still has meaning, but actual chest shapes may have any random shape between the plus and minus two standard deviation lines.

Plots of these transverse X-ray variables versus each other are shown in Figures C10 and C11. When these sections are reconstructed to form a generalized total thorax, V_{Chmax} (chest height) will also have a tolerance assigned to it. Again, the meaning of connecting V_{Chmax} + 2σ to A + 2σ, B + 2σ, etc., must be determined. Hence, plots of V_{Chmax} vs. width (B), total depth (C + A) and the anterior depth (C) are shown in Figures C12-C14. Very little correlation can be seen in any of the five graphs. Numerical values supporting this visual assumption of scatter follow:

For level 10, male (80 radiograms):

C vs A	R*= -.25	(*R = Spearman Rank
B vs A	R = .1897	correlation coefficient)
B vs C	R = .1566	

In another test, where simple linear regressions were tried:

B vs C	Correl. = .2307	B = 6.94 + .48 · C
C vs A	Correl. = -.1998	C = 7.79 - .0719 · A
B vs A	Correl. = .1766	B = 4.765 + .133 · A

the normality of A, B, and C was approached by determining if the skewness of the data was significant. Again, level 10, from the 80 male radiograms:

Results

Parameter	Data Points	Skewness	Significant
A	79	1.57	yes
B	68	.415	no
C	69	.063	no

the only parameter not normal was A, the posterior measurement. Since this dimension is not relevant to the heart location, the lack of normality is not serious. As a result:

1. Data is normal, and hence the standard deviation has meaning. However,

2. No correlation exists between the normalizing parameters A, B, and C. This means that the area enclosed by the ± 2σ lines in Figures 29 to 31 represents the limits of random curves, and that the closed curves shown have no real meaning; e.g., a curve going from B + 2σ to C + 2σ is just as probable as one going from B + 2σ to C - 2σ. The same holds true for V_{Chmax} vs A, B, and C.

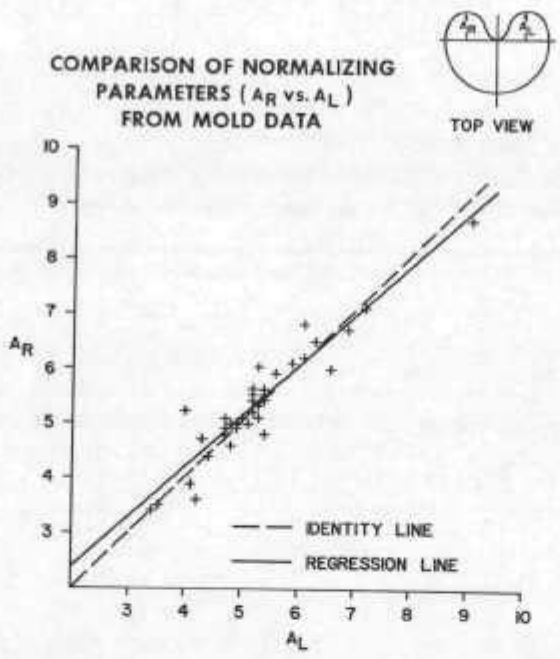

Figure C1

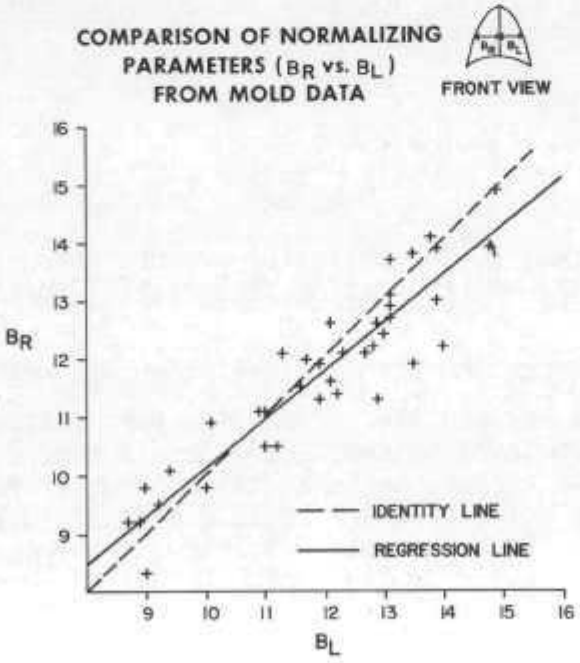

Figure C2

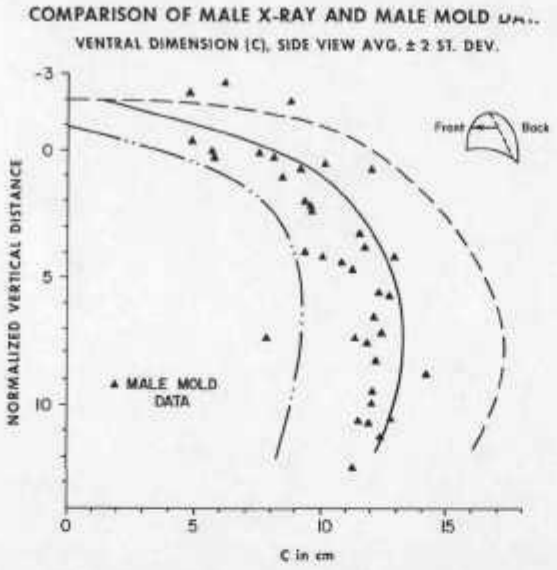

Figure C3

COMPARISON OF MALE AND FEMALE X-RAY DATA

DORSAL DIMENSION (A), SIDE VIEW AVG. ± 2 ST. DEV.

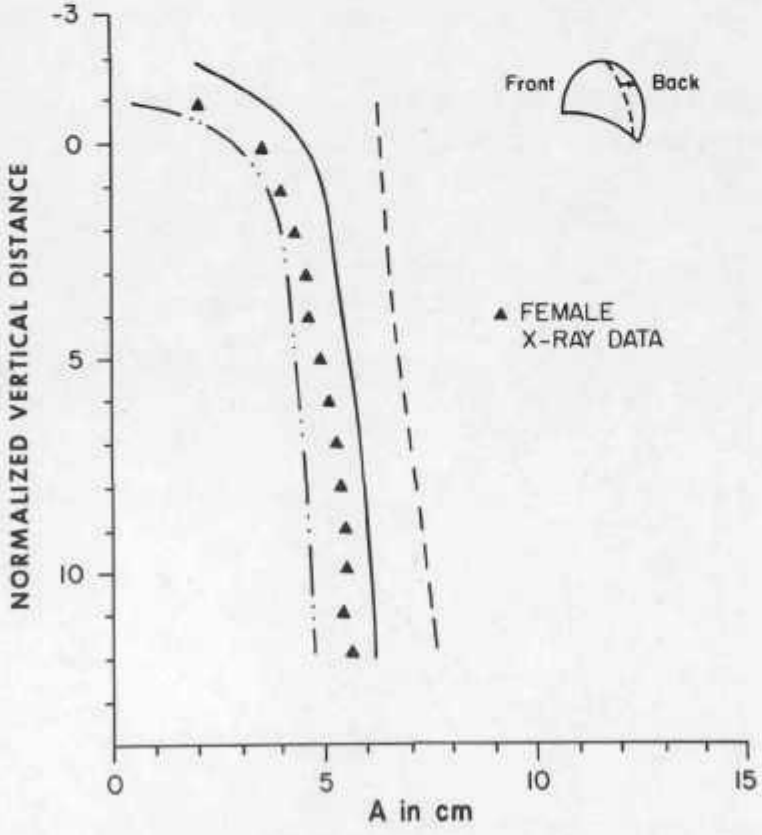

Figure C4

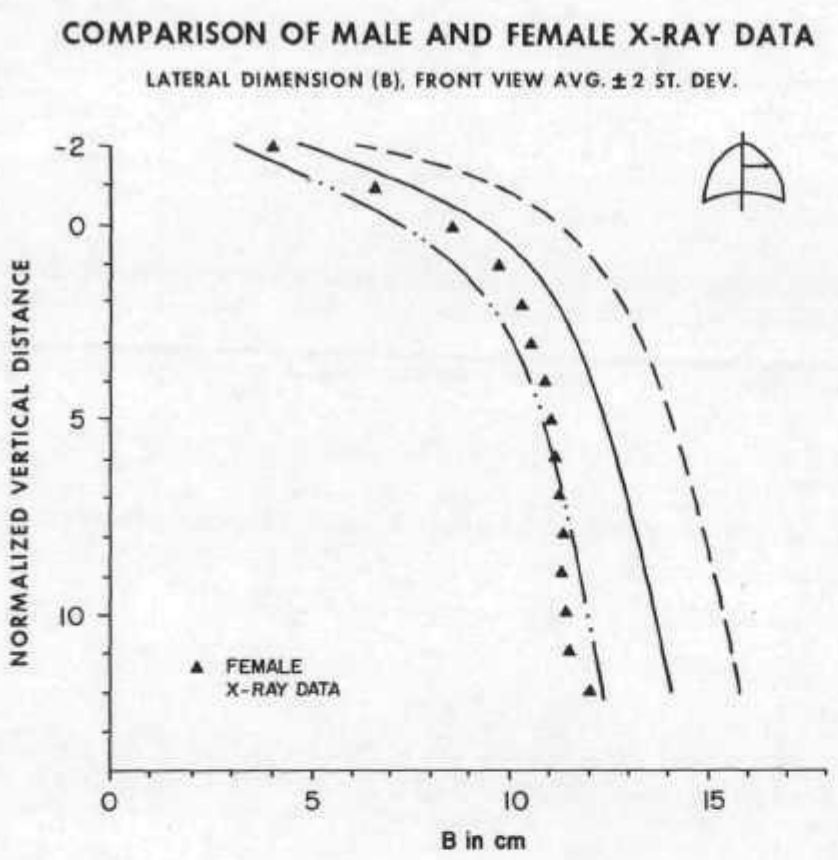

Figure C5

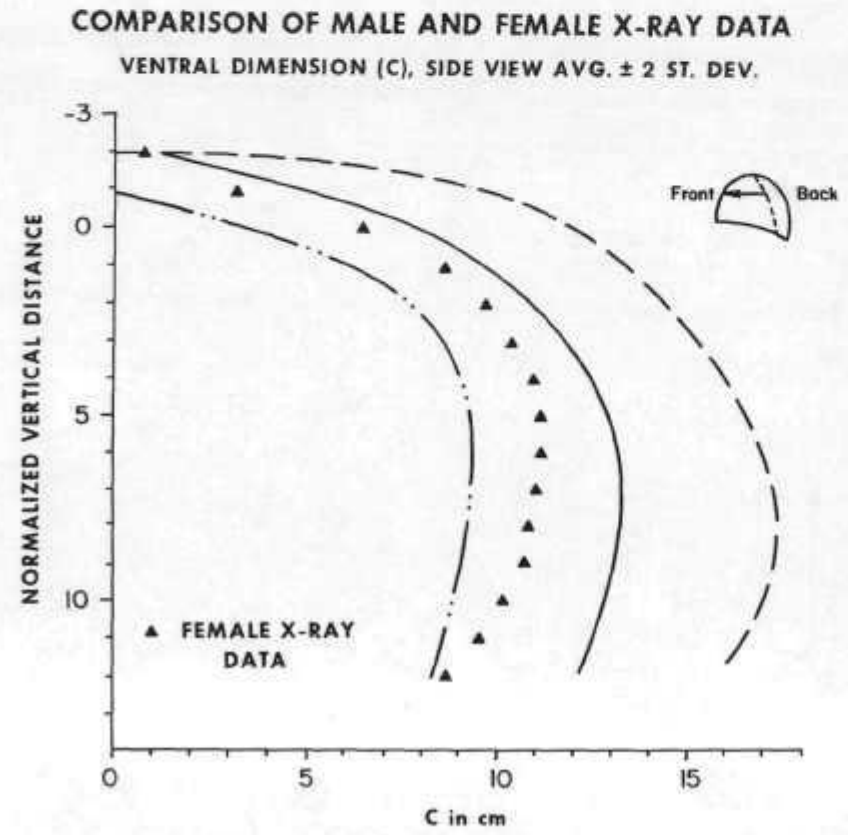

Figure C6

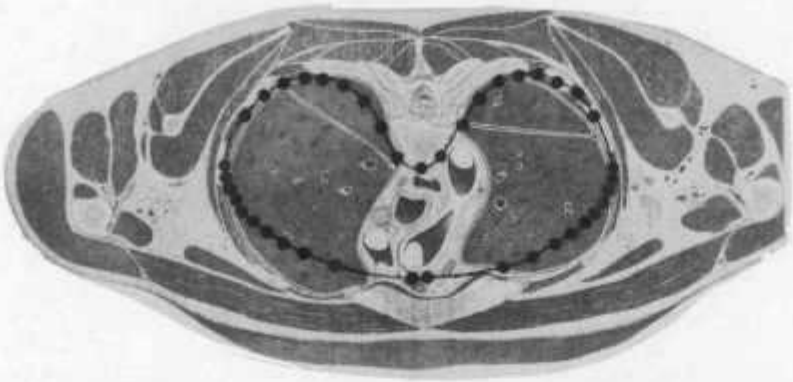

Figure C7

COMPARISON OF MODEL WITH ACTUAL SECTION

MIDDLE THORAX

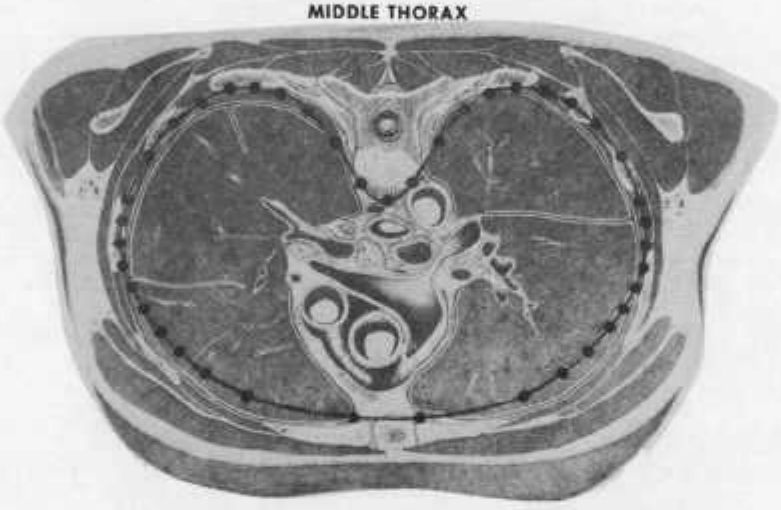

Figure C8

COMPARISON OF MODEL WITH ACTUAL SECTION

LOWER THORAX

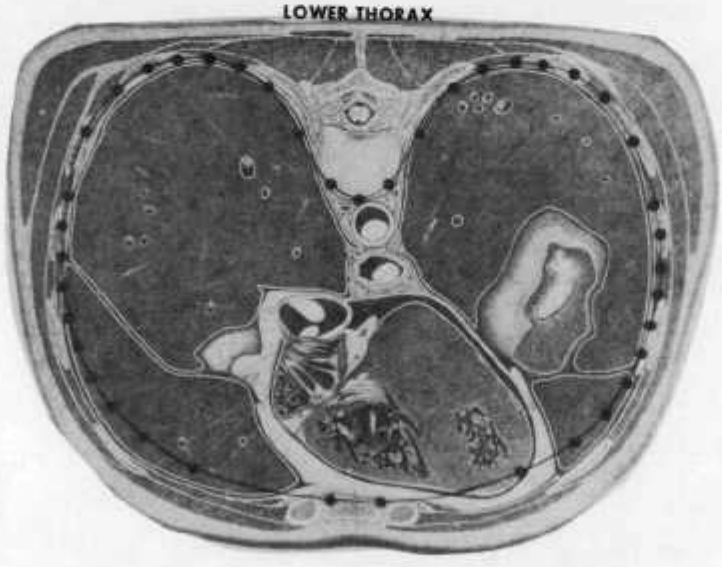

Figure C9

COMPARISON OF MODEL WITH ACTUAL SECTION

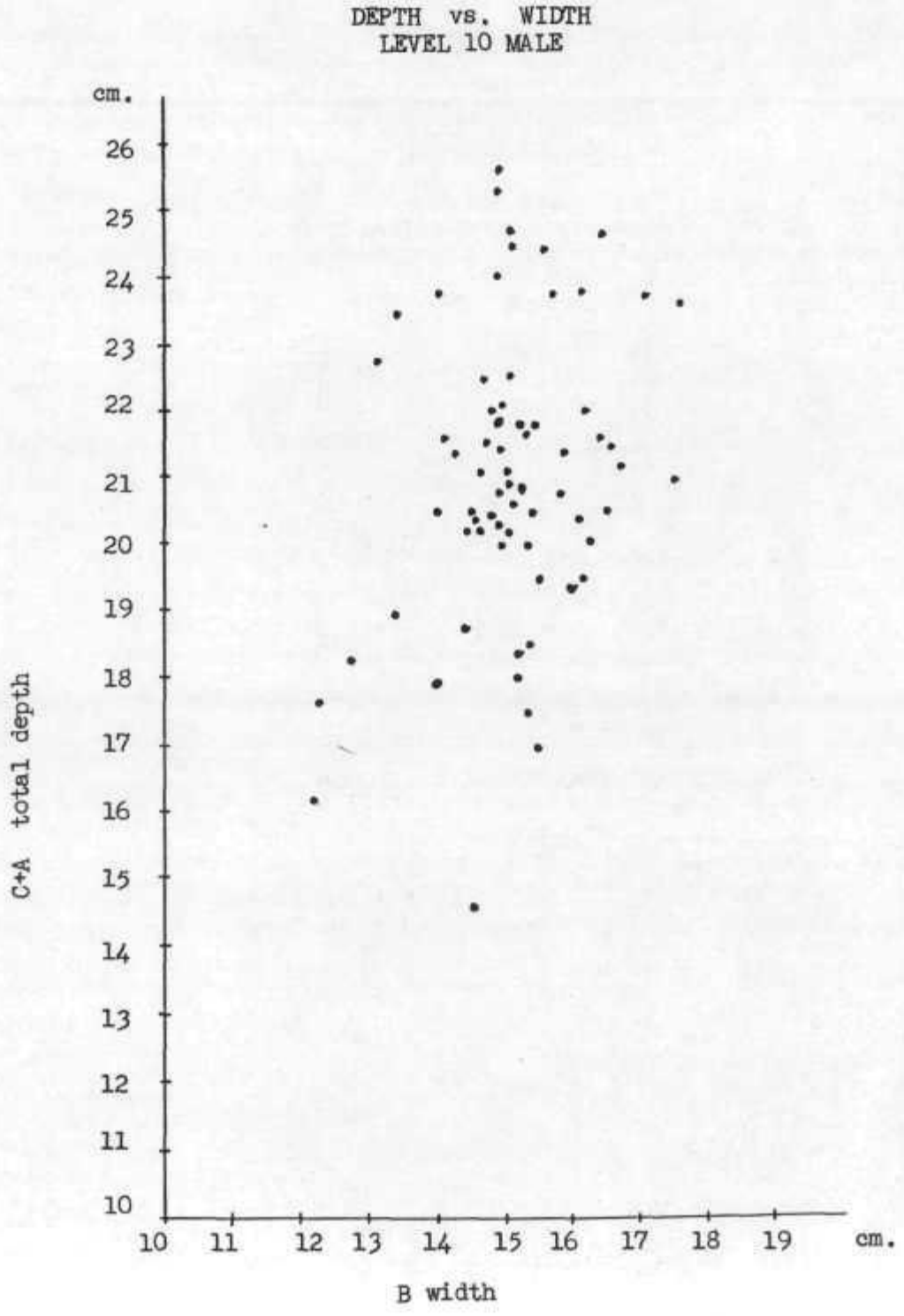
DEPTH vs. WIDTH
LEVEL 10 MALE
cm.
26
25
24
23
22
21
20
19
18
17
16
15
14
13
12
11
10
C+A total depth
10
11
12
13
14
15
16
17
18
19
cm.
B width

Figure C10

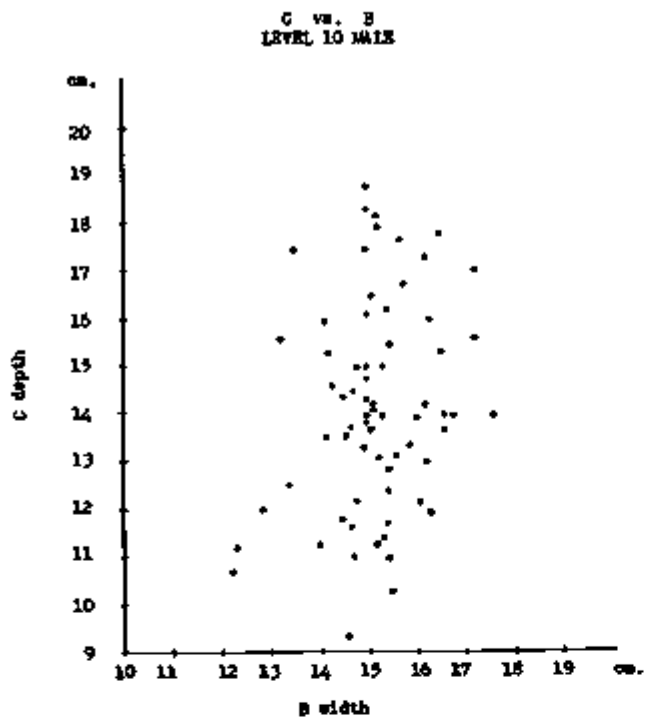

Figure C11

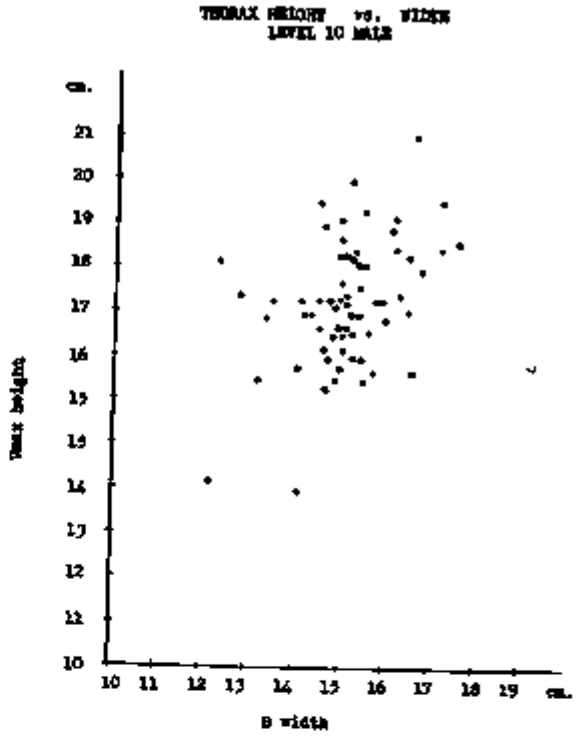

Figure C12

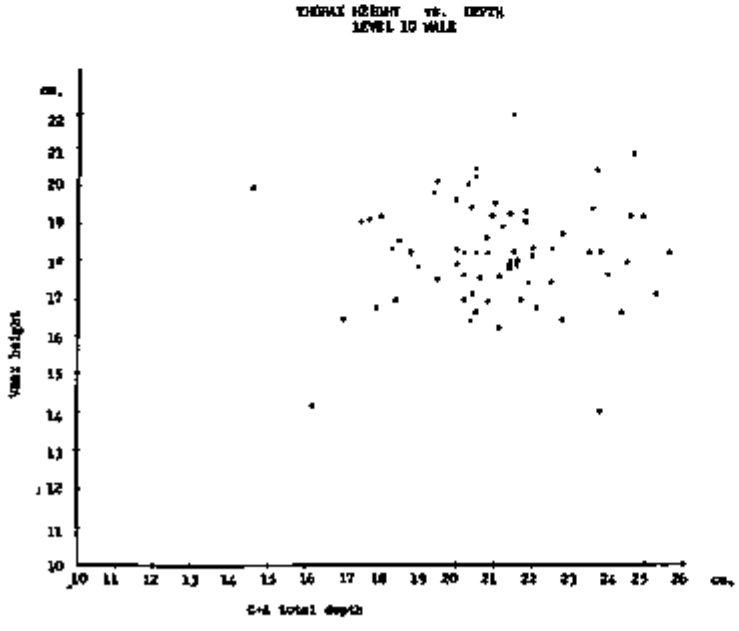

Figure C13

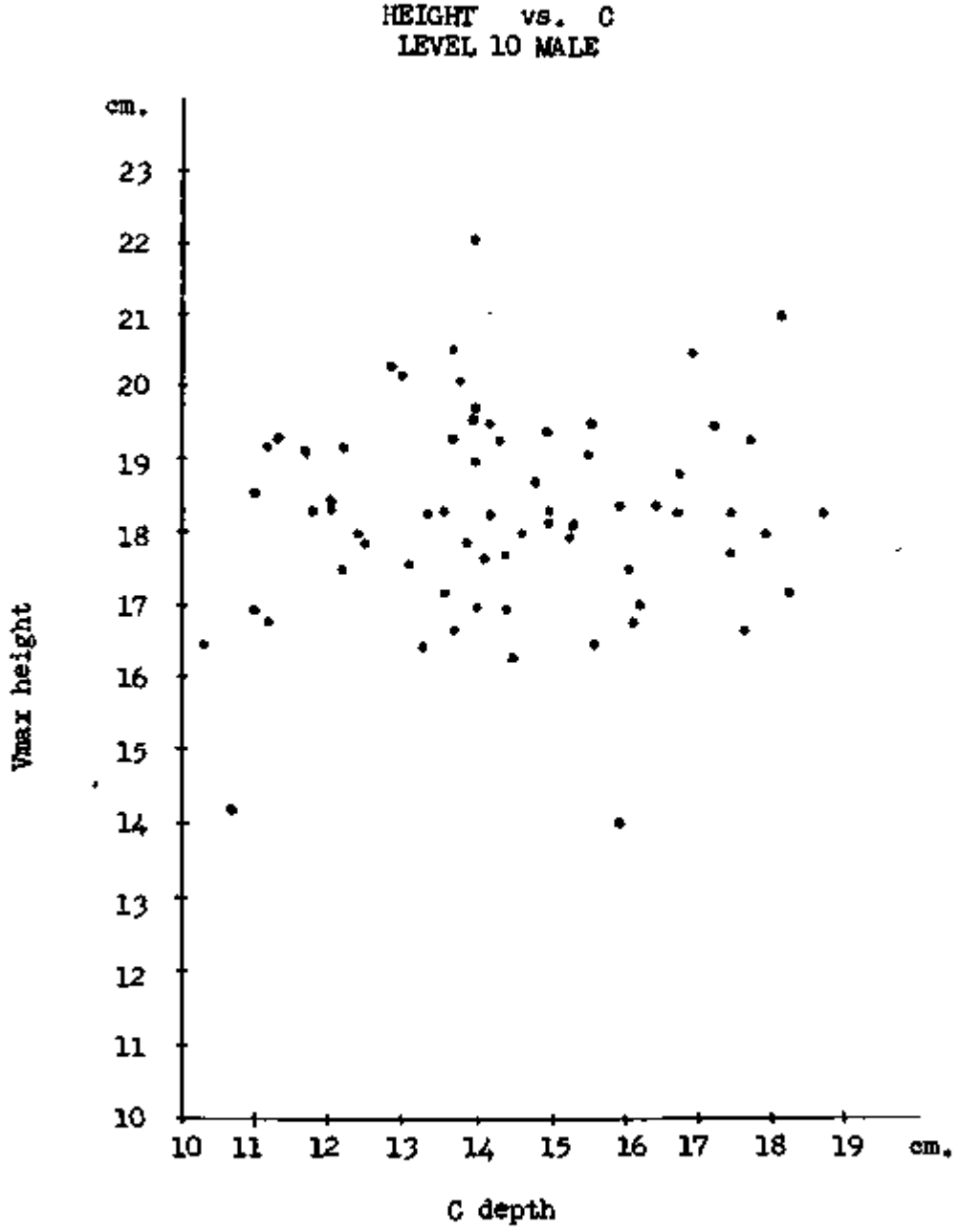
HEIGHT vs. C
LEVEL 10 MALE
cm.
23
22
21
20
19
18
17
16
15
14
13
12
11
10
Vmax height
10 11 12 13 14 15 16 17 18 19 cm.
C depth

Figure C14

APPENDIX D
PERICARDIAL SHAPE INFORMATION

Table 1

PERICARDIAL SHAPE MODEL INFORMATION

FEMALE AND MALE DATA

Pericardial Reference Level 3

	$\frac{X_a}{X_p MAX}$	$\frac{X_b}{X_p MAX}$	$\frac{Y_a}{Y_p MAX}$	$\frac{Y_b}{Y_p MAX}$
Mean	.548	.493	.492	.493
Standard Deviation	.061	.114	.132	.194
Number of Data Points	4	4	4	4

Pericardial Reference Level 4

	$\frac{X_a}{X_p MAX}$	$\frac{X_b}{X_p MAX}$	$\frac{Y_a}{Y_p MAX}$	$\frac{Y_b}{Y_p MAX}$
Mean	.465	.494	.442	.450
Standard Deviation	.092	.110	.050	.106
Number of Data Points	7	7	7	7

Pericardial Reference Level 5

	$\frac{X_a}{X_p MAX}$	$\frac{X_b}{X_p MAX}$	$\frac{Y_a}{Y_p MAX}$	$\frac{Y_b}{Y_p MAX}$
Mean	.50	.496	.407	.423
Standard Deviation	.134	.074	.081	.053
Number of Data Points	7	7	7	7

Pericardial Reference Level 8

	$\frac{X_a}{X_p MAX}$	$\frac{X_b}{X_p MAX}$	$\frac{Y_a}{Y_p MAX}$	$\frac{Y_b}{Y_p MAX}$
Mean	.441	.493	.394	.361
Standard Deviation	.115	.097	.102	.094
Number of Data Points	7	7	7	7

Table 2

FROM SPEC. # 3.00TO SPEC. # 7.00
LEFT SIDE
ANTERIOR
SLICES USED IN AVERAGE= 4.00

ZINT	AVG	STDEV	PRCT
0.0000	1.0000	0.0000	0.0000
0.1000	0.9827	0.0157	1.5990
0.2000	0.9526	0.0288	3.0215
0.3000	0.9236	0.0318	3.3779
0.4000	0.8799	0.0367	4.1747
0.5000	0.8367	0.0341	4.3173
0.6000	0.7660	0.0411	9.3866
0.7000	0.6539	0.0730	15.1636
0.8000	0.5572	0.0951	17.0707
0.9000	0.4119	0.1146	27.8800
1.0000	0.0000	0.0000	0.0000

FROM SPEC. # 3.00TO SPEC. # 7.00
LEFT SIDE
POSTERIOR
SLICES USED IN AVERAGE= 4.00

ZINT	AVG	STDEV	PRCT
0.0000	1.0000	0.0000	0.0000
0.1000	0.9608	0.0231	2.3471
0.2000	0.9682	0.0316	3.2607
0.3000	0.9177	0.0386	4.2009
0.4000	0.8593	0.0656	7.6836
0.5000	0.7816	0.1076	14.0530
0.6000	0.7098	0.1094	14.8043
0.7000	0.6367	0.0851	13.0164
0.8000	0.4813	0.1428	29.6717
0.9000	0.3266	0.1100	33.5679
1.0000	0.0000	0.0000	0.0000

FROM SPEC. # 3.00TO SPEC. # 7.00
RIGHT SIDE
ANTERIOR
SLICES USED IN AVERAGE= 4.00

ZINT	AVG	STDEV	PRCT
0.0000	1.0000	0.0000	0.0000
0.1000	0.9800	0.0040	0.4036
0.2000	0.9511	0.0193	2.0242
0.3000	0.9102	0.0463	5.0287
0.4000	0.8719	0.0716	8.2087
0.5000	0.8026	0.0974	12.0630
0.6000	0.7316	0.1260	17.2270
0.7000	0.6560	0.1747	26.7560
0.8000	0.5469	0.1778	32.4079
0.9000	0.4116	0.1928	46.6103
1.0000	0.0000	0.0000	0.0000

FROM SPEC. # 3.00TO SPEC. # 7.00
RIGHT SIDE
POSTERIOR
SLICES USED IN AVERAGE= 4.00

ZINT	AVG	STDEV	PRCT
0.0000	1.0000	0.0000	0.0000
0.1000	0.9841	0.0152	1.5490
0.2000	0.9746	0.0281	2.8831
0.3000	0.9528	0.0478	4.9041
0.4000	0.9081	0.0693	7.6319
0.5000	0.8706	0.0821	9.4236
0.6000	0.8063	0.0966	11.9797
0.7000	0.7160	0.1316	18.3800
0.8000	0.6159	0.1626	26.4017
0.9000	0.4908	0.1730	35.2467
1.0000	0.0000	0.0857	[illegible]

PERICARDIAL SHAPE MODEL

DATA P.L.3.

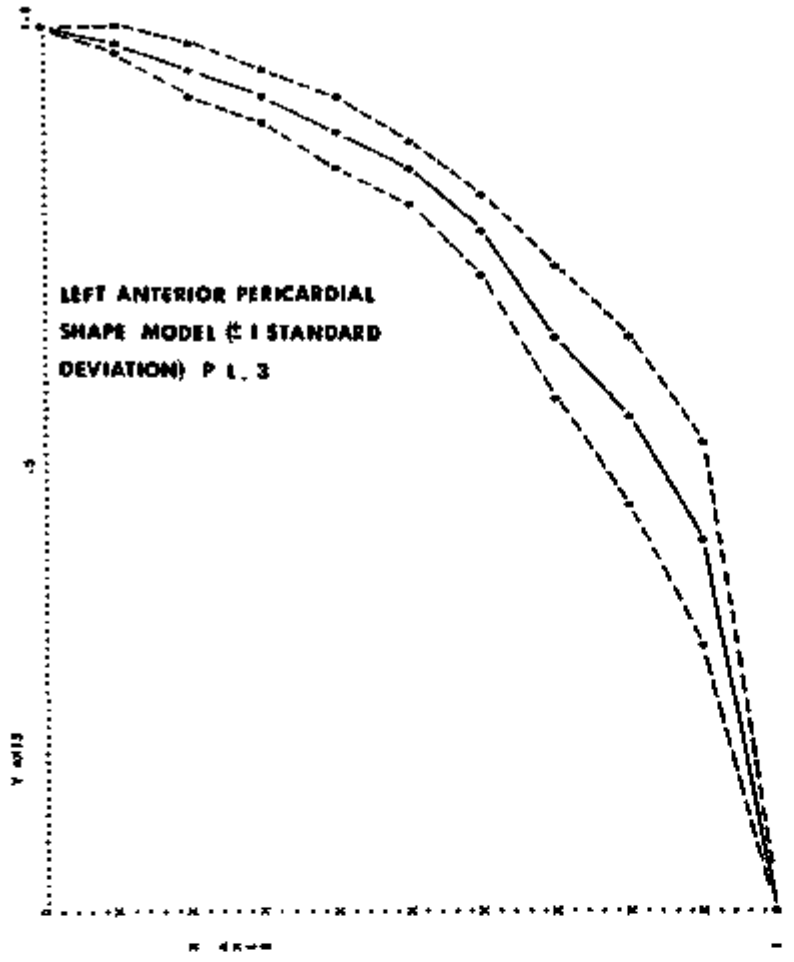

Figure 1

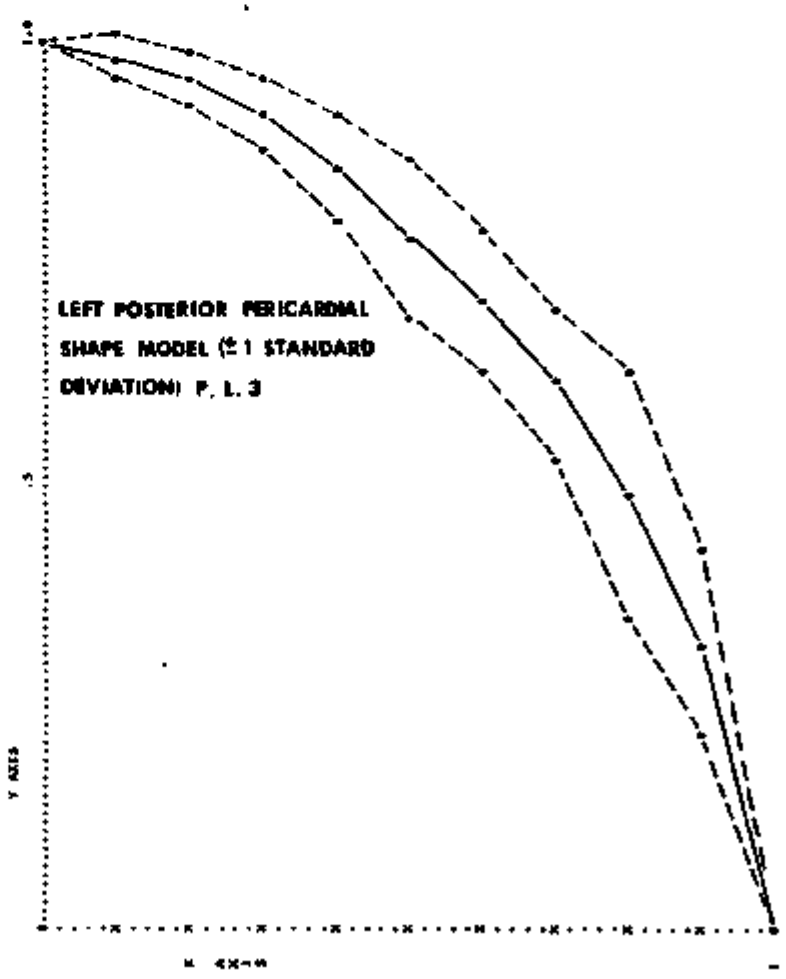

Figure 2

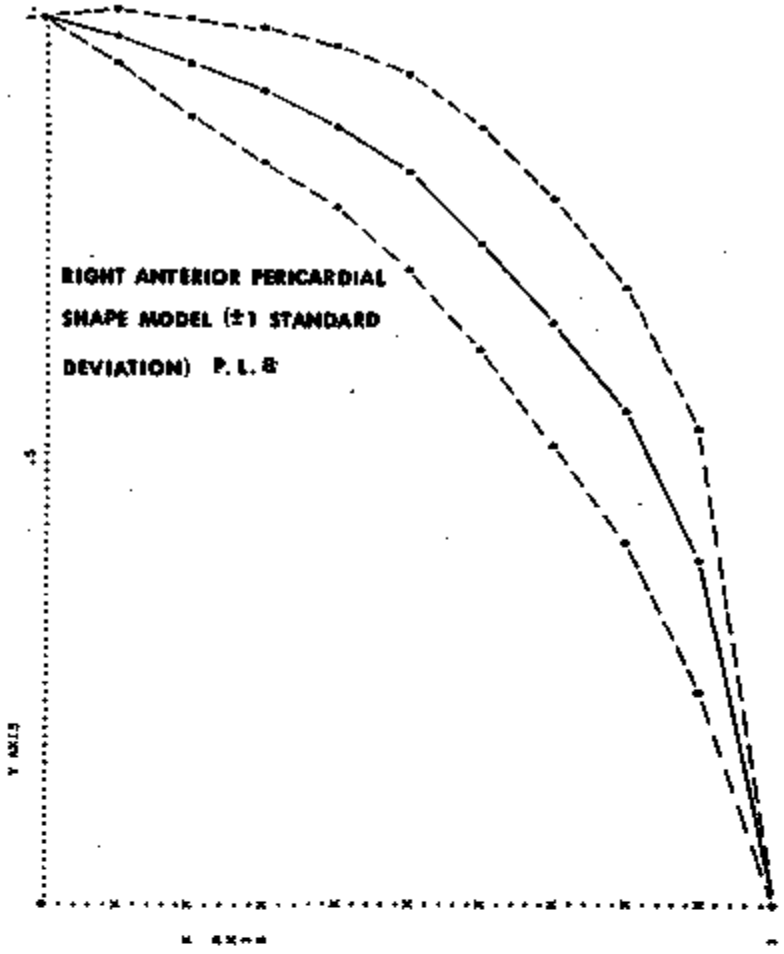

Figure 3

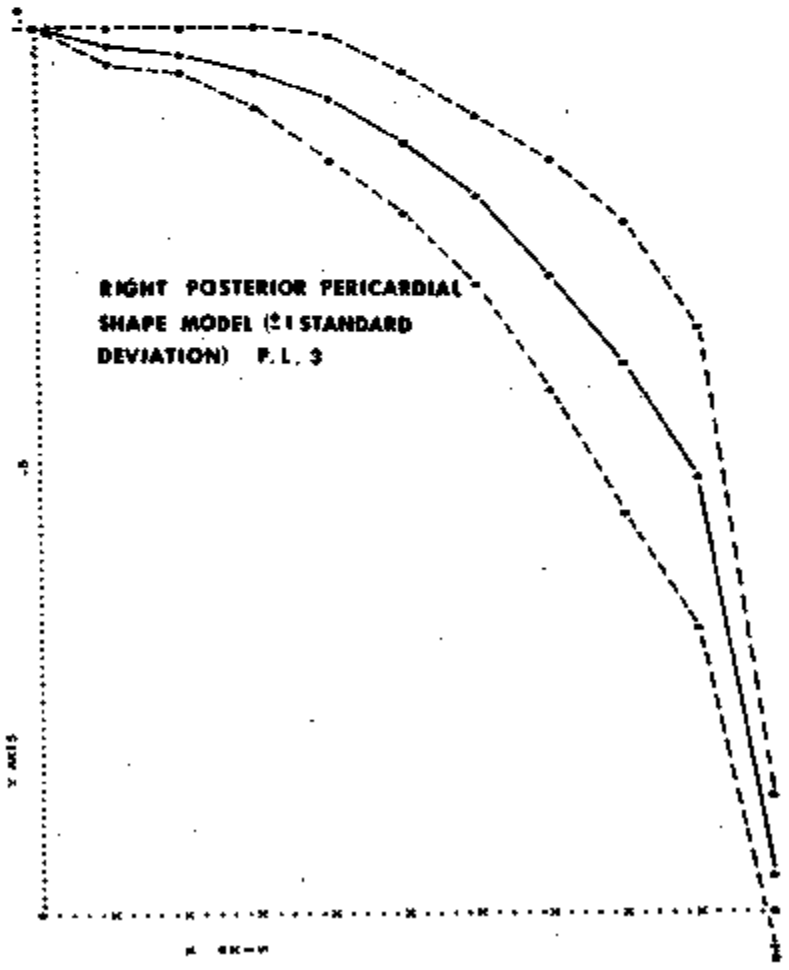

Figure 4

Table 3

FROM SPEC. # 1.00TO SPEC. # 7.00
LEFT SIDE
ANTERIOR
SLICES USED IN AVERAGE= 7.00

XINT	AVG	STDEV	PRCT
0.0000	1.0000	0.0000	0.0000
0.1000	0.9928	0.0116	1.1668
0.2000	0.9728	0.0180	1.8517
0.3000	0.9455	0.0257	2.7014
0.4000	0.9163	0.0393	4.3224
0.5000	0.8659	0.0585	6.7542
0.6000	0.8044	0.0781	9.7067
0.7000	0.7121	0.1008	14.1512
0.8000	0.5721	0.1134	19.6658
0.9000	0.3930	0.1025	26.0769
1.0000	0.0000	0.0000	0.0000

FROM SPEC. # 1.00TO SPEC. # 7.00
LEFT SIDE
POSTERIOR
SLICES USED IN AVERAGE= 7.00

XINT	AVG	STDEV	PRCT
0.0000	1.0000	0.0000	0.0000
0.1000	0.9891	0.0143	1.4434
0.2000	0.9727	0.0196	2.0120
0.3000	0.9486	0.0309	3.2900
0.4000	0.9068	0.0440	4.8603
0.5000	0.8460	0.0600	6.0326
0.6000	0.7594	0.0803	10.2661
0.7000	0.6058	0.0905	12.0712
0.8000	0.5068	0.0810	10.8037
0.9000	0.4033	0.0876	11.8216
1.0000	0.0000	0.0000	0.0000

FROM SPEC. # 1.00TO SPEC. # 7.00
RIGHT SIDE
ANTERIOR
SLICES USED IN AVERAGE= 7.00

XINT	AVG	STDEV	PRCT
0.0000	1.0000	0.0000	0.0000
0.1000	0.9888	0.0078	0.7889
0.2000	0.9638	0.0178	1.8532
0.3000	0.9366	0.0414	4.2335
0.4000	0.9055	0.0796	8.3662
0.5000	0.8602	0.1043	10.1081
0.6000	0.7948	0.1009	14.0110
0.7000	0.7136	0.1512	21.1432
0.8000	0.5951	0.1763	29.9513
0.9000	0.4029	0.1905	45.5983
1.0000	0.0000	0.0000	0.0000

FROM SPEC. # 1.00TO SPEC. # 7.00
RIGHT SIDE
POSTERIOR
SLICES USED IN AVERAGE= 7.00

XINT	AVG	STDEV	PRCT
0.0000	1.0000	0.0000	0.0000
0.1000	0.9884	0.0115	1.1616
0.2000	0.9760	0.0240	2.4613
0.3000	0.9601	0.0332	3.4585
0.4000	0.9259	0.0523	5.6548
0.5000	0.8638	0.0738	8.2864
0.6000	0.8108	0.0826	10.1980
0.7000	0.7266	0.1175	16.1725
0.8000	0.6151	0.1393	22.6265
0.9000	0.3979	0.1153	28.9659
1.0000	0.0000	0.0000	0.0000

PERICARDIAL SHAPE MODEL

DATA P.L.4

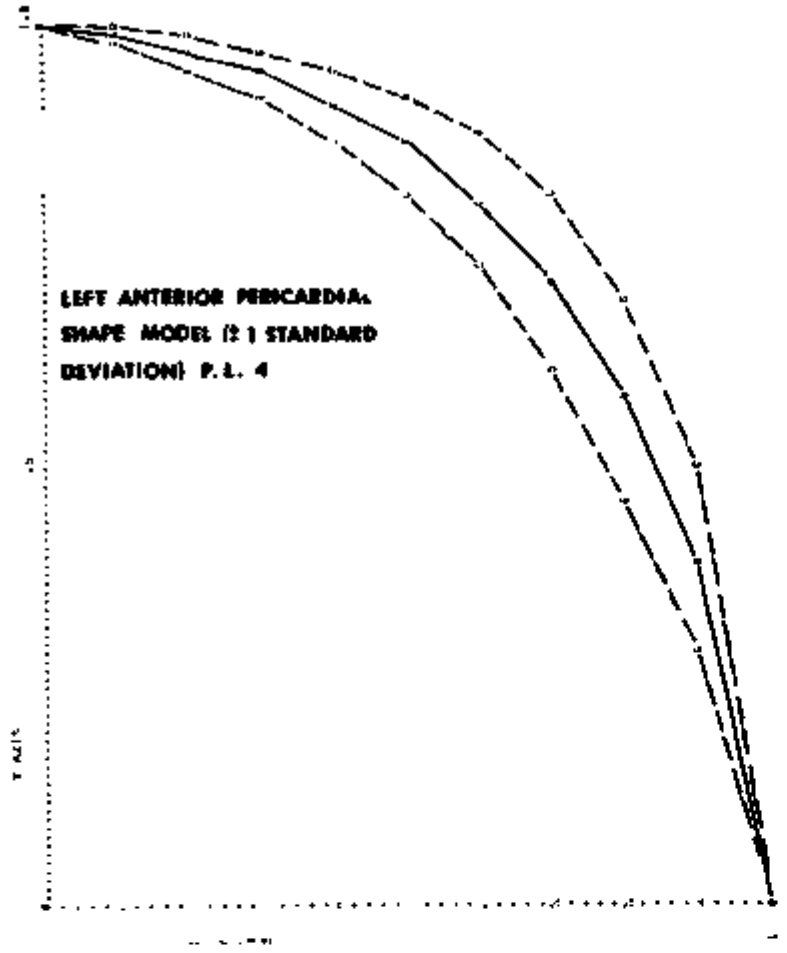

Figure 5

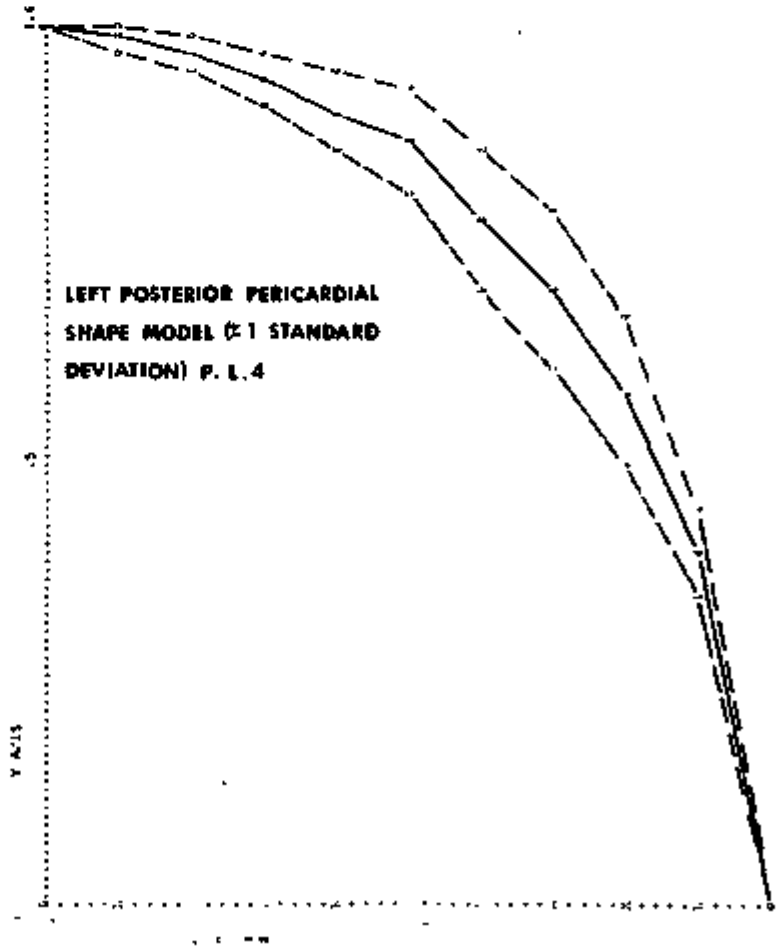

Figure 6

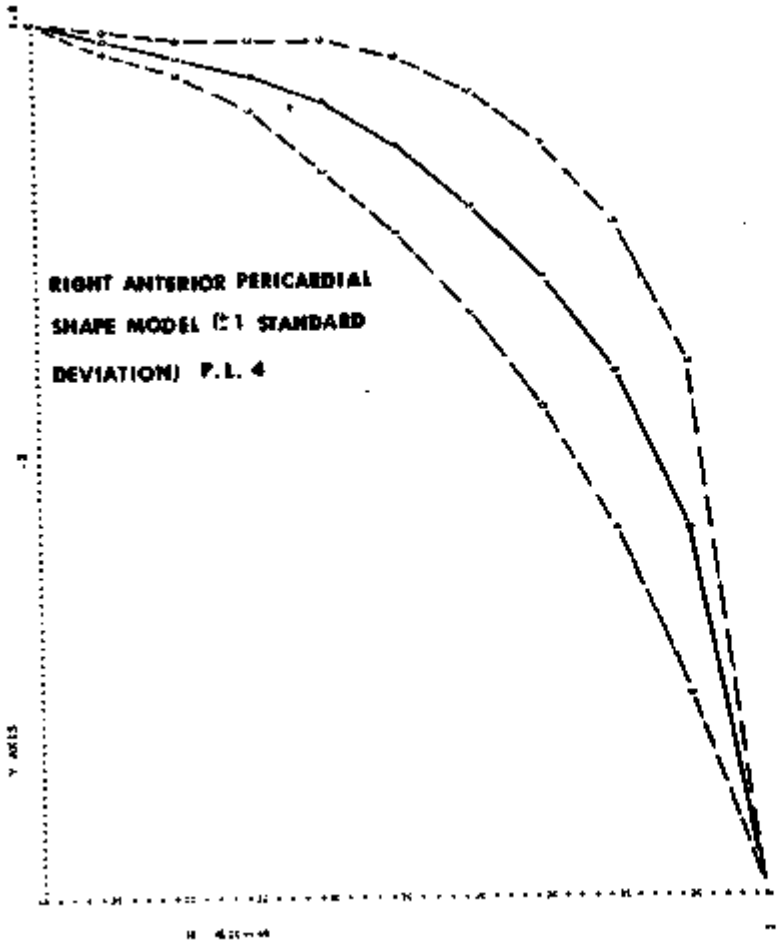

Figure 7

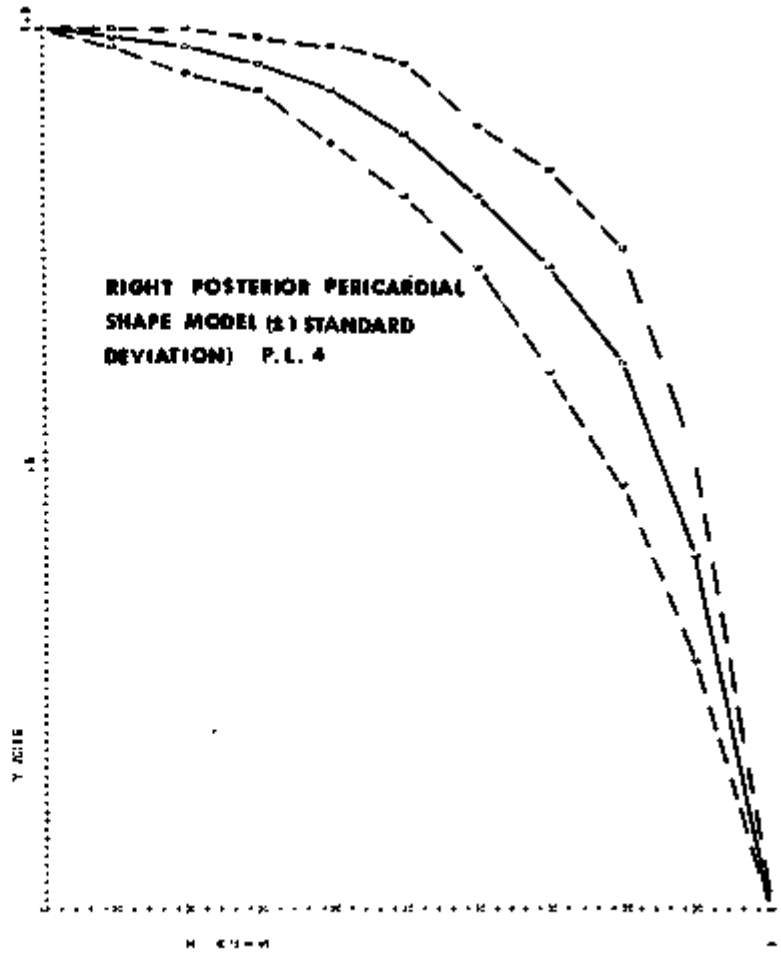

Figure 8

Table 4

PERICARDIAL SHAPE MODEL

DATA F.L.S

FROM SPEC. # 1.00TO SPEC. # 7.00
LEFT SIDE
ANTERIOR
SLICES USED IN AVERAGE= 7.00

XINT	AVG	STDEV	PRCT
0.0000	1.0000	0.0060	0.0050
0.1000	0.9949	0.0114	1.1660
0.2000	0.9752	0.0159	1.5080
0.3000	0.9403	0.0050	3.0626
0.4000	0.9135	0.0472	5.1540
0.5000	0.8767	0.0668	7.6295
0.6000	0.8201	0.0566	11.5595
0.7000	0.7460	0.0921	12.3662
0.8000	0.6381	0.0779	19.0195
0.9000	0.4484	0.1426	6.5630
1.0000	0.0000	0.0000	0.0000

FROM SPEC. # 1.00TO SPEC. # 7.00
LEFT SIDE
POSTERIOR
SLICES USED IN AVERAGE= 7.00

XINT	AVG	STDEV	PRCT
0.0000	1.0000	0.0000	0.0000
0.1000	0.9909	0.0114	1.1474
0.2000	0.9606	0.0206	2.1296
0.3000	0.9462	0.0303	3.2213
0.4000	0.9069	0.0030	4.7301
0.5000	0.8693	0.0374	6.0164
0.6000	0.8076	0.0551	6.0103
0.7000	0.7292	0.0546	6.2032
0.8000	0.6145	0.0737	11.9937
0.9000	0.4324	0.0580	12.9421
1.0000	0.0000	0.0000	0.0000

FROM SPEC. # 1.00TO SPEC. # 7.00
RIGHT SIDE
ANTERIOR
SLICES USED IN AVERAGE= 7.66

XINT	AVG	STDEV	PRCT
0.0000	1.0000	0.0000	0.0060
0.1000	0.9636	0.0134	1.2573
0.2000	0.9060	0.0605	2.5017
0.3000	0.9412	0.0360	3.6000
0.4000	0.9177	0.0510	5.5301
0.5000	0.8760	0.0705	6.0777
0.6000	0.8199	0.0500	10.9811
0.7000	0.7422	0.1173	15.2617
0.8000	0.6266	0.1421	22.3376
0.9000	0.4407	0.1701	36.5901
1.0000	0.0000	0.0000	0.0000

FROM SPEC. # 1.00TO SPEC. # 7.00
RIGHT SIDE
POSTERIOR
SLICES USED IN AVERAGE= 7.66

XINT	AVG	STDEV	PRCT
0.0000	1.0000	0.0044	0.0000
0.1000	0.9807	0.0056	0.9533
0.2000	0.9741	0.0207	2.1305
0.3000	0.9556	0.0287	2.6546
0.4000	0.9407	0.0012	4.4761
0.5000	0.8733	0.0624	7.1062
0.6000	0.7523	0.0555	7.5600
0.7000	0.7012	0.0916	14.5621
0.8000	0.5615	0.1017	17.4063
0.9000	0.3648	0.0310	6.7640
1.0000	0.0000	0.0000	0.0000

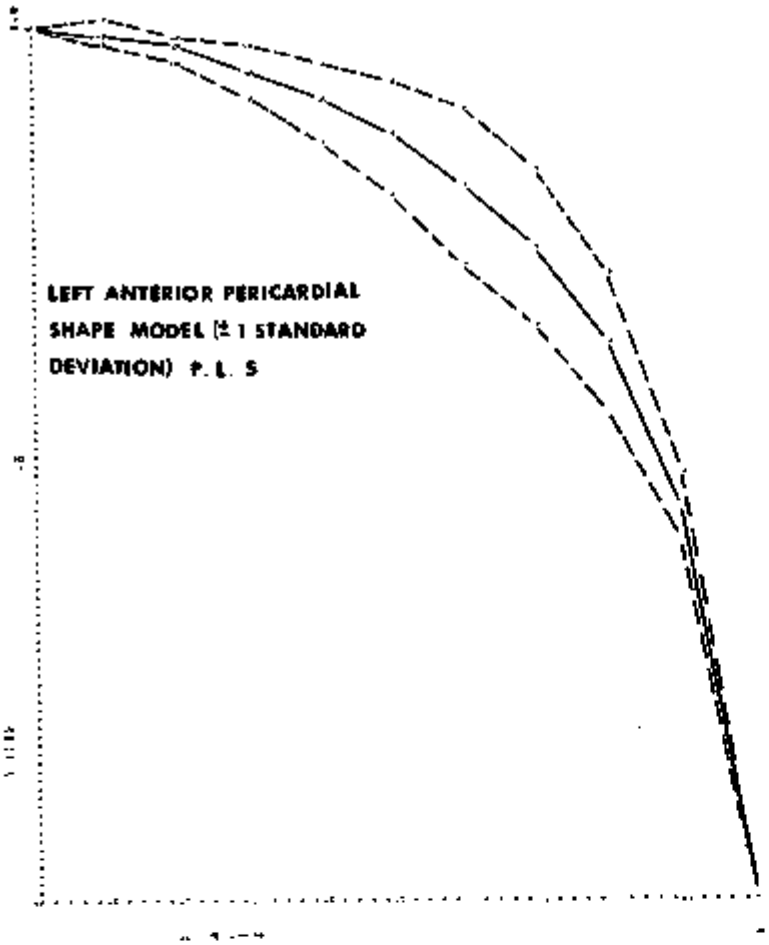

Figure 9

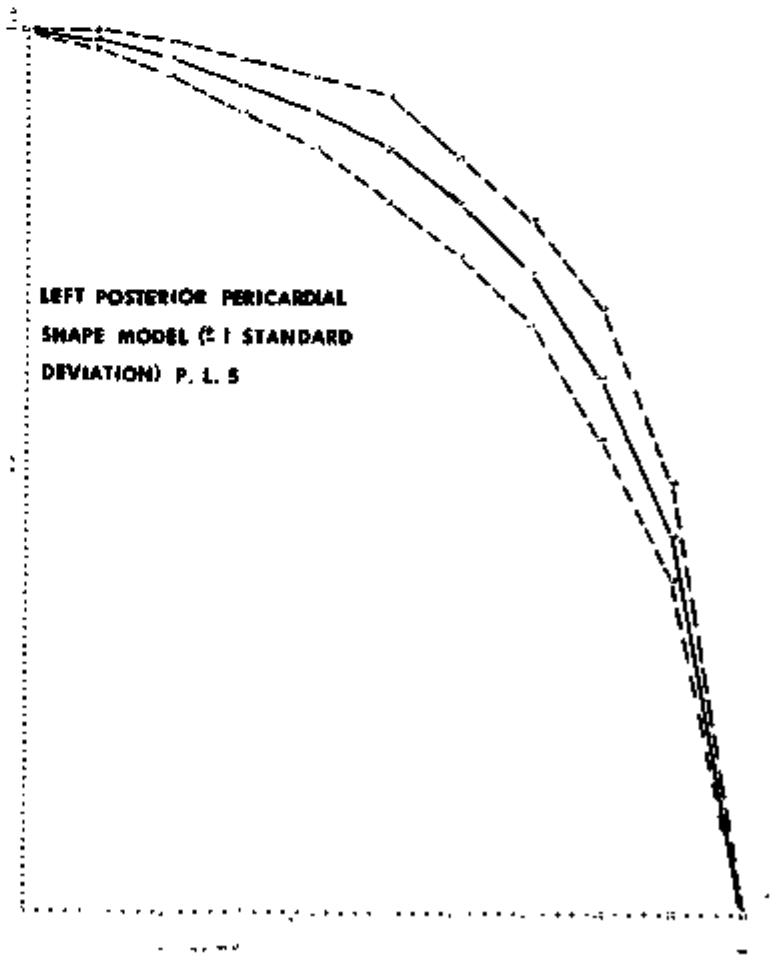

Figure 10

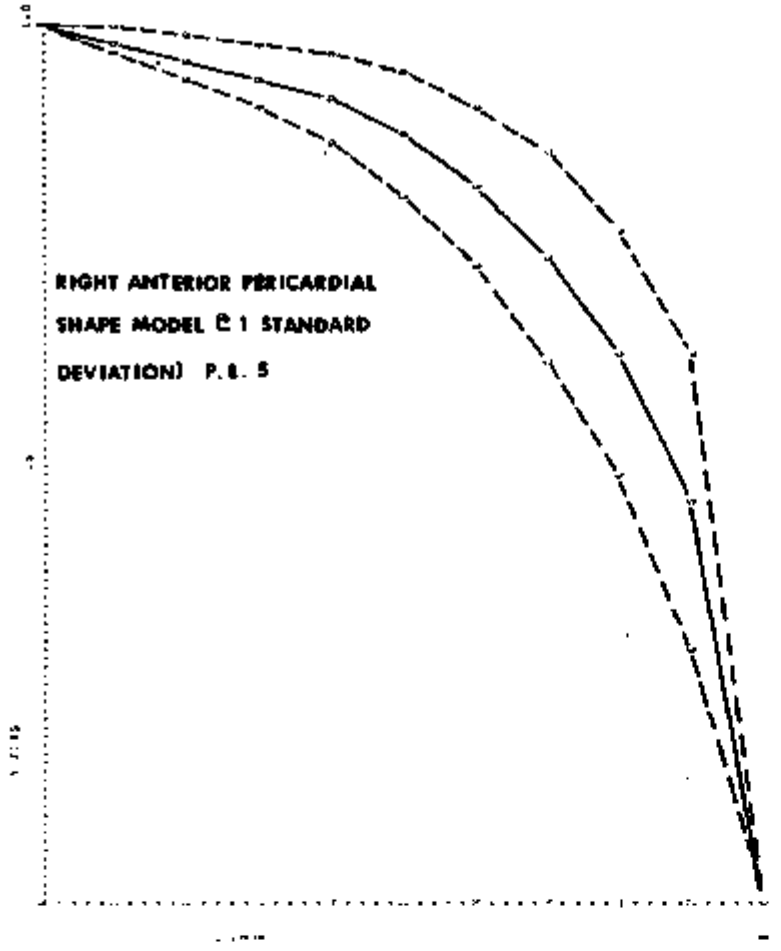

Figure 11

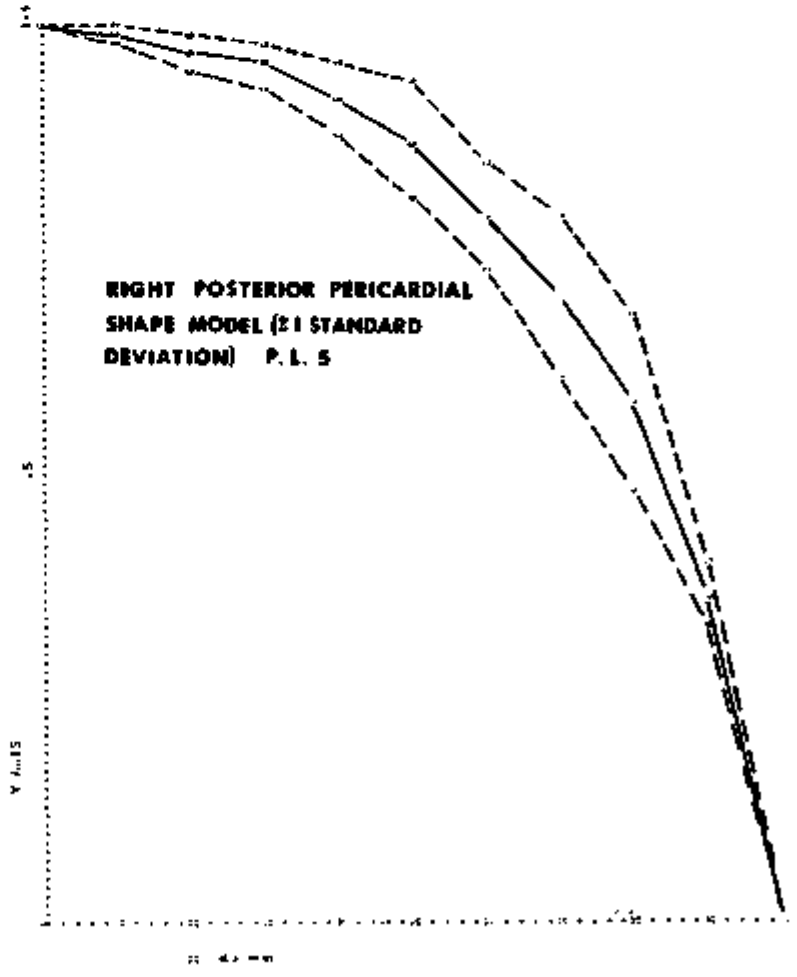

Figure 12

Table 5

FROM SPEC. # 1.0000 TO SPEC. # 7.00
LEFT SIDE
ANTERIOR
SLICES USED IN AVERAGE= 7.00

XINT	AVG	STDEV	PRCT
0.0000	1.0000	0.0000	0.0000
0.1000	0.9865	0.0281	2.8356
0.2000	0.9759	0.0279	2.8565
0.3000	0.9643	0.0279	2.8974
0.4000	0.9498	0.0366	3.7449
0.5000	0.9314	0.0498	5.2718
0.6000	0.8505	0.0592	6.9698
0.7000	0.7934	0.0882	11.1185
0.8000	0.7117	0.1327	16.6478
0.9000	0.5814	0.1567	31.0547
1.0000	0.0000	0.0000	0.0000

FROM SPEC. # 1.0000 SPEC. # 7.00
LEFT SIDE
POSTERIOR
SLICES USED IN AVERAGE= 7.00

XINT	AVG	STDEV	PRCT
0.0000	1.0000	0.0000	0.0000
0.1000	0.9817	0.0158	1.6064
0.2000	0.9537	0.0304	0.3734
0.3000	0.9281	0.0386	0.1573
0.4000	0.8927	0.0495	5.5449
0.5000	0.8299	0.0769	9.1541
0.6000	0.7488	0.1083	10.8575
0.7000	0.6469	0.1194	14.4003
0.8000	0.5046	0.1134	22.3681
0.9000	0.3471	0.1049	30.9264
1.0000	0.0000	0.0000	0.0000

FROM SPEC. # 1.0000 SPEC. # 7.00
RIGHT SIDE
ANTERIOR
SLICES USED IN AVERAGE= 7.00

XINT	AVG	STDEV	PRCT
0.0000	1.0000	0.0000	0.0000
0.1000	0.9160	0.0306	3.1324
0.2000	0.9465	0.0552	5.8033
0.3000	0.9183	0.0750	8.1619
0.4000	0.8609	0.0903	10.5945
0.5000	0.8292	0.1092	13.1724
0.6000	0.7558	0.1287	16.6161
0.7000	0.6649	0.1433	21.3383
0.8000	0.3584	0.1461	36.1439
0.9000	0.3981	0.1531	38.2882
1.0000	0.0000	0.0000	0.0000

FROM SPEC. # 1.0000 SPEC. # 7.00
RIGHT SIDE
POSTERIOR
SLICES USED IN AVERAGE= 7.00

XINT	AVG	STDEV	PRCT
0.0000	1.0000	0.0000	0.0000
0.1000	0.9909	0.0097	0.9813
0.2000	0.9657	0.0133	1.3810
0.3000	0.9380	0.0256	2.7568
0.4000	0.8923	0.0710	7.9877
0.5000	0.8462	0.0981	11.5945
0.6000	0.7867	0.1270	16.1693
0.7000	0.7481	0.1514	21.3876
0.8000	0.6072	0.1692	27.8527
0.9000	0.3982	0.1681	38.1700
1.0000	0.0000	0.0000	0.0000

PERICARDIAL SHAPE MODEL

DATA P.L.S

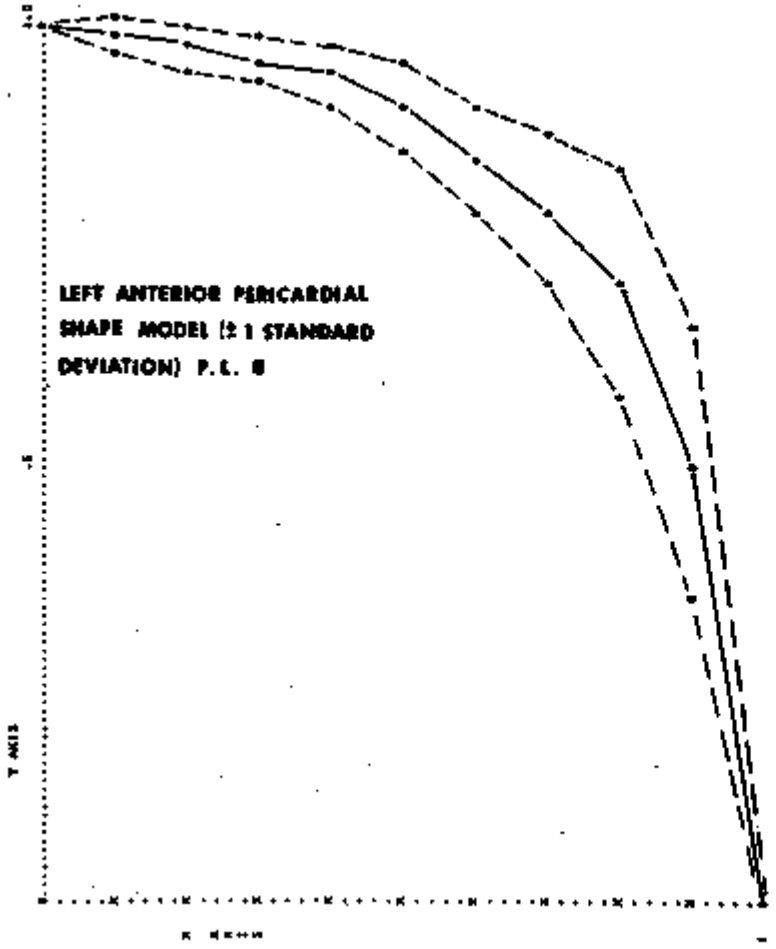

Figure 13

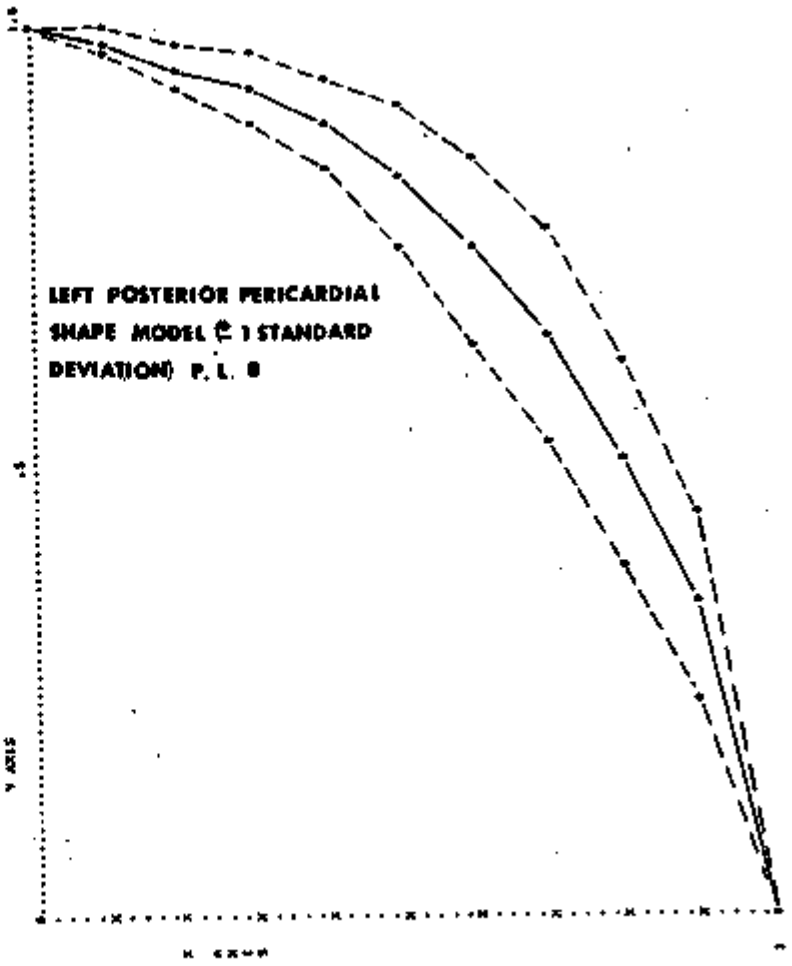

Figure 14

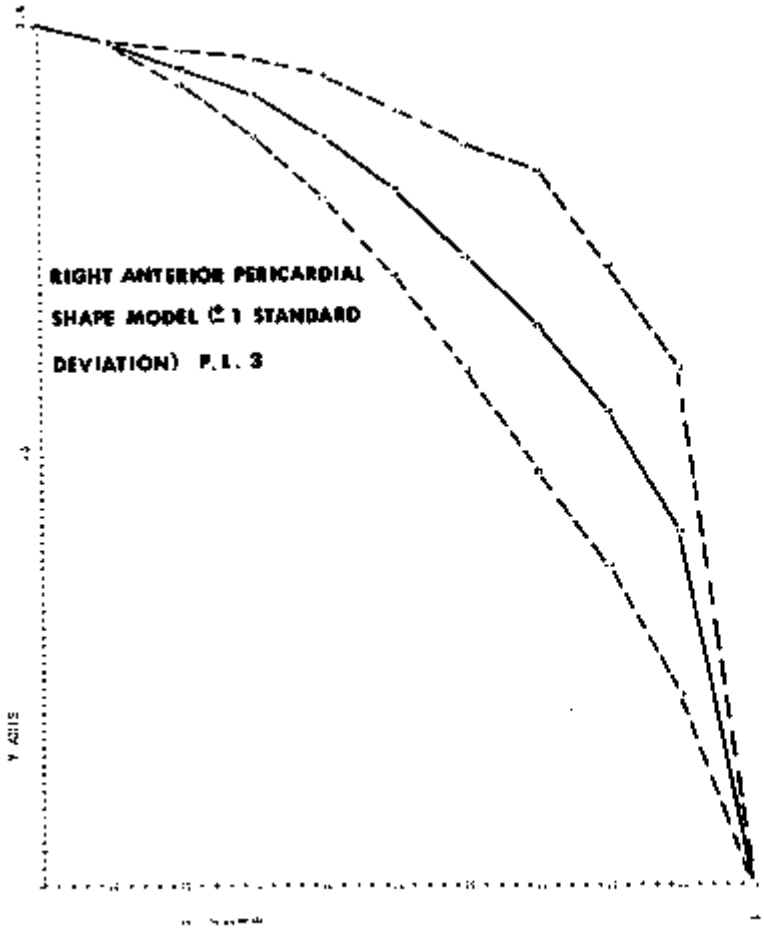

Figure 15

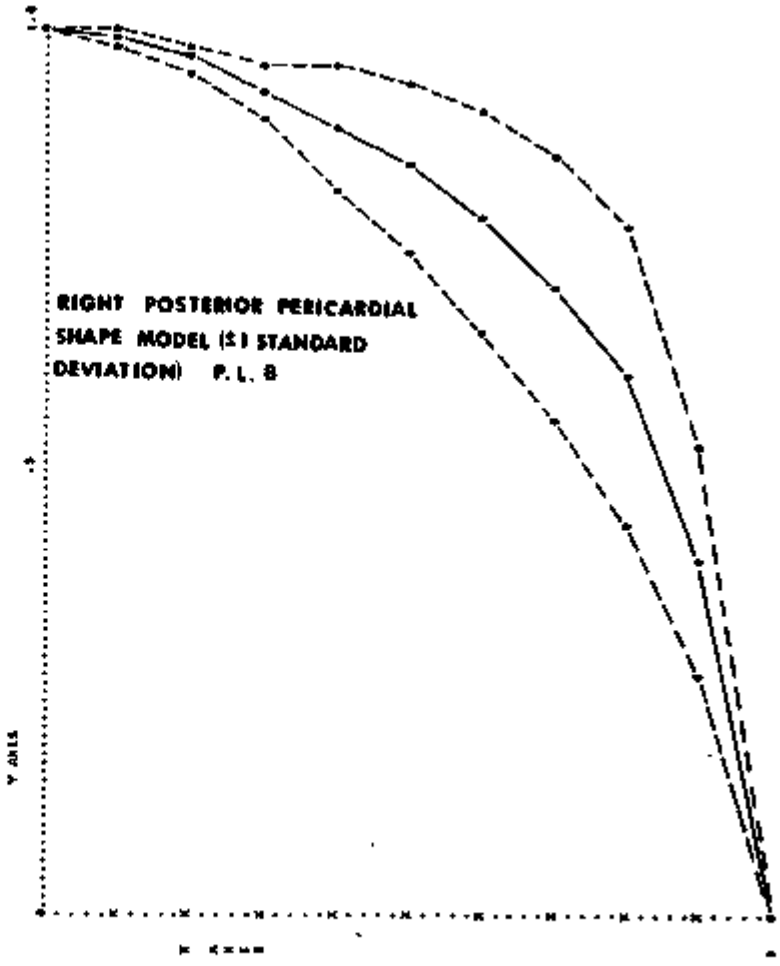

Figure 16

APPENDIX E

INDIRECT METHOD FOR VERIFYING VASCULAR CONNECTION LOCATION

The scarcity of radiograms of patients with prosthetic tricuspid and pulmonary valves necessitated development of a supplementary method for locating these particular anastomosis points for a total artificial heart. Application of the method depends upon accurate knowledge of two valves in each of the three dimensions. Using these dimensions (for mitral and aortic valves) and an "intravalvular model" described below, the other two valve locations were calculated. A flow chart of the technique is shown in Figure E1. Blocks 1 and 2 provide data for the absolute distance between the aortic and mitral valves, while both cadavers and published anatomy data provide a base for the intravalvular model.

A. Description of Intravalvular Model

The purpose of this model is to establish a three dimensional spatial relationship between the valves so that knowledge of two valves allows predictions to be made on the other two. Figure E2 will be used to help describe the approach for the x direction. Three equations define the following variables:

$$\text{(Equation 1)} \quad M_x = T_m - T_A$$

$$\text{(Equation 2)} \quad R_1{}^x = \frac{T_A}{T_M}$$

$$\text{(Equation 3)} \quad R_2{}^x = \frac{T_p}{T_M}$$

where M and R refer, in general, to absolute measurements and ratios respectively. M_x has been determined from cadavers or radiograms with two or more prosthetic valves visible in both the P-A and lateral views. The ratios $R^x{}_1$ and $R^x{}_2$ are derived from either cadavers or published sections of frozen cadaver slices in which all four valves are superimposed ("overlayed") into each of the three dimensions. The three equations can now be solved for the three unknowns (T_M, T_A and T_B).

First, eliminating T_M using equations 1 and 2:

$$M_x = T_M - T_A = \left[\frac{T_A}{R_1{}^x} - T_A\right] = T_A\left[\frac{1}{R_1{}^x} - 1\right]$$

$$\text{(Equation 4)} \quad T_A = \frac{M_x\, R_1{}^x}{1 - R_1{}^x}$$

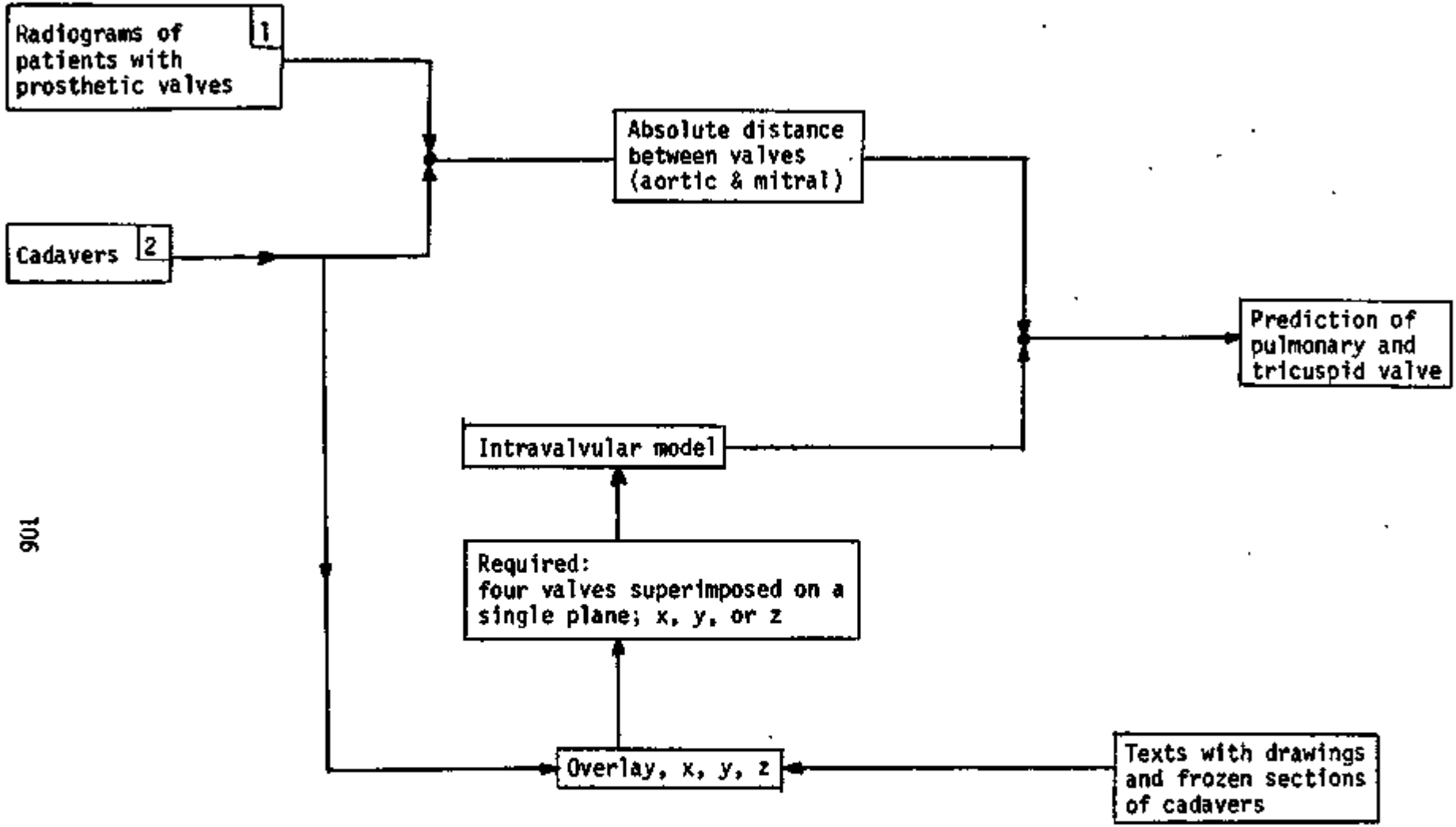

INDIRECT APPROACH FOR LOCATING PULMONARY AND TRICUSPID VALVES

Figure E1

ANATOMY OVERLAY METHOD

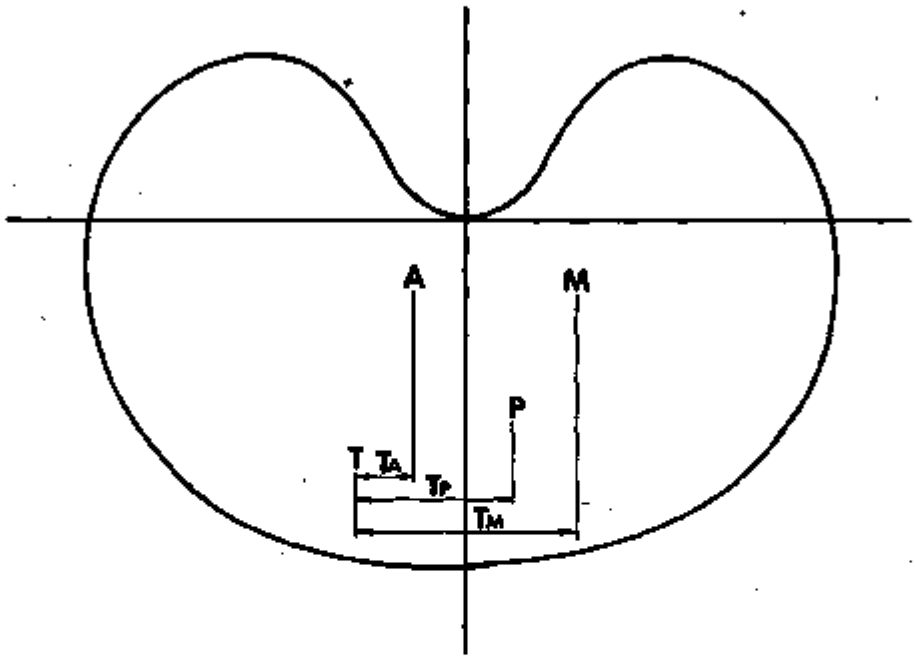

Transverse slice

Figure E2

This locates the tricuspid valve. Equation 3 can then be used to solve for T_p, the dimension specifying the pulmonary valve.

$$\text{(Equation 5)} \quad T_p = R_2^x T_M = \frac{R_2^x T_A}{R_1^x}$$

The same method is used in the y and z dimensions (Figure E3). Necessary additional ratio information (R_1^y, R_2^y, R_1^z and R_2^z) are defined below, along with the accompanying equation for the M variable.

$$\text{(Equation 6)} \quad M_y = P_m - P_A$$

$$\text{(Equation 7)} \quad R_1^y = P_A / P_m$$

$$\text{(Equation 8)} \quad R_2^y = P_T / P_m$$

$$\text{(Equation 9)} \quad M_z = P_m - P_A$$

$$\text{(Equation 10)} \quad R_1^z = P_A / P_T$$

$$\text{(Equation 11)} \quad R_2^z = P_m / P_T$$

B. Results

For the sake of comparison, data for the intravalvular was divided into two groups: overlays of frozen cadaver sections and overlays of artists drawings of cadavers. Hence, ratio values for the model (R_1^x, R_2^x, etc.) can be found in Tables E1 and E2. Distances between the values (M_x, M_y, etc.) are shown in Table E3. Predictions based on these last three tables are presented in Section 5.0. Table E4 shows overlay results when referenced to the chest wall in the x direction only. This allows some estimation of the values if pericardium is not visible.

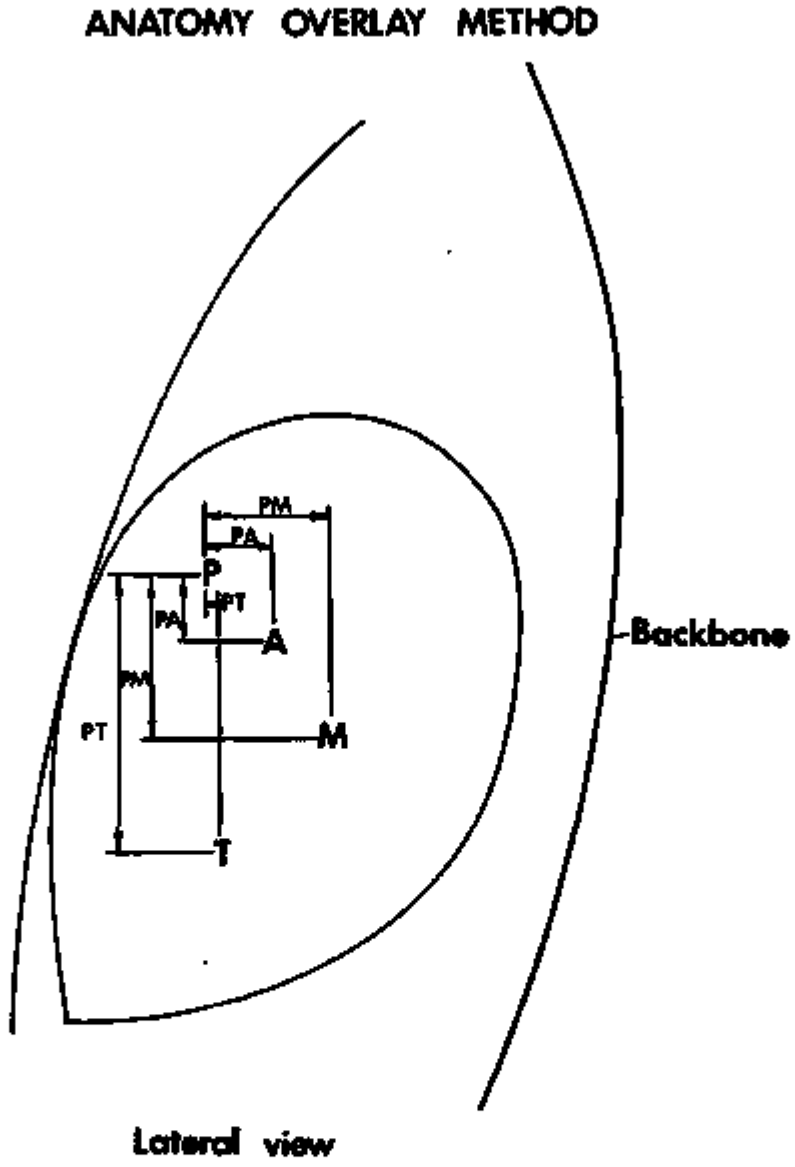
ANATOMY OVERLAY METHOD
PM
PA
P
PT
PA
A
PM
PT
M
T
Backbone
Lateral view

Ffgure E3

Table E1

Intravalvular Model

Variables	Anatomy Overlays (male and female)					
	x dimension		y dimension		z dimension	
	$R_1^x = \frac{T_A}{T_M}$	$R_2^x = \frac{T_P}{T_M}$	$R_1^y = \frac{P_A}{P_M}$	$R_2^y = \frac{P_T}{P_M}$	$R_1^z = \frac{P_A}{P_T}$	$R_2^z = \frac{P_M}{P_T}$
mean	.21	.955	.581	.183	.397	.684
S.D.	.286	.409	-	-	-	-
NDAPTS	8	8	1	1	1	1

Table E2

Intravalvular Model

Variables	Published drawings of cadavers					
	x dimension		y dimension		z dimension	
	$R_1^x = \frac{T_A}{T_M}$	$R_2^x = \frac{T_P}{T_M}$	$R_1^y = \frac{P_A}{P_M}$	$R_2^y = \frac{P_T}{P_M}$	$R_1^z = \frac{P_A}{P_T}$	$R_2^z = \frac{P_M}{P_T}$
mean	.565	.894	.39	.54	.304	.612
S.D.	.16	.084	-	-	.073	.068
NDAPTS	5	5	1	1	9	9

Table E3

Distance Between Valves

Variables	Radiograms of patients with prosthetic valves					
	Aortic to mitral (males only) in cm			Tricuspid to mitral (male and female) in cm		
	M_x	M_y	M_z	x	y	z
mean	1.26	2.47	1.46	3.08	3.14	.82
S.D.	1.16	.633	.536	1.58	.905	.738
NDAPTS	9	8	9	3	2	3

Table E4

Valve Locations Referenced to Chest Wall

Variables	x direction only (male and female)			
	$\frac{A_{CHMID}}{B}$	$\frac{P_{CHMID}}{B}$	$\frac{T_{CHMID}}{B}$	$\frac{M_{CHMID}}{B}$
mean	+.0075	+.156	-.029	+.17
S.D.	.061	.077	.095	.096
NDAPTS	8	8	8	8

APPENDIX F

VALVE ORIENTATION METHOD

Data for the angle or orientation of the valves is summarized in Table F1. Figures in Section 8.0 do not refelct this data. As shown in Figure F1, $Mangle_x$ is the angle between the central flow axis (i.e., direction of flow) and the horizontal.

Table F1

Valve Orientation Data
(Males Only)

	Aortic Valve		Mitral Valve		Tricuspid Valve	Pulmonary Valve
Variables	A $ANGLE_x$	A $ANGLE_y$	M $ANGLE_x$	M $ANGLE_y$	T $ANGLE_x$	P $ANGLE_x$
Mean	125	90.6	150.9	19.8	167	100.5
S.D.	11.4	12.2	9.2	6.6	6.09	14.01
NDAPTS	16	15	12	10	4	4

VALVE ORIENTATION METHOD

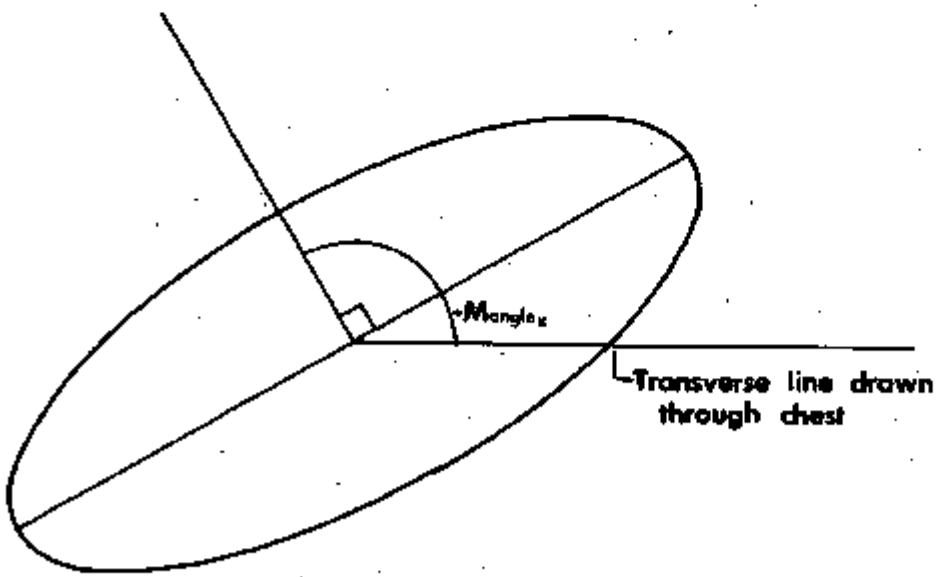

Figure F1

Mitral valve (P-A view)

APPENDIX G
GREAT VESSEL RATIO DATA

SUPERIOR VENA CAVA REFERENCED TO PERICARDIUM VS PERICARDIAL LEVEL (P-A VIEW)

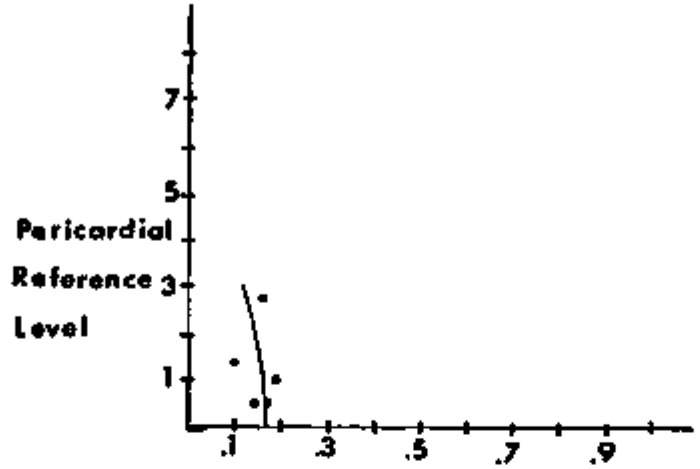

SUPERIOR $\frac{VC_x^P}{X_{pmax}}$

Figure E1

SUPERIOR VENA CAVA REFERENCED TO PERICARDIUM vs PERICARDIAL LEVEL (LATERAL VIEW)

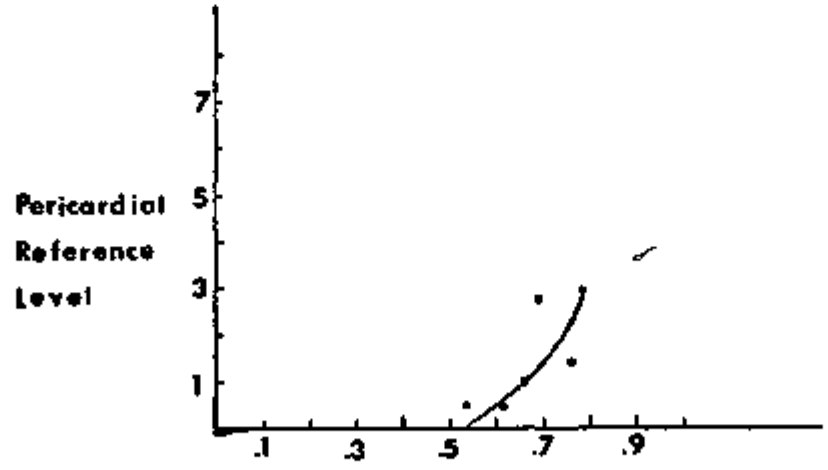

SUPERIOR $\frac{VC_y^P}{Y_{pmax}}$

Figure E2

SUPERIOR VENA CAVA REFERENCED TO
CHEST WALL vs PERICARDIAL LEVEL

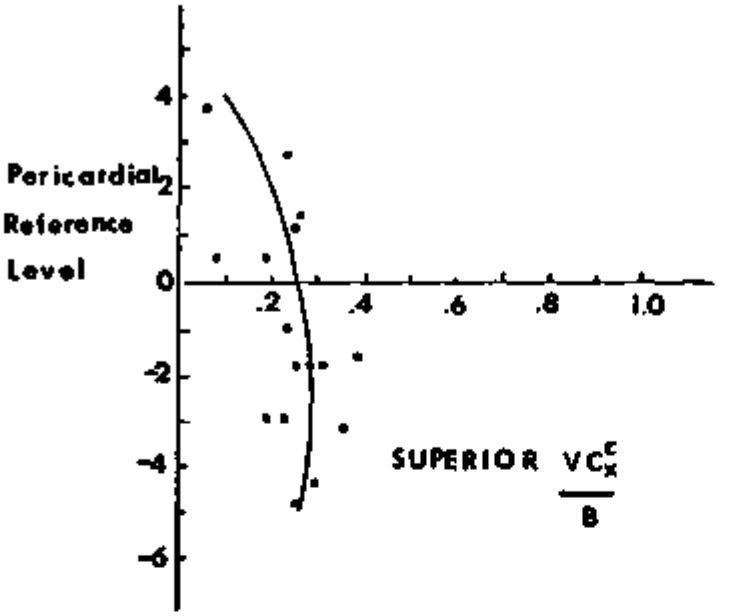

Figure E3

SUPERIOR VENA CAVA REFERENCED TO
CHEST WALL vs PERICARDIAL LEVEL
(LATERAL VIEW)

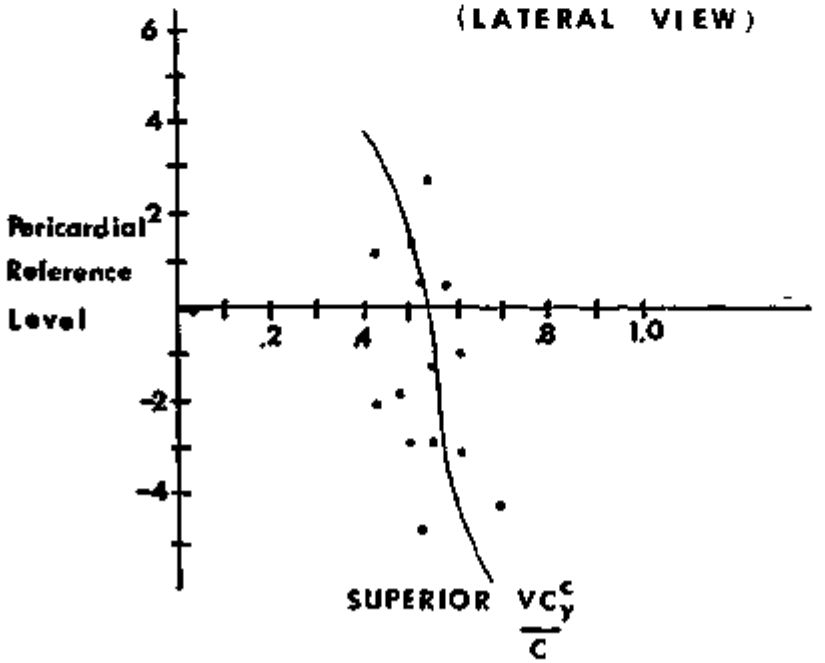

Figure E4

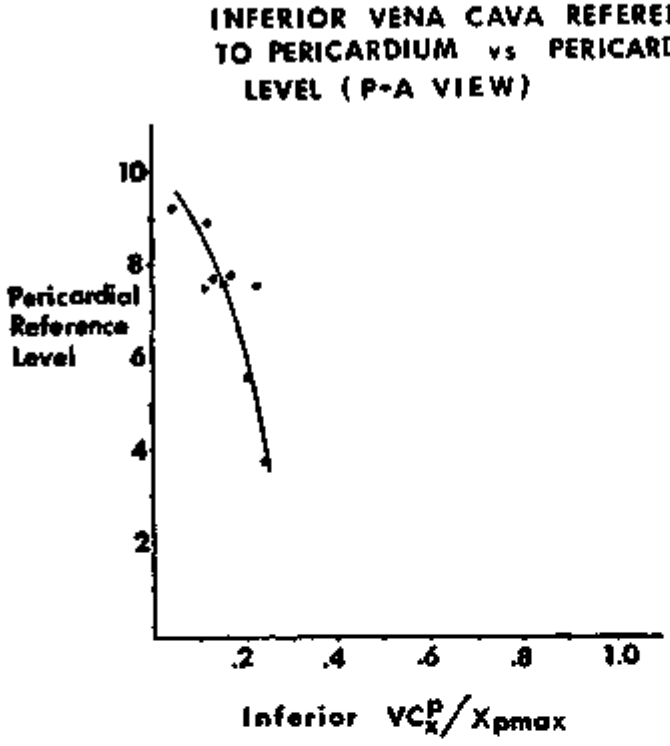

Figure E5

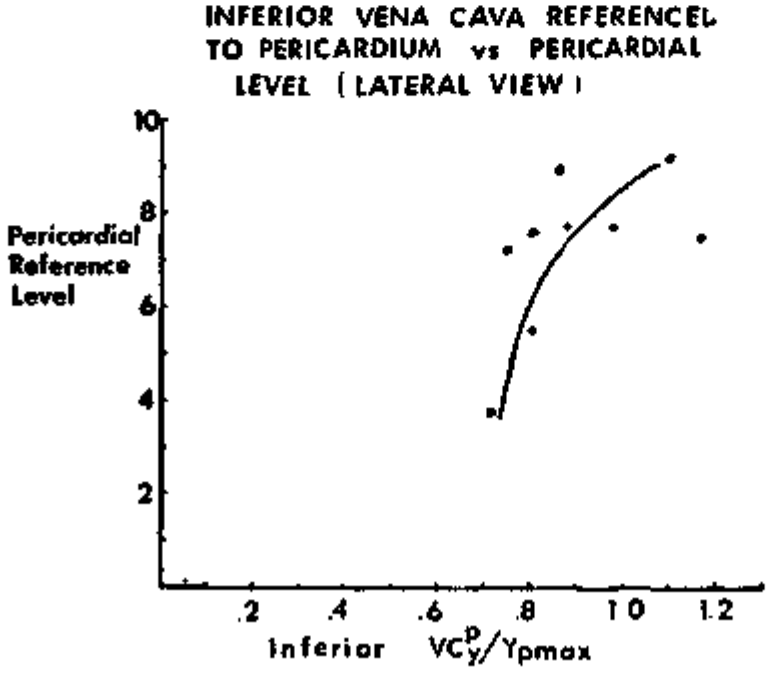

Figure E6

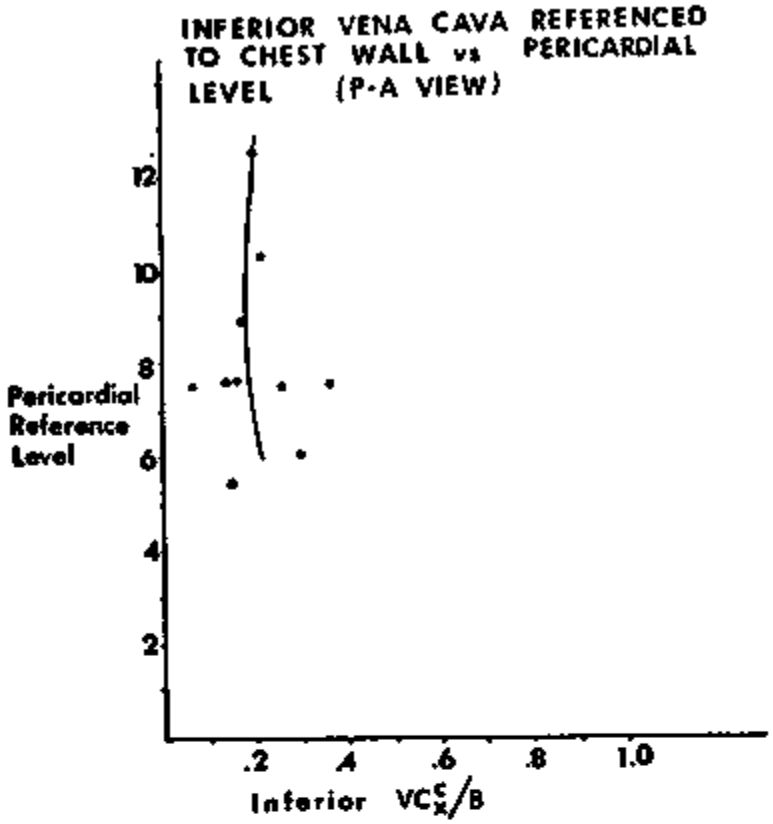

Figure E7

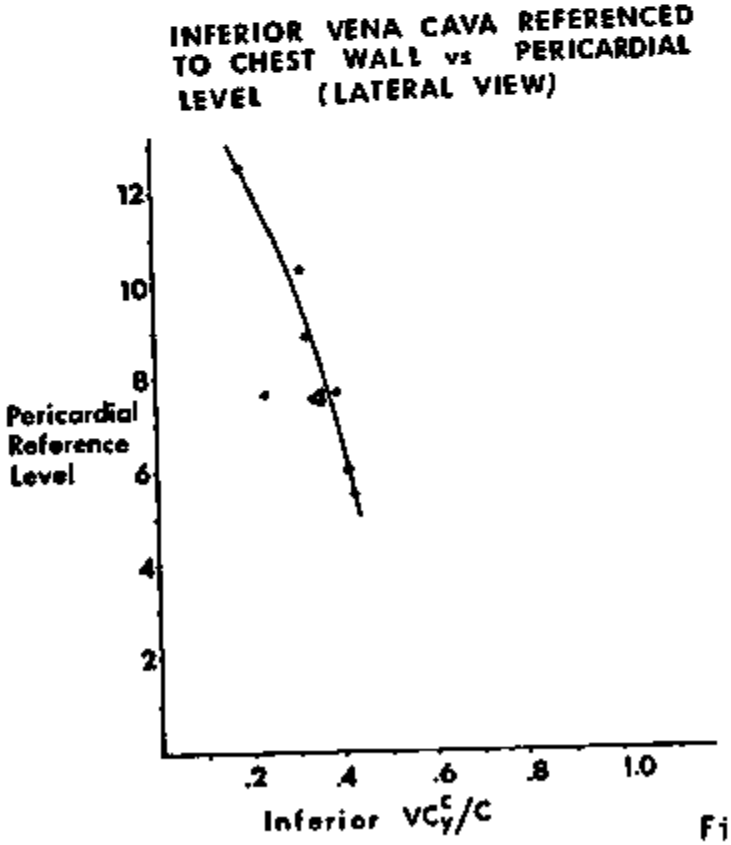

Figure E8

ASCENDING AORTA REFERENCED TO
PERICARDIUM vs PERICARDIAL LEVEL
(R-A VIEW)

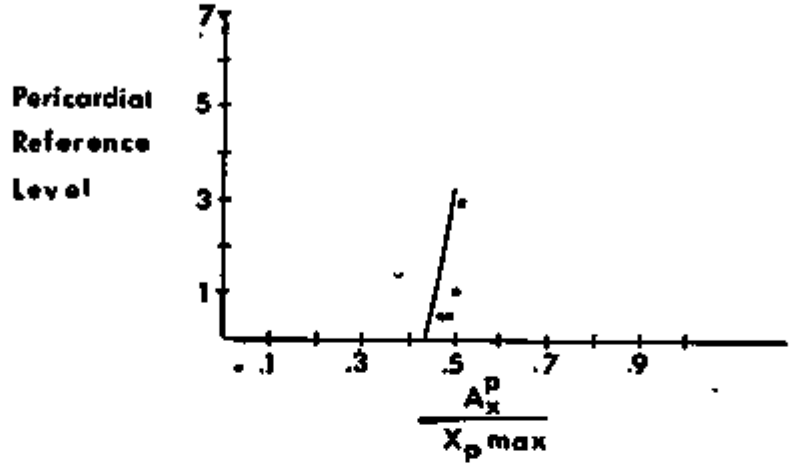

Figure E9

ASCENDING AORTA REFERENCED TO
PERICARDIUM vs PERICARDIAL LEVEL
(LATERAL VIEW)

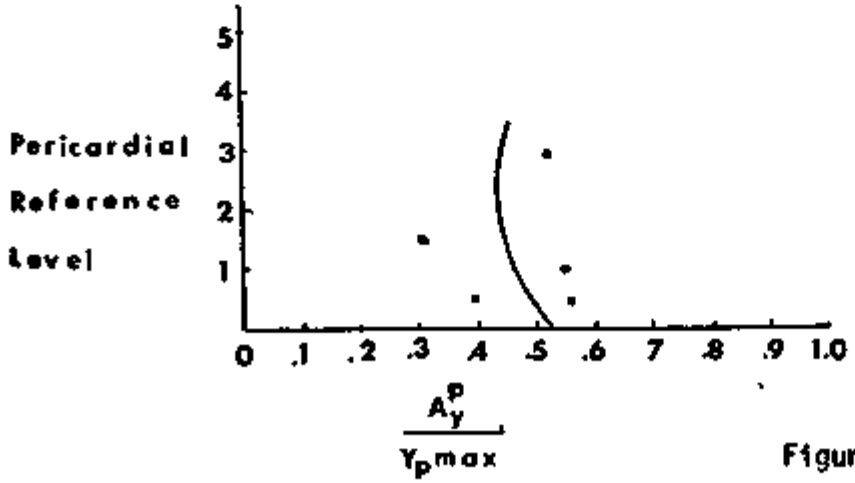

Figure E10

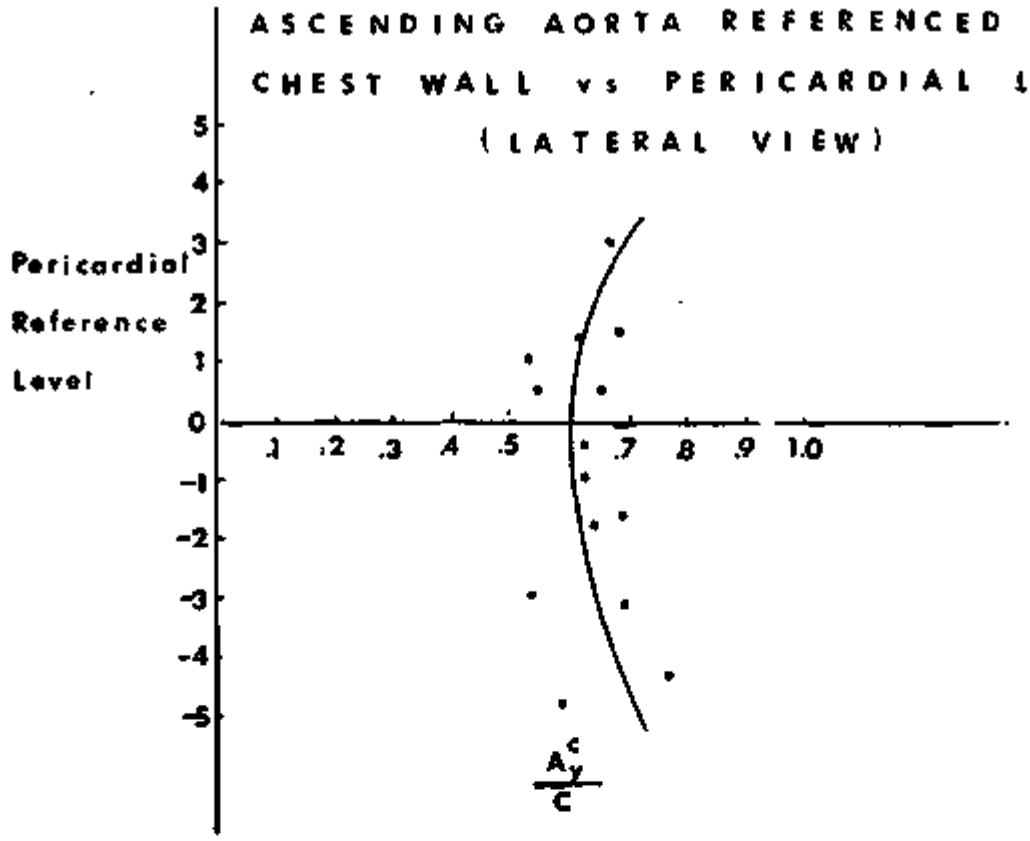

Figure E11

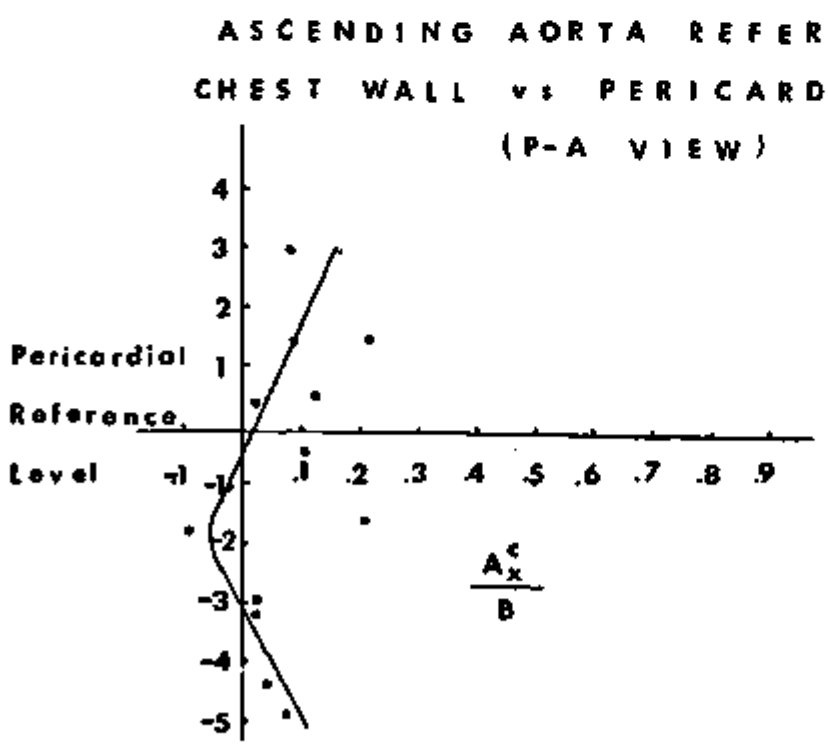

Figure E12.

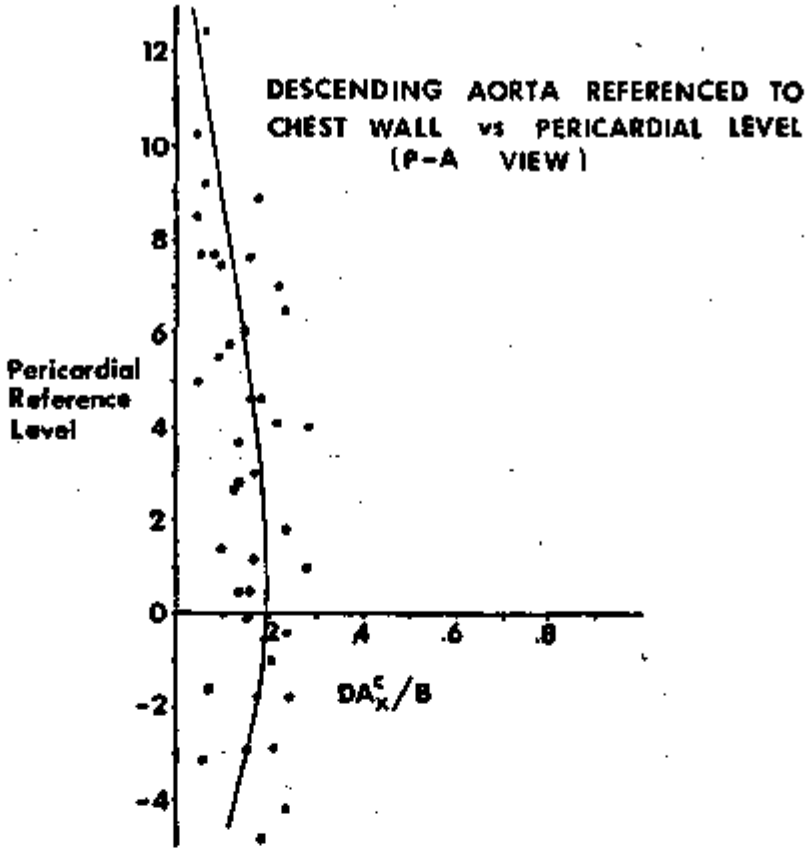

Figure E13

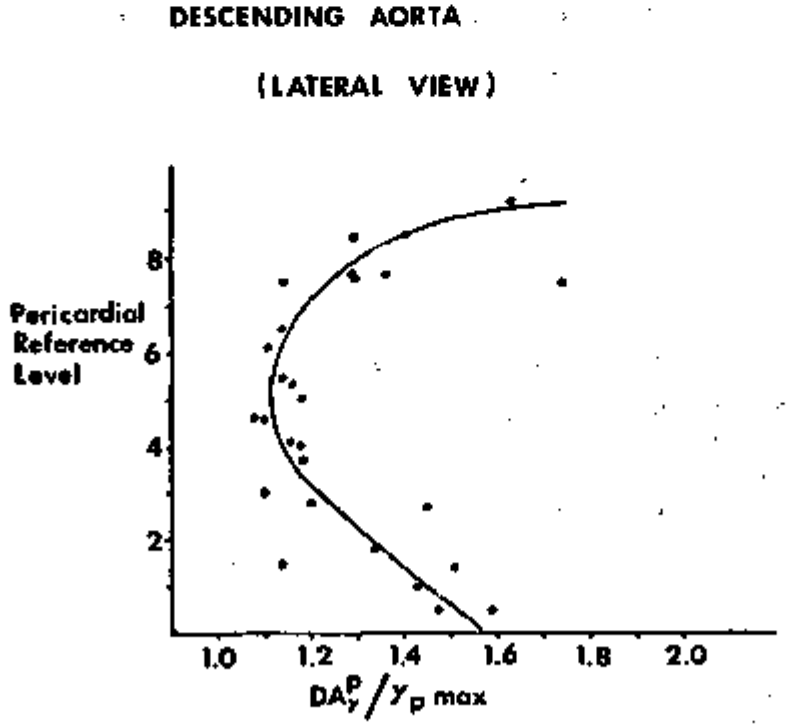

Figure E14

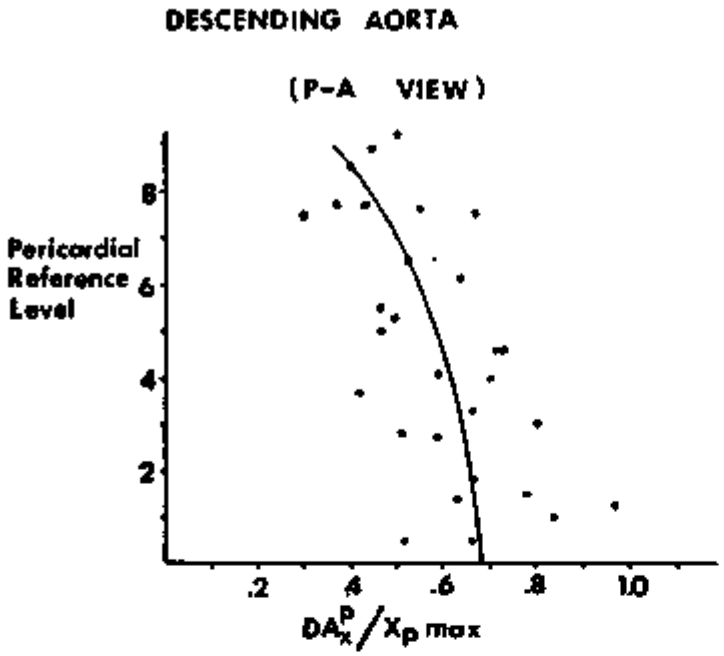

Figure E15

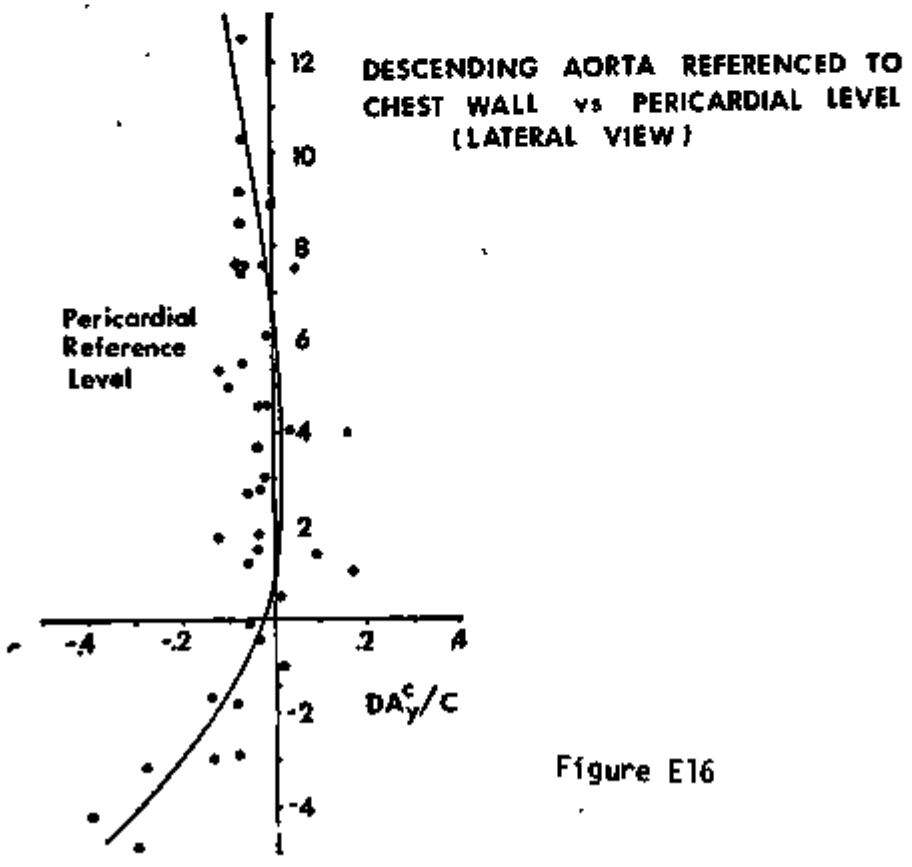

Figure E16

References

1. Urzua, J., Kiraly, R.J., Wright, J.I., Cloesmeyer, R. and Nose, Y.: A rationally designed artificial heart for calves. Trans. ASAIO, 20:660, 1974.

2. Aldrich, J.G., Chambers, J.A., Daly, B.D.T., Migliore, J.J., Newgard, P., Huffman, F.N. and Norman, J.C.: An electrically actuated left ventricular assist device (E-A LVAD) in vivo testing. Trans. ASAIO, 20:655, 1974.

3. Robinson, W.J., Igo, S.R., Daly, B.D.T., Migliore, J.J., Hughes, D.A., Edmonds, C.H., Fugua, J.M., Huffman, F.N. and Norman, J.C.: An abdominal left ventricular assist device (ALVAD): chronic hemodynamic analyses in the calf. Trans. ASAIO, 20:709, 1974.

4. Eycleshymer, A.C. and Schoemaker, D.M.: A Cross-Section Anatomy. New York: D. Appleton-Century Co., 1938.

5. Pernkopf, E.: Topographische Anatomie des Menschen. Muchen: Urban & Schwarzenberg, 1943.

6. Morton, D.J.: Manual of Human Cross Section Anatomy. Baltimore: Williams and Wilkins, 1944.

7. Sobotta, J.: Atlas of Human Anatomy, Vol. III. New York: G.E. Stechert & Co., 1928.

8. Doyen, E., Bouchon, J.P., and Doyen, R.: Atlas d'anatomie topographique. Paris: A. Maloine, 1911.

9. Hovelacque, A., Monod, O., and Evrard, H.: Treize coupes horizontales du thorax. Paris: Librairie Maloine, 1938.

10. Nishi, S., Oha, H., Sasa, T., Otsuki, K., and Hasegawa, T.: Clinical demonstration of axial transverse cross section of adult. Tokyo: Kanehara, 1949.

11. Nishi, S. (ed.): Atlas of Human Anatomy. Tokyo: Kanehara, 1956.

12. Roy-Camille, R.: Coupes horizontales du tronc. Paris: Masson, 1959.

13. Zdansky, E., and Boyd, L.-J.: Roentgen Diagnosis of the Heart and Great Vessels. New York: Grune & Stratton, 1965.

14. Ungerleider, H.E., and Clark, C.P.: A study of the transverse diameter of the heart silhouette with prediction table based on the teleroentgenograms. Amer. Heart J., 17:92, 1932.

15. Touro-Kaisila, K.: Heart size determination by photofluography. Acta. Radiol. Suppl., 295:3, 1970.

16. Larsson, H. and Kjellberg, S.R.: Roentgenological heart volume determination with special regard to pulse rate and the position of the body. Acta. Radiol., 29:159, 1948

17. Bergstrom, K.: Roentgenological heart volume determination in model experiments. Influence of the size, configuration and position of the heart and of the position of the diaphragm. Acta Soc Med Upsal, 74:49, 1969

18. Bergstrom, K., Erikson, U., Gustafsson, B.: Roentgenological determination of the heart volume, the influence of projection and body position. Acta Soc Med Upsal, 74:81, 1969.

19. Kremens, Victor: Deomonstration of the pericardial shadow on the routine chest roentgenograms: A new roentgen finding. Radiology, January 1955, p. 72.

20. Hultgren, H.N, Hubis, H., Shumway, N.: Cardiac function following prosthetic aortic valve replacement. Amer Heart J, 77:585, 1969.

21. Ungerleider, H.E., Gubner, R.: Evaluation of heart size measurements. Amer Heart J, 24:494, 1942.

22. Jonsell, S.: A method for the determination of the heart size by teleroentgenography (A Heart Volume Index). Acta Radiologica, 20:325, 1939.

23. Kjellberg, S.R., Lonroth, H. and Rudhe, U.: The effect of various factors on the roentgenological determination of the cardiac volume. Acta Radiol, 35:413, 1951.

24. Bergstrom, K., Backlund, L., Erikson, U. and Gustafsson, B.: Heart volume and its relation to measures of circulatory function in healthy young men. Acta Med Scand, 185:471, 1969.

25. Bergstrom, K. and Erikson, U.: A study of formulae and methods for determination of the heart volume. Acta Soc Med upsalien, 70:279, 1965.

26. Danzer, C.S.: The cardio-thoracic ratio: An index of cardiac enlargement. Am J Med Sci, 157:513, 1919.

27. Keats, T.E., Zenge, I.P.: Cardiac mensuration by the cardiac volume method. Radiology, 85:850, 1965.

28. Glover, L., Baxley, W.A., and Dodge, H.T.: A quantitative evaluation of heart size measurements from chest roentgenograms. Circulation, 47:1289, 1973.

29. Stein, P.D., Lewinson, H. and Potts, K.H.: Cardiac size and left ventricular performance: Lack of correlation with silhouette measurement. JAMA, 229:1614, 1974.

30. Eckner, F.A.O., Brown, B.W., Davidson, D.L. and Glagov, S.: Dimensions of normal human hearts. Arch Path, 88:497, 1969.

31. Burton, A.C.: The importance of the shape and size of the heart. Amer Heart J, 54:801, 1957.

32. Kaneko, K., Simonson, E. and Schmitt, O.H.: Relationship between the position of chest electrodes (Frank and SVEC-III Systems) and the anatomic position of the heart. Amer Heart J, 74:58, 1967.

33. Oberman, A., Myers, A.R., Karnnas, T.M. and Epstein, F.H.: Heart size of adults in a natural population. Circulation, 35:724, 1967.

34. Merklin, R.J.: Position and orientation of the heart valves. Am J Anatomy, 125:375, 1969.

35. Abbott, M.E.: Atlas of Congenital Cardiac Disease, New York: The American Heart Association, Inc., 1954.

36. White, Alan F., Dinsmore, R.E. and Buckley, Mortimer: Cineradiographic evaluation of prosthetic cardiac valves. Circulation, XLVIII:882, 1973.

37. Takahashi, S.: An Atlas of Axial Transverse Tomography and its Clinical Application, New York: Springer-Verlag, 1969.

38. Rushmer, R.F.: The size and configuration of the heart, in Cardiovascular Dynamics. Philadelphia: W.B. Saunders Co., 1970, pp. 328-353.

39. Kubik, S., and Healey, J.E.: Surgical Anatomy of the Thorax. Philadelphia: W.B. Saunders, 1970, p. 135, 171.

40. Brecher, G.A. and Galletti, P.: Functional anatomy of cardiac pumping, in Handbook of Physiology, sect. 2, Vol. II. Washington, D.C.: Am. Physiological Society, 1963, p. 764.

41. Johnson, S.A., Robb, R.A., Greenleaf, J.F., Ritman, E.L., Gilbert, B.K., Storma, M.T., Sjostrand, J.D., Donald, D.E., Herman, G.T., Sturm, R.E., and Wood, E.H.: Dynamic three-dimensional reconstruction of beating heart and lungs from multiplanar roentgen-television images. Mayo Clin Proc, 49:958, 1974.

42. Young, I.T., Walker, J.E., and Bowie, J.E.: An analysis technique for biological shape. Information and Control, 25:357, 1974.

43. Urzua, J., Sudilovsky, O., Panke, T., Kiraly, R., Nose, Y.: Anatomical constraints for the implantation of an artificial heart. J Surg Research, 17:262, 1974.

44. Annual Progress Report "Available Space for a Totally Implantable Cardiac Prosthesis" C00-2208-6, April, 1974, Cleveland Clinic Foundation.

45. Annual Progress Report "Available Space for a Totally Implantable Cardiac Prosthesis" C00-2208-3, April 1973, Cleveland Clinic Foundation.

46. Urzua, J., Kiraly, R., Lent, F., Nose, Y., Sudilovsky, O., Panke, T.: A Totally implantable artificial heart; anatomical space availability. Proc 25th ACEMB, 14:112, 1972.

47. Urzua, J., Kiraly, R., Jacobs, G., Agishi, T., Sudilovsky, O., Panke, T., Lent, F., Picha, G., Nose, Y.: Anatomical feasibility of a totally implantable artificial heart for human implantation, ASAIO Abstracts, 2:67, 1973.

48. Jacobs, G., Agishi, T., Urzua, J., Kiraly, R., Nose, Y.: Human chest dimensions for artificial heart design, ASAIO Abstracts, 3:33, 1974.

49. Jacobs, G., Agishi, T., Kiraly, R., Nose, Y.: Definition of the spatial constraints of the human thorax for implanting an artificial heart (Abstract) Med Instru, 8:138, 1974.

50. Jacobs, G., Agishi, T., Kiraly, R., Nose, Y.: Human chest dimensions relative to cardiac replacement, Proc 27th ACEMB, 16:46, 1974.

51. Roesler, H.: Clinical Roentgenology of the Cardiovascular System. Springfield: Charles C. Thomas, 1943.

52. Kruger, R.P., Townes, J.R., Hall, D.L., Dwyer, S.J., and Lodwick, G.S.: Automated radiographic diagnosis via feature extraction and classification of cardiac size and shape descriptors. IEEE Trans Bio-Med Engin, BME-19:3, 1972.

53. Deaver, J.B., Surgical Anatomy, III. Philadelphia: Blakiston's Son and Co., 1926, p. 405.